Cell death in the intestinal epithelium: the molecular basis for mouse resistance to *Shigella flexneri* infection

By

Justin Roncaioli

A dissertation submitted in partial satisfaction of the

requirement for the degree of

Doctor of Philosophy

in

Molecular and Cell Biology

in the

Graduate Division

of the

University of California, Berkeley

Committee in charge:

Professor Russell E. Vance, Chair
Professor Laurent Coscoy
Professor Sarah Stanley
Professor Daniel Portnoy

Fall 2022

Cell death in the intestinal epithelium: the molecular basis for mouse resistance to *Shigella flexneri* infection

Justin Roncaioli

Abstract

Cell death in the intestinal epithelium: the molecular basis for mouse resistance to *Shigella flexneri* infection

By

Justin Roncaioli

Doctor of Philosophy in Molecular & Cell Biology

University of California, Berkeley

Professor Russell E. Vance, Chair

Shigella species, the causative agents of bacillary dysentery or shigellosis, infect more than 250 million people each year and are a major driver of diarrheal associated morbidity and mortality world-wide. *Shigella* induces severe gastrointestinal disease by colonizing and disseminating within the epithelial lining of the human colon and rectum, events that drive significant inflammation in the gut. Despite this heavy disease burden, little is known about the molecular determinants of pathogenesis during infection and the adaptive immune correlates of protection up re-infection, due largely to the lack of an inexpensive, tractable, and physiologically relevant mammalian model of shigellosis. Indeed, a detailed understanding of the immune response to this pathogen is critical for the development of vaccines to *Shigella*, none of which has been effective enough at eliciting protection to be licensed for use in humans. Mice are an ideal system to model human specific disease because of their short generation time, the relatively low cost and effort to maintain a mouse colony for research, and the extensive immunological and genetic tools that have been established in this organism over the past half-century. Wild-type laboratory mice, however, are intrinsically resistant to high doses of oral *Shigella* challenge and the genetic and mechanistic underpinnings of this resistance have remained largely unknown. My dissertation examines the host innate immune factors in mice that dictate resistance to oral *Shigella* infection. In the first chapter I review what is currently known about *Shigella* pathogenesis, discuss the animal models that have been used to establish this understanding, and provide background on innate immune pathways in humans and mice that sense *Shigella.* In the second chapter I describe the genetic basis of resistance to *Shigella* infection in mice and show that NAIP–NLRC4 inflammasome-deficient mice are susceptible to *Shigella* infection and serve as a physiologically relevant model of dysentery. In the third chapter, I use this model to expand our understanding of innate immune resistance to *Shigella* infection and show that a redundant, layered hierarchy of cell death in intestinal epithelial cells is key to this resistance. Finally, in the fourth and final chapter, I describe how our findings advance the field and comment on how our new model of *Shigella* infection can be leveraged to learn more about the immune response to this deadly intestinal pathogen.

Acknowledgements

There are countless people that I must thank for carrying me through these past 6 years to the finish line of my PhD. To begin, I would like to acknowledge my supervisor, Russell Vance, who believed in me enough to let me join the Vance Lab. I really appreciate how Russell trusted me and my decisions and allowed me to grow into my own as a scientist. I admire his creative, curious, and meticulous approach to science and his ability to keep the mood light and joyous in the lab. He is one of the best professional role models I have had up to this point in my life.

I owe an immense Thank You to the members of the Vance Lab for providing a supportive, encouraging, and fun lab environment during my time here. Peter, Shally, Katie, and Kristen were my confidants, party buddies, and commiserators in the lab and I could not have done it without them. I'd also like to thank Justin, Daisy, Elizabeth, Brenna, Marian, and Charlotte for being excellent friends and colleagues. I am in great debt to former postdocs Bella Rauch and Patrick Mitchell, my initial mentors in the lab, whom I loved working with and deeply admire. I'd also like to thank Andrew, Moritz, Dmitri, Stefan, and Kevin for being incredible sources of knowledge and advice. I'm especially thankful for Kevin, who's rigorous and determined approach will greatly advance *in vivo Shigella* research. Livia and Janet, my bay-mates over the past 6 years, have both kept me honest and provided me with a space to vent my frustrations and excitements. It has been great to be able to mentor Janet and see her grow and really start to dig into the questions surrounding the adaptive immune response to *Shigella* infection. Finally, I would like to thank Fitty, Jocelyn, and Roberto, our research technicians and lab managers. Roberto has been the perfect take-down partner and mouse house manager – I owe him endlessly for the late nights he saved me from having. And it has been a pleasure to mentor Fitty from early 2020 through the pandemic and watch her mature as a scientist. I'm looking forward to seeing where her curiosity leads her in the next few years!

I'd like to extend a Thank You to my colleagues in the Immunology Division of MCB, especially those in the Barton Lab. There are too many of you to thank, but I've always appreciated the supportive environment that we fostered together and the energy that you brought to our weekly floor meetings, our retreats, and our competitive games of rage-cage during floor parties.

My previous scientific mentors Roddy O'Sullivan, Daven Presgraves, Amanda Larracuente, and Emily Landeen have been profound influences as well, and I have them to thank for instilling confidence in me and showing me that graduate school and science were places in which I could succeed. And a special Thank You to Cammie Lesser, who has been a source of support and guidance since we first started with *Shigella* and somehow trusted that we would figure everything out.

Thornton, Josh, Maya, Tess, Paige – I have you all to thank for being incredible housemates and friends. Our laughs, chats, and late nights got me through graduate school. And I'm also super grateful to Gabriella, Ellie, Arik, Nora, and Laura for being great and trusting friends who were up always up for a new adventure. A huge Thank You to Gabriella for sharing Warriors and Yankees super-fandom with me and the many great moments that came with it. Luke and Dan N. – thank you for being great run partners throughout the years. Nora – thank you for being such a fun and creative follies partner and friend. And Soctopus and the MCBallers – thanks for providing that athletic outlet each week that I always craved.

To my many other friends throughout graduate school: Josh, Raymond, Michael M., Rafael, George, Amy, Huntly, Melissa, Phil, Hannah, Erik, Jesse, Davis, Matthew, Rob, Nick, Victoria, Shaina, Eli, Parker, Tina, Natalie, Derek, Jesus, Kristi and many more – I couldn't have done this without you. Michael, Jamie, Brian, Simeng, Joe M., and Tim – thanks for providing a much needed outlet and for always lending an ear or joining me on a vacation. And my friends from home, Ethan and Kevin - thank you for sticking with me through all of this!

Of course, I would not be here without my family, especially Mom and Dad, Derek and Corinne (and baby G!), Matt and Deanna, and Aunt Sandy. I want to thank you for supporting me, loving me, and believing in me. Things were not always easy over the past 6 years and I am grateful to have had you to lean on. And finally, there is no way I would have made it through this PhD without my partner through nearly all of it, Perri. Thank you for being so understanding, patient, resilient, goofy, kind, and loving and for sharing a home with me. I thank you, I owe you, and I love you. <3

Table of Contents

Chapter One. Introduction

1.1 *Shigella* and shigellosis

Bacterial of the genus *Shigella* are diarrheal pathogens that are closely related to (and in fact cluster within) *Escherichia coli*. They are named after Kiyoshi Shiga, who isolated the most virulent species *Shigella dysenteriae* in 1898. *Shigella flexneri*, *S. sonnei*, and *S. boydii* make up the three remaining pathogenic members of the *Shigella* genus, each of which is genetically similar but differentiated by serotype. *Shigella* species possess a 220kb virulence plasmid which distinguishes them from avirulent *Escherichia coli* and is required for host pathogenicity upon infection [2].

Shigella species are gram negative, non-spore-forming, facultative anaerobic bacilli that infect humans and other primates. *Shigella* is transmitted via the fecal-oral route, and in some humans, as few as 10-100 bacteria are sufficient to cause disease. This low infectious dose drives outbreaks and endemicity in regions of the world where residents lack sufficient access to clean, treated drinking water. In recent years, over-use of antibiotics has driven a rise in antibiotic resistant strains. Furthermore, there exist no effective, licensed vaccines against *Shigella*. Taken together, these factors have contributed to the emergence of *Shigella* as the leading bacterial cause of diarrhea and diarrheal-associated childhood mortality [2-6].

Shigellosis, or *Shigella*-dependent dysentery, is driven by bacterial invasion of the epithelial lining of the colon and rectum. Invasion and colonization of this niche is dependent on the *Shigella* virulence plasmid, which encodes a type three secretion system (T3SS) necessary for IEC invasion and an arsenal of effectors that aid in inhibition of the innate immune response, residence in the epithelial cell cytosol, and dissemination to the cytosol of adjacent epithelial cells. These events drive widespread colonic inflammation and manifest symptomatically as fever, severe abdominal cramping, and bloody, neutrophilic diarrhea. *Shigella* infections are restricted to the intestine and are self-limiting, typically resolving within 7 days of symptom onset. In immunocompromised adults, the elderly, and children experiencing malnutrition, however, *Shigella* infections can persist for weeks and drive complications including toxic megacolon, renal failure, severe dehydration, low platelet and red blood cell counts, post-reactive arthritis, and fatality [2, 7, 8].

1.2 The infectious life cycle of *Shigella*

1.2.1 Accessing the intestinal tissue

Despite the limitations of modeling *in vivo Shigella* infection, progress has been made in characterizing the key steps in *Shigella* pathogenesis. To establish an infection, *Shigella* must first overcome the physiochemical conditions of the digestive tract and establish a stable niche among the endogenous host gut microbiota. While the details of how *Shigella* initially establishes a niche in the lower gastrointestinal tract are poorly understood, studies in mice have shown that colonization resistance from the endogenous host microbiome is a barrier to *Shigella* residence in the gut lumen and fecal contents [9-11]. Indeed, *Shigella sonnei* encodes a functional T6SS that provides a competitive advantage against other *Shigella* species and *E. coli* and promotes *Shigella* persistence in the colon of mice treated with antibiotic prior to infection [10].

After establishing a sufficient niche in the colonic lumen, *Shigella* is thought to access intestinal tissue by crossing the mucous layer that lines the epithelium and

utilizing specialized M (microfold)-cells, which passively sample the intestinal contents, to transit to the lamina propria of the gut. M-cells reside over lymphoid follicles enriched for macrophages and other antigen presenting cells, which can phagocytose the invading bacteria. The role of macrophages during *Shigella* infection is poorly understood, but it is hypothesized that *Shigella* rapidly induces the lysis of these cells through inflammasome-dependent pyroptosis. The release of processed IL-1β from pyroptotic macrophages is believed to initiate the inflammatory response to *Shigella* infection. Pyroptosis also releases *Shigella* into the extracellular environment of the lamina propria at the basolateral surface of intestinal epithelial cells. Extensive studies in cell lines and human organoids indicate that *Shigella* is particularly poor at invading intestinal epithelial cells at their apical surface (in contrast to other pathogens like *Salmonella*) but is effective at invading basolaterally. Thus, it is thought that the transit through M-cells and uptake and release by macrophages are key steps in delivering the pathogen to the basolateral surface of the intestinal epithelium [3, 7, 8].

1.2.2 Colonizing the intestinal epithelium

While the precise role of the virulence plasmid in these aforementioned steps is not well characterized, the plasmid is essential for the next step in the *Shigella* infectious life cycle: the invasion of the intestinal epithelium. Genes critical for invasion, including the structural components of the T3SS and the transcriptional regulators VirF and VirB are encoded in a 31kb pathogenicity island called the entry region. The expression of genes within this island is triggered by specific *in vivo* physiochemical conditions and a shift to 37°C, leading to the assembly of the T3SS, a long, needle-like structure which spans the bacterial inner and outer membrane and protrudes through the host cell membrane. A first wave of effectors is expressed and secreted through this structure into the epithelial cell cytosol, remodeling host actin to allow for bacterial uptake into a vacuole and subsequent escape from this vacuole into the host cytosol. One critical effector expressed on the virulence plasmid is the protein IcsA, an adhesin and actin nucleator essential for cytosolic actin-based motility [3, 7, 8].

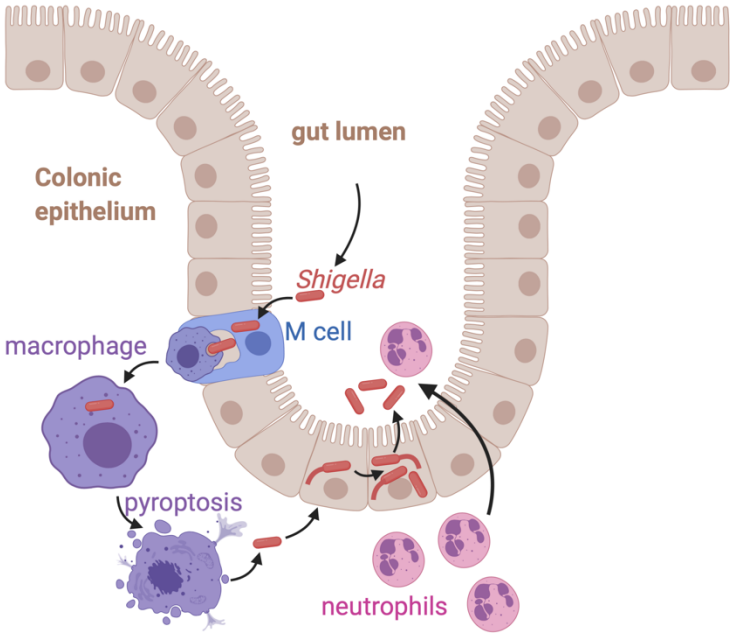

Figure 1.1. Accepted mode of *Shigella* Pathogenesis
Shigella is believed to access intestinal tissue via transport through M-cells. In the lamina propria, *Shigella* is phagocytosed by macrophages, which undergo T3SS and inflammasome-dependent pyroptosis. Bacteria release from pyroptotic cells can invade the basolateral side of the intestinal using the T3SS and several secreted effectors that promote bacterial uptake and promote cell survival. Vaculoar lysis upon invasion allows *Shigella* to enter the cytosol, where it replicates and nucleates actin to promote motility and dissemination to adjacent cells. Activation of innate immune sensors within IECs drives inflammation, neutrophil influx, and diarrhea.

Following invasion and escape into the cytosol, *Shigella* establishes its niche within the intestinal epithelium. The T3SS secretes a second wave of effectors which dampen the host immune response, promote cell survival, and make the host cell cytosol a more hospitable site in which to replicate. A key step in the establishment of this cytosolic niche and successful replication within it is the subversion or inhibition of host innate immunity and cell death pathways, a topic I will explore in detail later in this chapter. *Shigella* uses IcsA-dependent actin-based motility to move throughout the cytosol, evade autophagy, and to protrude and disseminate into adjacent cells. These steps again require the expression of the T3SS, which is critical for vacuolar rupture and cytosolic colonization upon invasion of an adjacent cell. Subsequent dissemination events ultimately initiate infection foci that spread throughout the epithelium. IcsA-deficient *Shigella* strains are largely unable to colonize the intestinal epithelium and cause disease, suggesting that these dissemination steps are essential for *Shigella* virulence, host inflammation, and pathogenesis [3, 7, 8].

1.2.3 The initiation of inflammation and pathogenesis

A key step in the initiation of inflammation during *Shigella* infection is the activation of the pro-inflammatory NF-κB signaling pathway within intestinal epithelial cells. The NF-κB signaling pathway can be activated in IECs by surface and endosomal Toll-like receptors (TLRs) that signal through MyD88 and cytosolic pattern recognition receptors (PRRs) Nod-like receptors 1 and 2 (NOD1 and NOD2) and alpha-kinase 1 (ALPK1). While it remains unclear if epithelial TLRs sense *Shigella* during infection, *in vitro* studies have shown that epithelial NOD1 and NOD2 recognize *Shigella* cell membrane peptidoglycan fragments γ-D-glutamyl-*meso*-diaminopimelic acid (iE-DAP) and muramyl dipeptide (MDP) [12, 13], respectively, and epithelial ALPK1 recognizes the *Shigella* metabolite ADP-β-D-manno-heptose (ADP-Hep) [14]. Both NOD1/2 and ALPK1 activation leads to robust NF-κB signaling, the transcriptional upregulation of several pro-inflammatory genes, and the subsequent secretion of cytokines from cells in the infected intestinal epithelium [14, 15]. Although *Shigella* encodes numerous effectors to dampen NF-κB activation and signaling, both infected and neighboring bystander IECs participate in the inflammatory process by secreting the NF-κB-dependent neutrophil chemoattractant IL-8 or CXCL1. It is thought that this cytokine, in combination with IL-1β, drives the robust recruitment of immune cells, including inflammatory monocytes, macrophages, NK-cells, and neutrophils [7, 8].

Neutrophil recruitment to the intestine and feces of human patients is a key hallmark of shigellosis but the exact role of neutrophils during infection remains largely unclear. Indeed, neutrophils have been implicated in both the exacerbation and resolution of *Shigella* infection. Neutrophil transmigration through the intestinal epithelium, for instance, might contribute to the destabilization of the intestinal epithelial barrier and provide an additional route for *Shigella* to translocate to the intestinal lamina propria and invade the epithelium [8]. Furthermore, neutrophils have been shown to be detrimental in some intracellular bacterial infections by potentiating inflammatory signals without clearing the pathogen [16]. It is plausible that similar events might occur *Shigella* infection, especially since the bacteria that seem to drive pathology are largely protected from neutrophil killing by residing within intestinal epithelial cells. However, it is likely that neutrophil recruitment into the lumenal contents of the colon leads to

phagocytosis and neutrophil extracellular trap (NET) release within this compartment, events which might ultimately promote bacterial clearance [7, 17].

1.2.4 Resolution of Infection

In immune-competent, healthy adults, *Shigella* infections are typically self-limiting and resolve within 7 days of symptom onset [2]. Three distinct events may contribute to infection resolution: (1) bacterial clearance by innate immune cells and effector mechanisms, (2) bacterial clearance by the adaptive immune system, and (3) bacterial loss of the virulence plasmid. The acute nature of most *Shigella* infections suggests that bacterial clearance is most likely driven by innate immune mechanisms, although antibody production and cellular adaptive immunity likely hastens resolution in infections that last more than 10 days. *Shigella* species experience spontaneous virulence plasmid loss at 37°C and bacteria that lose the plasmid experience a significant growth advantage [18]. When cultured at 37°C, virulence plasmid loss drives an outgrowth of non-virulent *Shigella* usually within 72 hours. While there is high selective pressure to maintain the plasmid during infection, it remains unclear whether virulence plasmid loss does occur *in vivo*, an event that would hasten infection resolution.

1.3 Modelling *Shigella* infection

Despite its high infectiousness in humans, oral *Shigella* challenge in mice does not lead to disease [9, 11]. The lack of a physiological mouse model that accurately recapitulates human shigellosis has remained a major impediment to progress in understanding how *Shigella* causes disease and how the immune system responds to infection. However, advances have been made using non-traditional animal models, human and primate challenge studies, and in vitro studies using both cell lines and primary cells. Here, I describe the models used to study *Shigella* infection and virulence, highlight the discoveries made in these systems, and outline their advantages and limitations.

1.3.1 Studying *Shigella* during human infection

The first controlled human *Shigella* challenge studies were performed in 1946 by Shaughnessy, et al. in healthy incarcerated adults [19] to determine the infectious dose of certain *Shigella* strains and to evaluate the dynamics of infection and the efficacy of a vaccine candidate. Researchers reported that the incubation period for shigellosis was remarkably short, with most individuals who experienced dysentery developing symptoms within 12 hours of challenge. The researchers also used intramuscular injection of irradiated, heat killed *Shigella* as a vaccination strategy, but vaccinated individuals did not appear to be more protected than unvaccinated controls. While the limitations of this study were numerous and the results were mixed, it set the precedent and guidelines for future human *Shigella* challenge studies in the decades to follow. A systematic literature review of human *Shigella* challenge studies in 2012 identified 18 independent human challenge studies with 47 different dose/strain combinations [20] that have been conducted since this original study. These human experiments have since provided insights on attack rate (~75%), minimal sufficient dose for infection (10^2 bacteria) in certain individuals, and protection upon re-infection [20]. However, the

variability in strains used, infection conditions, and human cohort status has lead to difficulties in a comprehensive interpretation of these results.

Many obstacles exist when performing human challenge studies. While the initial human *Shigella* challenges were performed in incarcerated people to establish large cohorts for infection, this practice is largely considered ethically untenable today, as it is difficult to obtain unadulterated consent from individuals who are incarcerated. Human challenge studies continue today, but the significant cost to recruit, house, and compensate individuals inherently restricts the sample size and lowers the power of each study. Another obvious limitation in human challenge studies is that researchers must take steps to mitigate the chances of severe infection and fatality, thus precluding studies of correlates of advanced disease. Furthermore, many of the detailed studies of pathogenesis that can be performed by sacrificing animal models cannot be performed in humans.

The largest strength of human challenge studies lies in their ability to determine vaccine efficacy or protection upon reinfection. A 1995 study [21] determined that initial infection of healthy human volunteers with *Shigella flexneri* strain 2a conferred a 70% reduction in re-infection relative to healthy, naïve controls. *Shigella* colonized the feces of both the resistant, re-challenged individuals and the susceptible naïve individuals, suggesting that fecal colonization can occur in humans even in the absence of disease. Interestingly, re-challenged individuals experienced a ~10-fold decrease in fecal colonization (peak excretion was ~10^7 CFU/gram of feces in naïve controls and ~10^6 CFU/gram of feces in re-challenged individuals), suggesting that primary challenge does indeed restrict the ability of *Shigella* to replicate within the gut upon re-challenge. Protection correlated with an increase in LPS specific IgA, IgM, and IgG antibody secreting cells, indicating that antibodies may be key in protection from re-infection. This study was key to establishing that humans do indeed mount an adaptive immune response to *Shigella* and that this response can protect against infection with a homologous or identical strain.

Despite extensive efforts, incremental progress has been made in understanding the immune correlates of protection during human infection in the last few decades. The only established parameter associated with significant protection from naturally occurring disease is anti-LPS serum antibodies [22, 23]. The durability of this protection and the ability of these antibodies to work against other *Shigella* species or serotypes is unclear and increasing epidemiological evidence indicates that re-infection by different serotype is a common occurrence in regions of *Shigella* endemicity [24]. Indeed, while the human challenge has been essential in establishing basic parameters of *Shigella* infection and host immunity, the limitations in experimental manipulation, the difficulty in performing and controlling each study, and the inconsistency in results across studies have illuminated the need for animal models that are less expensive and more experimentally tractable.

1.3.2 Primate challenge studies

Humans and non-human primates are the only species naturally susceptible to *Shigella* infection [8]. *Shigella*-dependent dysentery was first described in non-human primates in 1963 by tracking natural disease in a large (>1000 animals) primate colony of rhesus monkeys and hamadryas baboons over many years [25]. In the decades to follow, numerous accidental *Shigella* outbreaks in primate colonies at zoos and

research labs have been documented [26] and have contributed to our knowledge of transmission and epidemiology in this species and in humans.

The first experimental challenge studies in non-human primates occurred in the mid-1960s. Observations during these experiments have contributed significantly to our understanding of the steps of *Shigella* pathogenesis. Sacrifice of animals at the height of infection allowed for a detailed histological examination of intestinal tissue during the acute phase of infection, which revealed significant edema, lesions, cell death, and erosion of the colonic lining and robust neutrophil influx to the lamina propria and lumen of the gut [27, 28]. Fluorescent staining of *Shigella* and microscopy of intestinal tissue sections revealed for the first time that *Shigella* appears to invade intestinal epithelial cells of the colon [27, 29, 30]. Further microscopy studies in infected rhesus macaques showed that the follicle associated epithelium above lymphoid tissue was the first site targeted by *Shigella* in the gut, implicating these organs as initial sites of infection and dissemination [31, 32]. Indeed, the first evidence that *Shigella* effector IcsA is required for virulence *in vivo* is the result of experimental challenges in macaques [31, 33].

As new models of *Shigella* infection were developed in rabbits, guinea pigs, and mice (described in the following sections), the non-human primate model has become primarily associated with studies of *Shigella* vaccine efficacy and adaptive immunology [34, 35]. The genetic and thus immunological similarities between monkeys and humans render findings in monkeys most immediately translatable to humans. Vaccination studies are often easier to perform in non-human primates as researchers do not have to spend effort and funding to recruit and screen human participants and can largely control the parameters of infection and the direct monitoring of disease. Although non-human primates are immensely valuable organisms, extensive sample collection, biopsy, or sacrifice of these animals throughout the course of challenge or re-challenge also lends crucial insights into the progression of the immune response. These experimental manipulations cannot be performed or are more difficult to perform in humans. The intrusive nature of these studies, the value of each animal, and the expense to maintain an animal colony ensures that only the studies most translatable to human health are conducted in non-human primates [36]. For this reason, many of the more detailed studies of basic molecular pathogenesis caused by *Shigella* infection have been performed in smaller mammals.

1.3.3 Guinea pig and rabbit infection models

Studies in humans and primates paved the way for *in vivo Shigella* research, but much of what we now know about pathogenesis and disease has come from infections in guinea pigs and rabbits, which are more amenable to experimental manipulation, easier to maintain in research facilities, and less expensive to use than non-human primates. Both adult rabbits and guinea pigs are resistant to oral inoculation with *Shigella* [37, 38], so researchers have relied on non-traditional routes of infection to study *Shigella* in these animals.

The first guinea pig infection model used was the corneal infection model, commonly referred to as the “Sereny test”, which utilizes the swelling and inflammation of the eye to identify *Shigella* virulence factors required to induce inflammation [39]. Researchers studying host pathogenesis, however, have favored the ligated ileal loop model [37, 40-42] or the intrarectal challenge model [38, 43] in both rabbits and guinea pigs. While infection in these systems bypasses key steps that occur during natural oral

infection, each seems to recapitulate physiological aspects of *Shigellosis* including invasion of intestinal epithelial cells, inflammation, and neutrophil influx in the colon. Studies in these systems have lent insight into how *Shigella* associates with M-cells [44], invades colonocytes at different stages of infection [38, 45], and initiates an immune response [43], and have been particularly useful in phenotypic characterization of *Shigella* mutants [7]. Neutrophil depletions and IL-1R or IL-8 (CXCL1) blockade in the rabbit ligated ileal loop model, for instance, revealed that IL-1, IL-8, and neutrophil influx contribute significantly to tissue damage in the gut [46-48]. In recent years, researchers have developed an oral infant rabbit model of *Shigellosis* which features robust colonization of the feces and intestinal epithelium, weight-loss, and diarrhea [49]. While this experimental system is significantly less surgically invasive than the ileal loop infection models and utilizes the natural route of infection, it is difficult and costly to set up large group sizes for experiments when only using newborn animals.

While many of the basic discoveries of *Shigella* pathogenesis have been made in these rabbit and guinea pig models, the limited availability of genetic and immunological tools in these systems and the paucity of researchers that maintain a guinea pig or rabbit colony has precluded extensive research in these animals. Furthermore, while each of these model systems captures some aspects of human *Shigellosis*, none fully recapitulates the full course of pathogenesis.

1.3.4 Recent zebrafish models

In recent years, researchers have turned to a Zebrafish model of infection to better understand host pathogenesis. Despite their evolutionary distance from mammals, larval zebrafish are susceptible to intravenous infection with *Shigella.* A benefit of this organism is its genetic tractability and its quick development, which allows for relatively high-throughput experimentation in transgenic animals [50, 51]. Another major advantage of the zebrafish system is its optical accessibility for real-time imaging [50], which can be utilized to observe the interactions between fluorescently labeled cells and microbes *in vivo*. Importantly, hindbrain ventricle or caudal vein infection in zebrafish larvae both recapitulate aspects of human *Shigella* infection including epithelial cell invasion, cell death of macrophages, and localized inflammation, all which depend on the *Shigella* T3SS [50].

Studies in zebrafish larvae have revealed key roles of host septins in localizing to cytosolic *Shigella*, limiting actin-based motility, and promoting host autophagy - events which prevent inflammation and systemin infection [52]. Furthermore, live cell imaging of infection dynamics in this organism revealed a role for neutrophil scavenging in eliminating dead macrophages and other non-immune cells that fail to control *Shigella* replication [52]. Larval zebrafish lack a mature intestinal microbiome and adaptive immune system, aspects central to defense against *Shigella* in humans. However, development of an adult zebrafish gastrointestinal infection model which can transmit to naïve organisms and can develop protective immunity has opened the field to more advanced studies of immunity and transmission dynamics in this species [51].

The central disadvantage of using the Zebrafish model is its biological dissimilarity to humans and, thus, it is often unclear how studies of pathogenesis in this organism might translate to humans. Zebrafish reside naturally in water temperatures of ~28-30°C and raising their environmental temperature to 37°C to facilitate *Shigella* T3SS activation can induce a depressed host immune response and an upregulation of

the stress response, confounding studies of pathogenesis [50]. Finally, there is a need to develop more immunological tools and zebrafish specific antibodies to better study host-pathogen dynamics in this system.

1.3.5 *In vitro* modelling of *Shigella* infection

The major advantage of studying *Shigella* infection *in vitro* is the reductionist nature of this system that allows for straightforward hypothesis testing. The ease in setting up high-throughput assays that measure invasion, plaque formation, cell death, and cytokine secretion in cell lines has lead to studies that have lent insight into how shigella invades and survives within epithelial cells [53]. The combination of these assays with traditional biochemical techniques, genetic screening, and advanced imaging in recent years has greatly expanded our knowledge of the molecular interactions between *Shigella* effectors and host proteins and processes [8]. Particularly valuable studies in the last decade have used bacterial TnSeq and *Shigella* effector libraries or minimal systems to perform reverse and forward genetic screen in cell lines [54-56]. These screens have identified key proteins and virulence factors involved in the invasion and dissemination processes, activation of innate immune sensors and cell death pathways, and blockade or antagonism of these pathways.

One disadvantage of working in these *in vitro* systems, however, is that human epithelial cancer cell lines are susceptible to genomic instability and may lack key genes or pathways involved in sensing and responding to *Shigella*. For instance, HeLa cells appear to lack key components of inflammasomes pathways that can respond to *Shigella* and induce pyroptosis. To circumvent these limitations, researchers have had success in maintaining and infecting human-derived intestinal epithelial cell organoids [57-59], which are seeded into monolayers on trans-wells and differentiated to resemble a human *ex vivo* epithelium. Combination of these new systems with co-culture of additional cell types like neutrophils or adaptive immune cells specific to *Shigella* might begin to shed light on the integrated immune response to *Shigella*-infected IECs.

1.3.6 Mouse models of *Shigella* infection

Mice remain the optimal mammalian organism with which to model human disease in a laboratory setting because of their quick generation time (6 weeks), the established genetic and immunological tools in this organism, and the relatively low cost to maintain a colony. Despite the genetic (and thus biological) similarity between humans and mice, key differences between the species often dictate differential outcomes to infection with a single pathogen. *Shigella*, for instance, readily infects humans but does not cause overt disease in mice [9, 11, 60-62]. Uncovering the basis of this resistance in mice is the major focus of this dissertation (chapters two and three) and has been a specific area of study in the *Shigella* field for decades.

The first documented oral mouse *Shigella* challenge study was performed in 1956 by Rolf Freter [9]. Freter found that *Shigella* successfully colonized the feces of mice only when they were administered oral streptomycin prior to infection, indicating that the colonization resistance provided by the endogenous gut microbiota is a major barrier to infection in mice. A 1958 study performed by David McGuire [11] using streptomycin pretreatment indicated that despite high fecal colonization by *Shigella* following oral challenge, mice do not display the inflammatory hallmarks of human shigellosis, suggesting that there is an additional barrier to infection. Since these

original studies, there have been numerous attempts to model oral *Shigella* infection in mice employing immunocompromised, humanized mice [63], newborn mice [62], and mice receiving a zinc-deficient diet [61]. These studies have illuminated important aspects of innate defense, but no infection strategy seems to fully recapitulate the constellation of disease symptoms experienced in humans. Most importantly, there is little evidence that during these infections *Shigella* colonizes colonic epithelial cells, the known natural niche during human infection.

To circumvent the challenges of oral route infection in mice, researchers have made use of mouse intranasal/pulmonary [64, 65], intraperitoneal (I.P.) [66], rectal [60], and ligated intestinal loop *Shigella* infections [67, 68]. An advantage of the intranasal and I.P. infection routes is that mice do experience acute disease [65, 66]. Both intranasal and I.P. challenge at sufficient doses leads to weight-loss, inflammation of infected sites, and systemic dissemination of *Shigella.* A clear phenotype in these models makes them viable for testing virulence of *Shigella* mutants and for testing certain aspects of the host immune response to infection. However, the extent to which findings in these non-physiological models are relevant and informative to oral infection in humans is not always clear. Indeed, *Shigella* rarely disseminates to systemic sites during human infection, and thus, these models do not actually represent phases of infection that might occur naturally. Rectal and ligated intestinal loop challenges do target a relevant site of infection and are effective for studying host pathogen interactions at the epithelial barrier. Unfortunately, however, these challenges are artificial in that *Shigella* is not able to stably colonize these organs and initiate a full cycle of pathogenesis.

1.3.7 Hypotheses for the differential susceptibility of mice and humans

Mouse resistance to shigellosis might be mediated by defects in epithelial invasion, specific immune resistance mechanisms that exist in mice but not humans, or defects in mouse sensing and initiation of inflammation. Most enteric bacterial pathogens use fimbriae, an adhesive filamentous organelle protruding from the bacterial outer membrane, for host attachment. *Shigella* species have lost their fimbriae [69] and it has been hypothesized that the loss of this organelle might dictate a difference in epithelial cell attachment and invasion between mice and humans [8, 67]. Indeed, it has been proposed that *Shigella* to co-opt human α-defensin 5 (HD5), a host anti-microbial peptide, to enhance its adhesion specifically to human cells. Administration of HD5 during mouse colonic and ileal loop infection was reported to increase *Shigella* adhesion to macrophages and IECs but does not appear to promote epithelial cell invasion and colonization in this species [67, 70].

A second explanation for the differences in susceptibility between mice and humans is the differential production of the neutrophil chemoattractant CXCL1 (IL-8) due to mouse-specific defects in the innate sensors that produce this factor or mouse-specific defects in the expression of this factor itself [7, 60]. Mice that received an injection of recombinant human CXCL1 showed robust neutrophil recruitment to the colon following rectal *Shigella* challenge [60]. Importantly, inflammation was dependent on infection with virulent *Shigella.* These experiments suggest that CXCL1 is important for the initiation of inflammation in mice but that this cytokine is not produced during mouse challenge. The absence of CXCL1 production during mouse infection, however, does not mean that this chemokine cannot be produced under the right conditions. It is

possible that CXCL1 can be produced in mice but the pathways that lead to its upregulation and release are simply not being activated by *Shigella* because of a species-specific barrier that prevents colonization of IECs.

A third explanation is that mouse IECs are readily invaded by *Shigella* but a mouse-specific epithelial intrinsic defense mechanism eliminates the pathogen before it can provoke an immune response. Indeed, Chang et al. observed invasion of ileal epithelial cells within one hour of oral infection (without oral streptomycin treatment) in mice [71]. Interestingly, bacteria were rapidly cleared by 3 hours post-infection which was concomitant with mild tissue destruction and host cell death, suggest that host cell death might prevent persistent colonization of the intestinal epithelium by *Shigella*. Indeed, if these events occur before *Shigella* can begin to replicate and disseminate in the epithelium, they might be sufficient to preclude inflammation and disease during oral infection. In the sections below, I will review the emerging role of cell death as a critical defense mechanism against bacterial infection.

1.4 Cell death as an innate immune defense against intracellular pathogens

There is an increasing appreciation for programmed host cell death as an innate immune defense mechanism against intracellular pathogens [72]. Activation of cell death pathways in the context of infection is proposed to rapidly eliminate a pathogen's intracellular niche, exposing it to potent extracellular clearance mechanisms [72]. There are three central modes of programmed cell death – apoptosis, pyroptosis, and necrosis – and each can be triggered by pathogen associated molecular patterns (PAMPs), pathogen encoded activities, or host signals or cytokines released in the context of infection. Here, I review these cell death pathways, the sensors that initiate their activation, and their roles in recognizing and responding to pathogens.

1.4.1 Inflammasomes defend against intracellular pathogens via pyroptosis

Inflammasomes are cytosolic multi-protein complexes that initiate innate immune responses to pathogens by recruiting and activating pro-inflammatory caspases such as Caspase-1 [73]. Once activated, Caspase-1 cleaves and activates pro-inflammatory cytokines IL-1β and IL-18 and the pore forming protein Gasdermin-D (GSDMD). Activated GSDMD monomers localize to the cell plasma membrane, forming a large oligomeric pore that leads to cell permeabilization, release of activated cytokines, and a lytic cell death termed pyroptosis [74]. Several inflammasomes have been described, each with a unique sensing domain that recognizes bacterial and viral PAMPs, pathogen-dependent enzymatic activities, or cellular stress, and a second CARD (Caspase activation and recruitment domain) or PYRIN domain that participates in Caspase-1 recruitment.

The NAIP–NLRC4 inflammasome is a well characterized inflammasome that recognizes monomeric protein subunits of the bacterial flagellar apparatus or the T3SS that are aberrantly secreted through the T3SS during infection [73]. NAIP–NLRC4 inflammasome assembly occurs when a NAIP receptor recognizes and binds to its cognate ligand [75]. Humans encode one generalist NAIP protein (hNAIP) which can bind bacteria ligands flagellin, T3SS rod, and T3SS needle [76, 77]. Mice, on the other hand, encode four specialist NAIP proteins. NAIP5 and NAIP6 recognize flagellin, NAIP1 recognizes needle, and NAIP2 binds rod [75, 78]. Binding induces a

conformation change in the NAIP protein which promotes the recruitment of NLRC4 protein sub-units to form a multi-protein, ring-like structure that can recruit Caspase-1 (CASP1) directly or through the adaptor protein ASC [73, 79]. In the absence of Caspase-1, NAIP–NLRC4 can recruit Caspase-8 via ASC [80] which drives a backup cell death pathway with delayed kinetics and apoptotic morphology.

The NAIP–NLRC4 inflammasome is expressed in mouse and human immune cells but there is a growing appreciation for the role of this inflammasome in bacterial defense in the intestine epithelium. In mouse intestinal epithelial cells, activated NAIP–NLRC4 triggers IL-18 release, GSDMD-dependent pyroptosis, and the cell-intrinsic expulsion or ejection of infected cells from the epithelium without compromising barrier integrity [1, 81]. However, it remains unclear if NAIP-NLRC4 is active and performs similar effector functions in the human intestinal epithelium [82].

NAIP–NLRC4 inflammasome deficiency in mice results in various degrees of susceptibility to bacterial pathogens. NLRC4-deficient mice infected intranasally with *Legionella pneumophila* [83] or orally with *Salmonella typhimurium* [1, 81, 84] experience modestly increased bacterial loads in infected sites, increased bacterial dissemination, and succumb somewhat more rapidly to infection. During oral *Salmonella* infection, epithelial NLRC4 seems to be particularly important in defense, as mice that lack NLRC4 and cannot undergo IEC expulsion experience increases in bacterial burden in the intestinal epithelium [1, 81]. Interestingly, bacterial pathogens *Listeria monocytogenes* and *Salmonella typhimurium* have evolved to evade NAIP–NLRC4 inflammasome detection during systemic infection by downregulating their flagellin expression [85, 86]. The forced expressed of flagellin in these pathogens during systemic infection promotes rapid bacterial clearance which appears to depend on pyroptosis of infected macrophages and subsequent killing by neutrophils [86, 87]. These experiments underscore the importance of NAIP–NLRC4 activation and subsequent pyroptosis as a defense mechanism employed by the host against intracellular pathogens.

Caspase-11 (CASP11), the mouse ortholog of human Caspases-4 and -5, is a non-canonical inflammasome because the caspase serves as both the sensor and the executor. Caspase-11 directly senses lipopolysaccharide (LPS), the major component of the outer membrane of gram-negative bacteria, when pathogens colonize the cytosol of host cells. Caspase-11 cannot cleave and activate cytokines IL-1β and IL-18 but it does activate GSDMD, and thus, its primary function is to induce pyroptosis [88]. Caspase-11 is expressed in both immune cells and intestinal epithelial cells but its expression requires priming via TLR activation or type II interferon (IFN*γ*) [88, 89].

Caspase-11 is important for defense against several pathogens *in vivo* including *Salmonella typhimurium*, *Legionella pneumophila, Burkholderia thailandensis*, and *Francisella novicida.* Many intracellular, host-evolved pathogens that have detectable LPS have evolved mechanisms to alter their LPS structure or remain vacuolar during infection to evade detection by Caspase-11, further underscoring the role of this inflammasome in host defense [72, 90].

In intestinal epithelial cells, Caspase-11 appears to drive expulsion of infected IECs, although it is not clear whether this process is immediately coupled to inflammasome activation like it is downstream of NAIP-NLRC4 [89, 91]. In mice, Caspase-11-dependent cell death and expulsion prevents colonization of the intestinal

epithelium by *Salmonella*, especially in the absence of NAIP–NLRC4 or Caspase-1, suggesting that these inflammasomes are somewhat redundant and can defend in tandem against gram negative intracellular pathogens [89, 91]. There is mounting evidence that human Caspases-4 is indeed active in primed human intestinal epithelial cell lines and intestinal epithelial enteroids derived from human patients. Challenge of these cells with *Salmonella typhimurium* leads to Caspase-4 dependent pyroptosis, expulsion, and bacterial restriction [82, 89, 92], suggesting that this inflammasome might be critical for responses to enteric intracellular bacteria during human infections.

1.4.2 Caspase-8-dependent apoptosis defends against intracellular pathogens

Apoptosis is a form of non-inflammatory programmed cell death characterized by cytoplasmic shrinkage, blebbing of the intact plasma membrane, and chromatin condensation and nuclear fragmentation. Two apoptotic pathways have been described: the extrinsic pathway, which relies on extracellular signals through cell surface death domain receptors, and the intrinsic pathway, which is stimulated by mitochondrial cytochrome *c* release. Apoptosis acts through Caspases-2, -8, and-9, which integrate initial apoptotic signals, and executioner Caspases-3, -6, and -7, which cleave several substrates culminating in a commitment to cell death. Apoptosis is frequently used to delete unwanted or harmful cells, like those undergoing transformation, and there is a growing appreciation for its role in host defense against intracellular pathogens, inferred by the discovery of apoptosis inhibitors in several viruses and intracellular bacterial pathogens [72, 93].

In the context of pathogen infection, apoptosis can be initiated by extracellular TNFα cytokine signaling. TNFα engagement of TNFR1 typically results in the activation of signaling cascades which induces NF-κB and MAPK signaling and subsequent transcriptional upregulation and expression of pro-inflammatory cytokines and pro-survival proteins [94]. The inhibition or alteration of these pro-inflammatory signaling pathways by a pathogen, however, can trigger a switch to apoptotic cell death via Caspase-8. Thus, Caspase-8 acts as a “guard” of the NF-κB and MAPK pro-inflammatory signaling pathways and can promote the apoptotic clearance of pathogens seeking to dampen the host immune response [72, 93-95].

All cells possess the machinery to execute apoptosis and can employ this cell death pathway in various contexts. Intestinal epithelial cell apoptosis, for instance, is central to maintaining homeostasis of the epithelial barrier in the gut [96]. Apoptosis occurs spontaneously in intestinal epithelial cells at the end-phase of their migration and differentiation along the crypt-villus axis [97] and is critical in maintaining healthy epithelial turnover. However, elevated TNFα in the gut can trigger aberrant apoptosis of healthy IECs, disrupting barrier integrity and driving colitis in human patients and mouse models of irritable bowel disease (IBD) [97-99]. Importantly, apoptosis in IECs results in non-lytic cell expulsion or dislodgement from the intestinal epithelium, analogous to what occurs downstream of inflammasome activation in these cells [100, 101].

The role of apoptosis in the context of *in vivo* invasive enteric pathogen infection seems largely context dependent. During oral *Salmonella* infection of NLRC4-deficient mice, TNFα drives widespread, indiscriminate cell death and dislodgement at later time points of infection [84]. Here, apoptosis appears to be largely pathological and does not contribute to bacterial clearance within the intestinal epithelium. During *Clostridium*

difficile infection, intrinsic apoptosis appears to confer protection in mice [102] despite that fact that this pathogen does not invade IECs but attaches and injects toxins into them instead. At present, there is a critical need for more *in vivo* studies of the role of TNFα and apoptosis during enteric infection, as there is little evolutionary rationale for why this cytokine might be produced in the gut.

1.4.3 Necroptosis guards against pathogenic Caspase-8 blockade

Necroptosis is a programmed lytic cell death pathway that is activated during pathogen infection. Necroptosis can be triggered by Z-DNA or Z-RNA sensing via Z-DNA binding protein 1 (ZBP1) [103], but its activation has been more extensively studied in the context of Caspase-8 inhibition [72]. If a pathogen inhibits extrinsic apoptosis via Caspase-8 antagonism, Caspase-8 can no longer inhibit the RIPK1-dependent recruitment of RIPK3 to the TNFR1 complex. Recruitment and activation of RIPK3 allows this kinase to phosphorylate and activate MLKL, a pore forming protein that oligomerizes in the plasma membrane to drive cell lysis and necroptosis [104-107]. Thus, the necroptotic pathway guards the extrinsic apoptosis pathway and can sense when this pathway is disrupted by a pathogen, triggering an alternate pro-inflammatory form of cell death [72, 106, 108]. *Ripk3*$^{-/-}$ mice are susceptible to HSV-1 and vaccinia virus infection, suggesting that necroptosis is protective during viral infection [109]. However, whether necroptosis is important for *in vivo* defense against bacterial pathogens remains unclear.

1.5 The host-pathogen conflict between *Shigella* and cell death

This network of redundant, intersected, and guarded cell death pathways provides a formidable barrier to intracellular colonization by pathogens [72]. And yet, many professional pathogens, including *Shigella* species, are still able to achieve infection by evading or inhibiting host cell death. Antagonism or evasion of cell death allows for colonization of and replication within host cells, events that lead to increases in bacterial fitness and transmission but are concomitant with a strong host immune response that drives pathogenesis. Here, I review the innate immune pathways that sense *Shigella* and lead to cell death, particularly in intestinal epithelial cells. I then highlight the ways by which *Shigella* has evolved to counteract some of these cell death pathways to establish an intracellular niche.

1.5.1 *Shigella* activates NLRC4 and both activates and inhibits Caspase-4/11

Cytosolic delivery of *Shigella* T3SS needle and rod proteins (MxiH and MxiI) can activate both mouse NAIP1 and NAIP2 and human NAIP to drive NLRC4 inflammasome assembly [76, 77, 110, 111]. Given the importance of this inflammasome in intestinal defense [1, 81, 84], there is speculation that *Shigella* might have evolved a mechanism to block its activation [112]. However, infection of mouse BMDMs with *Shigella* indicates that there is still NLRC4-dependent cell death [112], suggesting that *Shigella* does not inhibit or suppress this pathway in mice. In the U937 human monocyte cell line, there appears to be MxiH and NLRC4-dependent cell death upon *Shigella* infection, as well, indicating that *Shigella*-dependent antagonism of NLRC4 does not occur in human either [76]. In human THP-1 cells, however, cell death upon infection appears to be largely NLRC4-independent but Capsase-1-dependent [112].

Simultaneous *Shigella* infection of THP1 cells and exogenous delivery of MxiH to the cytosol, revealed an apparent suppression of MxiH-dependent cell death, suggesting that *Shigella* might indeed encode a human-specific effector that counteracts NLRC4 inflammasome activation by directly inhibiting hNAIP or NLRC4 [112]. Additional studies are required to determine if *Shigella* can definitively suppress NAIP-NLRC4 activation specifically in human cells.

It is well established that *Shigella* LPS activates mouse Caspase-11 and human Caspase-4/5 [113-116]. Non-canonical inflammasome activation in either species is partially dependent on guanylate binding proteins (GBPs), which encapsulate cytosolic bacteria by binding to LPS and have been proposed to both liberate LPS from the bacterial outer membrane and serve as a recruitment platform for Caspase-4/11 [117, 118]. Indeed, *Shigella* encodes two effectors which can suppress the Caspase-4/11 pathway. IpaH9.8 is a *Shigella* ubiquitin ligase which targets GBPs for proteasomal degradation [119] and OspC3 is a *Shigella* effector with a novel enzymatic activity that modifies Caspase-4/11 via ADP-riboxanation [120], blocking auto-processing and initiation of pyroptosis [115, 120, 121]. Recent data suggest that OspC3 is important for virulence in the I.P. mouse model of *Shigella* infection [120, 121], but the roles of both OspC3 and IpaH9.8 would be clarified in a physiological oral-infection mouse model.

1.5.2 *Shigella* effector IpaH7.8 activates the mouse NLRP1B inflammasome but may antagonize human Gasdermins-D and E

Another *Shigella* ubiquitin ligase, IpaH7.8, appears to both activate and inhibit inflammasome-dependent cell death in the context of *Shigella* infection. IpaH7.8 targets the 129S1 mouse strain variant of the NLRP1B inflammasome but not the human NLRP1 inflammasome for degradation. Ubiquitylation of 129S1 NLRP1B by IpaH7.8 in mouse macrophages targets the N-terminus of this host protein for “functional degradation” via the proteasome, liberating the FIIND-CARD domains of the C-terminus to oligomerize and form an inflammasome that recruits Caspase-1 and leads to pyroptosis. NLRP1B, thus, has been proposed to serve as a decoy – a cell death initiator that mimics the intended targets of effector IpaH7.8 [122]. *Nlrp1* genes are rapidly evolving in humans and mice, suggesting that this inflammasome is in broad evolutionary conflict with bacterial ubiquitin ligases and viral proteases, which have also been shown to activate it [123, 124].

Two recent studies suggest that the ‘intended targets’ of IpaH7.8 are human Gasdermin proteins. Using an effector screen for inhibitors of LPS-dependent cell death in a human endothelial cell line, Luchetti et al. [56] reported that IpaH7.8 could ablate Caspase-11-dependent pyroptosis by targeting GSDMD for proteasomal degradation. This antagonism appears to be human specific, allowing the authors to speculate that the species-specific antagonism of this cell death executor explains the susceptibility of humans, but not mice, to *Shigella* infection. A parallel study by Hansen et al. [125] used a ubiquitin-activated interaction trap technique in human cells to identify GSDMB and not GSDMD as the intended substrate of IpaH7.8. The authors reported that GSDMB, when activated by granzyme release from natural killer cells (NK cells), did not localize to the host cell membrane but instead to cytosolic bacteria, where its pore-forming activity was shown to be directly bactericidal. Thus, the proposed function of IpaH7.8 in this context is to directly inhibit the bactericidal activity of human GSDMB. Regardless of the specific intended host target of IpaH7.8, it appears that its activity would increase

Shigella virulence during human infection by allowing for increased bacterial survival and replication in the host cell cytosol.

1.5.3 *Shigella* appears to inhibit apoptosis and necroptosis

Faherty et al., were the first to show that *Shigella* could inhibit intrinsic staurosporine-induced apoptosis in epithelial cells by the T3SS-dependent prevention of caspase-3 activation [126-128]. These studies, however, did not identify a specific *Shigella* effector or host target important for this inhibition. *Shigella* infection of epithelial cells leads to host cell DNA damage, triggering the intrinsic p53-dependent pro-apoptotic pathway [129]. This pathway, however, is antagonized by delivery of *Shigella* effector VirA, which targets calpastatin for degradation, ultimately resulting in the degradation of p53 and prevention of apoptosis [129]. A recent study suggests that *Shigella* LPS O-antigen can directly bind to and inhibit Caspases-3 and -7, blocking mitochondrial-dependent intrinsic apoptosis during *Shigella* infection [130]. These studies, taken together, indicate that *Shigella* infection can lead to the initiation of apoptosis in host cells but this cell death is delayed or incomplete because of the inhibition of downstream mediators of this pathway by *Shigella* effectors.

There currently exists little evidence for the activation of extrinsic apoptosis in the context of *Shigella* epithelial cell invasion. Importantly, however, *Shigella* encodes several effectors that dampen the NF-κB signaling cascade [131-137], an event known to sensitize cells toward Caspase-8-dependent extrinsic apoptosis [72, 98, 99]. A compelling study from Ashida et al. [138] recently revealed that *Shigella* effector OspD3 could suppress necroptotic cell death in HT29 human colon epithelial cells by degrading RIPK1 and RIPK3. Since necroptosis is triggered when Caspase-8-dependent extrinsic apoptosis is blocked, these findings suggested the existence of *Shigella*-dependent Caspase-8 inhibition that prevents apoptosis in infected human cells. Indeed, the authors identified OspC1 as an inhibitor of Caspase-8 and found that cells infected with an *ospC1*/*ospD3* double mutant *Shigella* strain did not undergo necroptosis and showed elevated Caspase-8 activity indicative of extrinsic apoptosis. This study is the first to report the existence of a bacterial strategy to inhibit both extrinsic apoptosis and necroptosis and subvert the built in cross-talk and redundancy between these two pathways. Furthermore, these findings reinforce the importance of extrinsic apoptosis and necroptosis as host defense mechanisms against *Shigella* intracellular colonization.

1.6 Concluding remarks

An important theme surfaces when considering these results in the context of host-pathogen evolution: there may exist many important innate immune pathways in nature but they may be difficult to uncover because they are blocked by professional pathogens or because they are redundant with other critical pathways. In the following two chapters, I will provide data to support the hypothesis that multiple, layered, and redundant cell death pathways define mouse resistance to *Shigella* infection. While these pathways may be antagonized in human cells, many appear to be active, uninhibited, and important in defense in mice, a finding that reflects the human specificity of *Shigella* and the evolutionary distance between these two mammalian species. Genetic removal of key cell death pathways renders mice susceptible to oral *Shigella* challenge, providing the first physiologically relevant mouse of shigellosis.

Ultimately, my thesis work illustrates the importance of cell death as an innate defense mechanism against intracellular bacteria and provides a window into the host-pathogen evolutionary arms race that occurs between a host-adapted intracellular pathogen and innate immune mechanisms it must subvert to establish an infection *in vivo*.

Chapter Two. NAIP–NLRC4-deficient mice are susceptible to shigellosis

2.1 Summary

Bacteria of the genus *Shigella* cause shigellosis, a severe gastrointestinal disease that is a major cause of diarrhea-associated mortality in humans. Mice are highly resistant to *Shigella* and the lack of a tractable physiological model of shigellosis has impeded our understanding of this important human disease. Here we propose that the differential susceptibility of mice and humans is due to mouse-specific detection of *Shigella* by the NAIP–NLRC4 inflammasome. We find that NAIP–NLRC4-deficient mice are highly susceptible to oral *Shigella* infection and recapitulate the clinical features of human shigellosis. Although inflammasomes are generally thought to promote *Shigella* pathogenesis, we instead demonstrate that intestinal epithelial cell (IEC)-specific NAIP–NLRC4 activity is sufficient to protect mice from shigellosis. In addition to describing a new mouse model of shigellosis, our results suggest that the lack of an inflammasome response in IECs may help explain the susceptibility of humans to shigellosis.

2.2 Introduction

Shigella is a genus of Gram-negative enterobacteriaceae that causes ~269 million infections and ~200,000 deaths annually, a quarter of which are of children under the age of five [4]. Disease symptoms include fever, abdominal cramping, and inflammatory diarrhea characterized by the presence of neutrophils and, in severe cases, blood [5]. There is no approved vaccine for *Shigella* and antibiotic resistance continues to rise [6]. *Shigella* pathogenesis is believed to be driven by bacterial invasion, replication, and spread within colonic intestinal epithelial cells (IECs). *Shigella* virulence requires a plasmid-encoded type III secretion system (T3SS) that injects ~30 effectors into host cells [3, 8]. The virulence plasmid also encodes IcsA, a bacterial surface protein that nucleates host actin at the bacterial pole to propel the pathogen through the host cell cytosol and into adjacent epithelial cells [139, 140].

A major impediment to studying *Shigella* is the lack of experimentally tractable *in vivo* models that accurately recapitulate human disease after oral inoculation. Although the infectious dose for *Shigella* in humans can be as low as 10-100 bacteria [141, 142], mice are resistant to high doses of oral *Shigella* challenge [9, 11]. Rabbits, guinea pigs, zebrafish, piglets, and macaques have been used to model human infection [38, 43, 52, 143-147] but the cost and/or limited tools in these systems impair detailed studies of pathogenesis. Oral streptomycin administration and other treatments facilitate *Shigella* colonization of the mouse intestinal lumen by ablating the natural colonization resistance provided by the microbiome [9, 61, 148]. However, antibiotic-treated mice do not present with key hallmarks of human disease, likely due to the failure of *Shigella* to invade and/or establish a replicative niche within the mouse intestinal epithelium.

Inflammasomes are cytosolic multi-protein complexes that initiate innate immune responses upon pathogen detection or cellular stress [79, 149]. The NAIP–NLRC4 inflammasome is activated when bacterial proteins, such as flagellin or the rod and needle proteins of the T3SS apparatus, are bound by NAIP family members. Importantly, the *Shigella* T3SS inner rod (MxiI) and needle (MxiH) proteins are both potent agonists of human and mouse NAIPs [76, 77]. Activated NAIPs then co-assemble with NLRC4 to recruit and activate the Caspase-1 (CASP1) protease [150,

151]. CASP1 then cleaves and activates the pro-inflammatory cytokines IL-1β and IL-18 and the pore-forming protein Gasdermin-D [152, 153], initiating a lytic form of cell death called pyroptosis. We and others recently demonstrated that activation of NAIP–NLRC4 in IECs further mediates the cell-intrinsic expulsion of infected epithelial cells from the intestinal monolayer [1, 81]. In the context of *Shigella* infection, it is generally accepted that inflammasome-mediated pyroptosis of infected macrophages promotes pathogenesis by initiating inflammation, and by releasing bacteria from macrophages, allowing the bacteria to invade the basolateral side of intestinal epithelial cells [8, 154, 155]. However, it has not been possible to test the role of inflammasomes in the intestine after oral *Shigella* infection due to the lack of a genetically tractable model. Here we develop the first oral infection mouse model for *Shigella* infection that recapitulates human disease, and demonstrate a specific host-protective function for inflammasomes in intestinal epithelial cells.

2.3 Results

2.3.1 B6.Naip-deficient mice are susceptible to shigellosis

The mouse NAIP–NLRC4 and CASP11 inflammasomes protect the intestinal epithelium from *Salmonella* [1, 81, 156]. Since *Shigella* invades the intestinal epithelium and also activates the mouse NAIP–NLRC4 inflammasome[76, 77], we hypothesized that NAIP–NLRC4 activation in IECs and subsequent cell death and expulsion might protect mice from shigellosis. A prediction from this hypothesis is that genetic removal

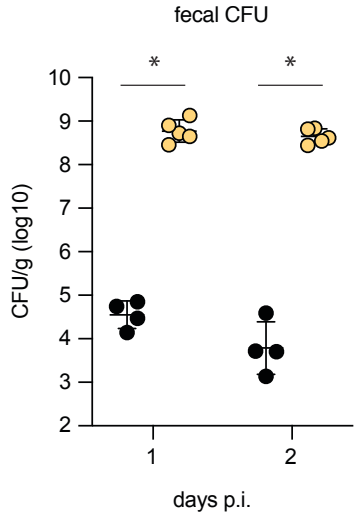

Figure 2.1. Antibiotic pre-treatment followed by oral route *Shigella* infection permits substantial lumenal colonization.
CFU determination per gram (g) feces of B6 WT mice that were treated orally with 25mg streptomycin sulfate (yellow) or water (black) and orally challenged the next day with $5x10^7$ CFU of WT *Shigella*. Feces were collected 1 and 2 days post-infection (p.i.). Data are representative of three experiments. Each symbol represents one mouse. Mann-Whitney test, $*P < 0.05$.

● H_2O + $5x10^7$ CFU

○ Streptomycin sulfate + $5x10^7$ CFU

of NAIP–NLRC4 pathway should render mice susceptible to *Shigella* infection. However, previous studies have demonstrated that the intestinal microbiota of mice provides an initial intrinsic barrier to mouse *Shigella* infection in the form of colonization resistance [9, 61, 148, 157]. To overcome this barrier we pretreated wild-type C57BL/6J mice orally with streptomycin antibiotic. Consistent with the studies cited above, we found that antibiotic pre-treatment followed by oral infection with $5x10^7$ CFU allows for robust *Shigella* colonization of the intestinal lumen and feces compared to vehicle-treated controls (Figure 2.1) and that high lumenal/fecal bacterial loads (>10^8 CFU/g feces) did not cause overt disease (Figure 2.2, 2.3).

To determine if inflammasomes contribute to the resistance of mice that are colonized with *Shigella*, we treated WT and *Casp1/11*$^{-/-}$ mice with streptomycin sulfate and challenge them with 5x10^7 CFU of *Shigella*. Mice that lack CASP1 and/or CASP11 are also more susceptible to oral infection with *Salmonella* Typhimurium [156]. In contrast, B6 WT and *Casp1/11*$^{-/-}$ mice that were treated with antibiotic and infected with *Shigella* were similarly resistant to *Shigella* infection, showing no signs of intestinal inflammation or disease (Figure 2.2). Thus, neither of the primary caspases associated with the canonical or non-canonical inflammasome are essential for resistance to *Shigella* in the mouse intestine.

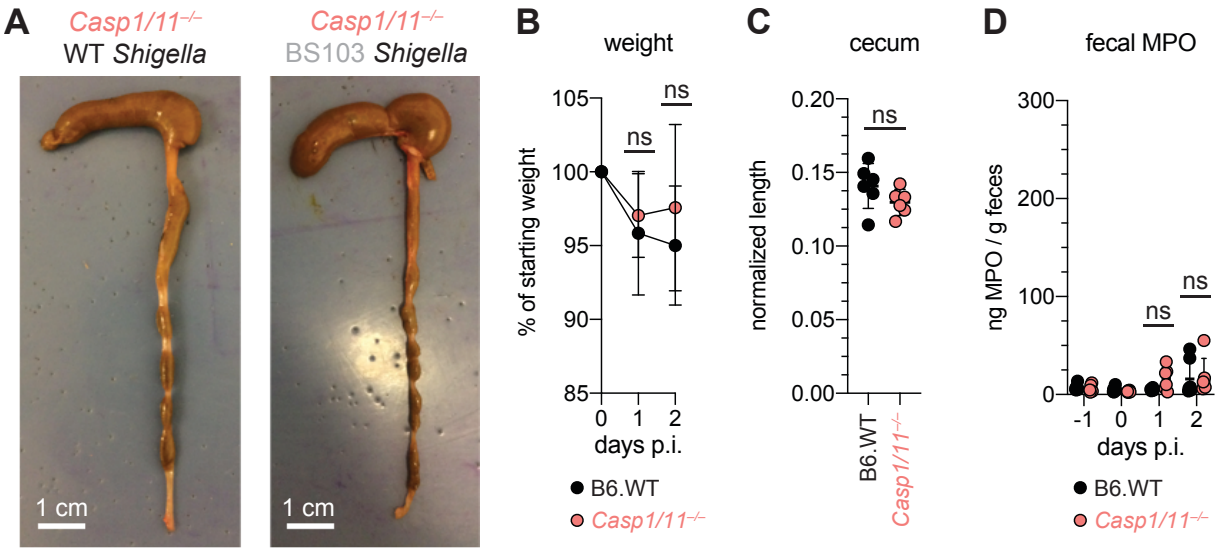

Figure 2.2. B6.*Casp1/11*$^{-/-}$ mice are resistant to oral *Shigella* challenge.
(**A–D**) B6.WT (black) and B6.*Casp1/11*$^{-/-}$ (peach) mice were treated orally with 25mg streptomycin sulfate and were orally challenged the next day with 5x10^7 CFU of either WT or BS103 (avirulent) *Shigella*. (**A**) Representative images of the cecum and colon dissected at 2 days post-infection (p.i.). (**B**) Mouse weights. (**C**) Quantification of cecum and colon lengths. Values were normalized to mouse weight prior to infection; cecum length (cm) / mouse weight. (**D**) MPO levels measured by ELISA from feces of B6.WT and B6.*Casp1/11*$^{-/-}$ mice collected -1 through 2 days p.i. Each symbol represents one mouse. Data are representative of three independent experiments. Mean ± SD is shown in (**B,C,D**), Mann-Whitney test, $^*P < 0.05$.

The NAIP–NLRC4 inflammasome can recruit Caspase-8 (CASP8) in the absence of CASP1, an event which leads to non-lytic cell death and delayed IEC expulsion [1]. We reasoned that this compensatory capacity of CASP8 may account for the resistance of *Casp1/11*$^{-/-}$ mice to *Shigella* infection. Thus, to test directly if the mouse NAIP–NLRC4 inflammasome mediates resistance to shigellosis, we orally infected streptomycin-pretreated B6 WT and Δ*Naip* mice with 5x10^7 CFU of *Shigella*. Δ*Naip* mice (also called *Naip1-6*$^{\Delta/\Delta}$ mice [158]) harbor a large chromosomal deletion that eliminates expression of all mouse *Naip* genes. Remarkably, *Shigella*-infected Δ*Naip* but not WT mice exhibited clear signs of disease (Figure 2.3). At two days post-challenge, Δ*Naip* mice had altered stool consistency (Figure 2.3A), cecum shrinkage, and thickening of the cecum and colon tissue (Figure 2.3A, B). Histological analysis of primary sites of infection (cecum, colon) revealed edema, epithelial hyperplasia, epithelial sloughing, and inflammatory infiltrate (predominantly neutrophils and mononuclear cells in the submucosa and mucosa) exclusively in Δ*Naip* mice (Figure

2.3C, D). In contrast, we did not observe any indicators of inflammation in Δ*Naip* mice infected with the avirulent BS103 strain (Figure 2.3C, D).

A defining feature of human shigellosis is the presence of neutrophils in patient stools [159]. The levels of myeloperoxidase (MPO, a neutrophil marker) were low or undetectable in the feces of mice following antibiotic treatment (Figure 2.3E), indicating that microbiota disruption did not itself promote neutrophilic inflammation. Following *Shigella* infection, however, fecal MPO from Δ*Naip* mice dramatically increased (Figure 2.3E). In contrast, MPO levels remained low in both B6 WT and *Casp1/11*$^{-/-}$ mice (Figure 2.2) or Δ*Naip* mice infected with the avirulent BS103 strain (Figure 2.3E). These results indicate that NAIP–NLRC4-deficient mice experience robust neutrophilic infiltrate consistent with human shigellosis.

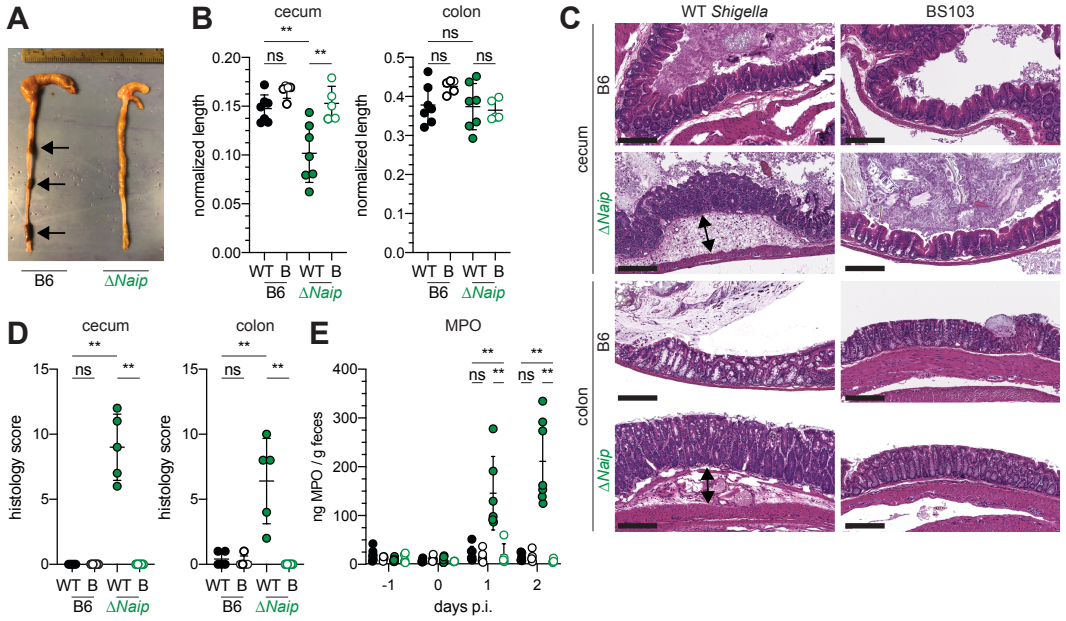

Figure 2.3. *Shigella*-infected B6.Δ*Naip* mice exhibit intestinal inflammation.
(**A–E**) B6.WT and B6.Δ*Naip* (green) mice (lacking expression of all *Naip* genes) treated orally with 25mg streptomycin sulfate were orally challenged the next day with 5x10^7 CFU of WT or BS103 ("B",non-invasive) *Shigella*. Endpoint harvests were performed at 48 hours post-infection (p.i.). (**A**) Representative images of the cecum and colon dissected from B6.WT and B6.Δ*Naip* mice. Note cecum tissue thickening (size reduction), macroscopic edema, and loose stool (absence of arrows). (**B**) Quantification of cecum and colon lengths. Values were normalized to mouse weight prior to infection; cecum length (cm) / mouse weight (g). WT, wild-type *Shigella* (filled symbols); B, BS103 (open symbols).(**C**) Representative images of H&E stained cecum and colon tissue from infected mice. Scale bar, 200 μm. (**D**) Blinded quantification of histology score (cumulative) for tissues in (**C**). Edema, hyperplasia, inflammatory infiltrate, and epithelial cell death were scored from 0-4. The final score is the sum of individual scores from each category. (**E**) MPO levels measured by ELISA from feces of B6.WT and B6.Δ*Naip* mice collected -1 through 2 days p.i. (**B**, **D, E**) Each symbol represents one mouse. Filled symbols, WT *Shigella*; open symbols, BS103. Data are representative of two independent experiments. Mean ± SD is shown in (**B**,**D**,**E**), Mann-Whitney test, **P* < 0.05, ***P* < 0.01, ****P* < 0.001.

2.3.2 B6.*Nlrc4*$^{-/-}$ mice are susceptible to shigellosis

To confirm that the NAIP–NLRC4 inflammasome confers resistance to *Shigella*, and to control for potential microbiota-associated phenotypes, we next infected streptomycin-pretreated B6.*Nlrc4*$^{+/-}$ and B6.*Nlrc4*$^{-/-}$ littermates, as well as B6 WT mice that had been co-housed with B6.*Nlrc4*$^{-/-}$ mice for three weeks prior to inoculation (*Nlrc4*$^{+/-}$ and B6 WT mice are hereby referred to collectively as *Nlrc4*$^{+}$). Consistent with

our prior results in Δ*Naip* mice, we observed thickening of the intestinal mucosa (Figure 2.4A), cecum shrinkage (Figure 2.4A, B), increased fecal MPO levels (Figure 2.4C), and acute weight loss (Figure 2.4D) in *Shigella*-infected B6.*Nlrc4*$^{-/-}$ mice but not B6.*Nlrc4*$^{+}$ littermates or co-housed mice. B6.*Nlrc4*$^{-/-}$ mice also had diarrhea, which was apparent by visual inspection of lumenal contents and quantified by the wet-to-dry ratio of fecal pellets (Figure 2.4E). Thus, B6.*Nlrc4*$^{-/-}$ mice phenocopy the disease susceptibility of B6.Δ*Naip* mice, and strongly suggest that the NAIP–NLRC4 inflammasome mediates the resistance of mice to *Shigella* infection.

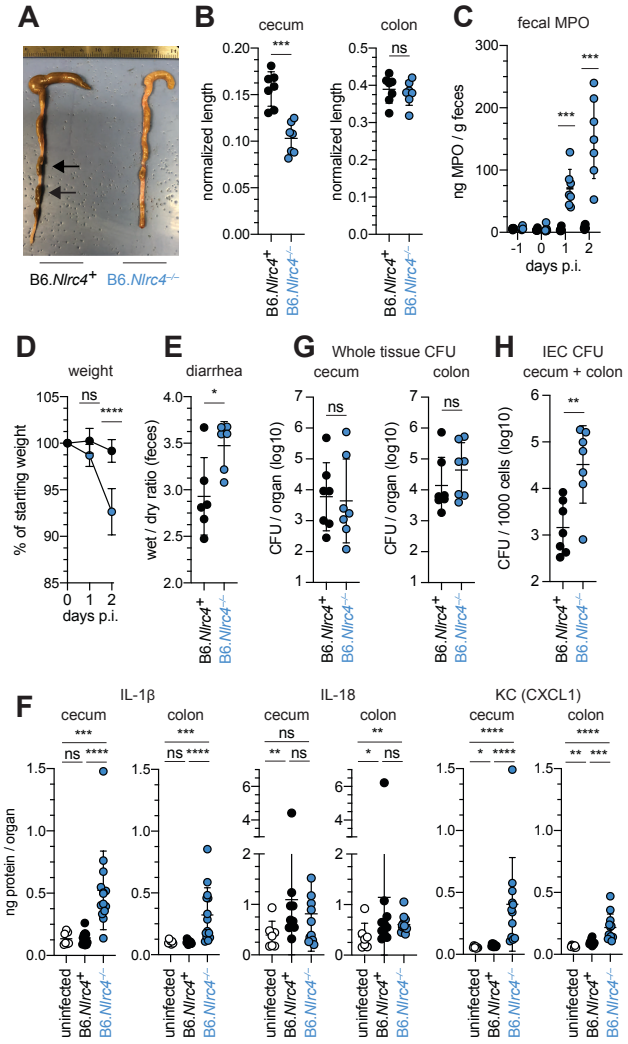

Figure 2.4. *Shigella*-infected B6.*Nlrc4*$^{-/-}$ mice exhibit intestinal inflammation and bacterial colonization of IECs. (**A–E**) B6.*Nlrc4*$^{+/-}$ and B6.*Nlrc4*$^{-/-}$ littermates were cohoused with B6.WT mice for a minimum of three weeks. Mice were infected with only WT *Shigella* as described for Figure 2. Endpoint harvests were performed 48 hours post-infection (p.i.). B6.*Nlrc4*$^{+/-}$ and B6.WT mice are collectively referred to as B6.*Nlrc4*$^{+}$. (**A**) Representative images of the cecum and colon dissected from B6.*Nlrc4*$^{+}$ and B6.*Nlrc4*$^{-/-}$ mice. Note the cecum tissue thickening (size reduction), macroscopic edema, and loose stool (absence of arrows). (**B**) Quantification of cecum and colon lengths. Values were normalized to mouse weight prior to infection; cecum length (cm) / mouse weight (g). (**C**) MPO levels measured by ELISA from feces of B6.*Nlrc4*$^{+}$ and B6.*Nlrc4*$^{-/-}$ mice collected -1 through 2 days p.i. (**D**) Mouse weights from 0 through 2 days p.i. Each symbol represents the mean for all mice of the indicated condition. (**E**) Quantification of feces weights before and after dehydration at 2 days p.i. A larger ratio indicates diarrhea. (**F**) IL-1β, IL-18, and KC levels measured by ELISA from tissue of B6.*Nlrc4*$^{+}$ and B6.*Nlrc4*$^{-/-}$ mice collected 2 days p.i. (**G**) CFU determination from gentamicin-treated whole tissue homogenates from the cecum or colon of infected mice. (**H**) CFU determination from the IEC enriched fraction of gentamicin-treated cecum and colon tissue (combined). (**B,C,E–H**) Each symbol represents one mouse. Data are representative of three independent experiments. Mean ± SD is shown in (**B-F**). Geometric mean ± SD is shown in (**F**, **G**). Mann-Whitney test, **P* < 0.05, ***P* < 0.01, ****P* < 0.001.

To compare the cytokine profiles of B6.*Nlrc4*$^{+}$ and B6.*Nlrc4*$^{-/-}$ mice, we performed ELISAs for pro-inflammatory cytokines IL-1β, IL-18, and the mouse chemokine and neutrophil attractant KC (CXCL1). IL-18 levels were similarly elevated in B6.*Nlrc4*$^{+}$ and B6.*Nlrc4*$^{-/-}$ mice relative to uninfected mice (Figure 2.4F). By contrast, IL-1β and KC levels were significantly elevated in B6.*Nlrc4*$^{-/-}$ relative to B6.*Nlrc4*$^{+}$ and uninfected mice (Figure 2.4F), consistent with the neutrophilic inflammation observed by histology and fecal MPO ELISAs. Since IL-1β is a pro-inflammatory cytokine released primarily from pyroptotic macrophages, we hypothesize that additional inflammasomes are likely active in this cell-type in the absence of NAIP–NLRC4 and may play a role in driving pathogenesis.

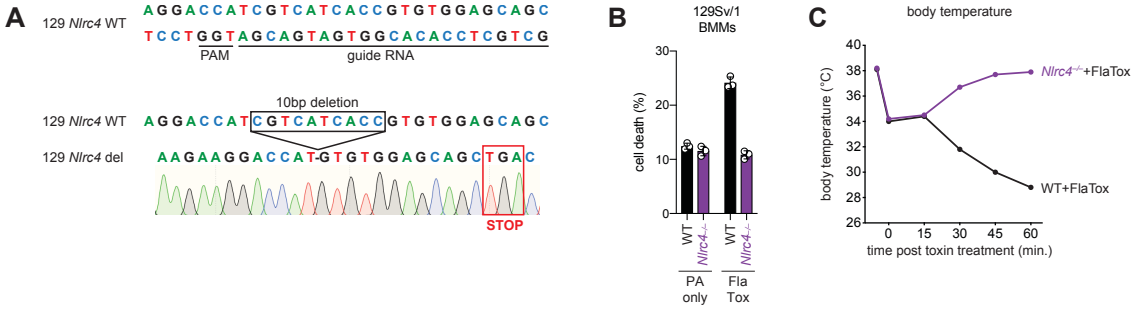

Figure 2.5. Construction and functional characterization of *Nlrc4* knockout mice on the 129S1/SvImJ genetic background.
(**A**) The targeted wildtype *Nlrc4* sequence (chromosome 17, NC_000083.6, exon 5) aligned to the *Nlrc4* guide RNA. The protospacer adjacent motif (PAM) is indicated. Below is a schematic of the Sanger sequencing verified product of CRISPR/Cas9-editing (129 *Nlrc4* del), which results in a 10 base pair deletion and an in-frame early TGA stop codon in exon 5 of *Nlrc4*. (**B**) Quantification of cell death in 129 WT or *Nlrc4*$^{-/-}$ bone marrow derived macrophages (BMMs) treated with 10μg/mL PA alone or PA + 10μg/mL LFn-FlaA (LFn fused to *Legionella pneumophila* flagellin, "FlaTox"). Cell death was measured 30 minutes post-infection by propidium iodide uptake and reported as percent death relative to 100% killing by treatment with Triton X-100. (**C**) WT or 129.*Nlrc4*$^{-/-}$ mice were injected intravenously with 0.2μg/g body weight PA + 0.1μg/g body weight LFn-FlaA and body temperature was monitored for the indicated times (minutes) post-treatment. The initial temperature decrease in all mice is due to isoflurane treatment.

Surprisingly, despite the clear differences in disease between *Shigella* infected B6.*Nlrc4*$^{+}$ and B6.*Nlrc4*$^{-/-}$ mice, we found no significant difference in the bacterial burdens of whole cecum or colon tissue (Figure 2.4G). To more e directly measure the intracellular colonization of IECs, the primary replicative niche for *Shigella*, we enriched IECs from the ceca and colons of infected B6.*Nlrc4*$^{+}$ and B6.*Nlrc4*$^{-/-}$ mice (see Methods). We found an ~20-fold difference in colonization in enriched IECs between B6.*Nlrc4*$^{+}$ and B6.*Nlrc4*$^{-/-}$ mice (Figure 2.4H), indicating that disease in our model correlates with invasion of and replication in IECs. Importantly, we observed no CFU differences in feces at the time of harvest, excluding the possibility that differences in IEC CFU were merely the result of differences in lumenal *Shigella* density. These data suggest that *Shigella* colonizes the intestinal tissue regardless of inflammasome activity, but can only specifically invade the epithelium and provoke disease in NAIP–NLRC4-deficient mice.

2.3.3 *Shigella* causes bloody diarrheal disease in 129.*Nlrc4*$^{-/-}$ mice

To determine whether the role of NAIP–NLRC4 in mediating protection against *Shigella* is robust across diverse mouse strains, we generated *Nlrc4*$^{-/-}$ mice on the 129S1 genetic background. 129.*Nlrc4*$^{-/-}$ mice have a 10bp deletion in exon 5 of the

Nlrc4 coding sequence, resulting in loss of NLRC4 function (Figure 2.5). Importantly, 129S1 mice are naturally deficient in CASP11, which responds to cytosolic LPS, and thus 129.*Nlrc4*$^{-/-}$ mice lack functional NAIP–NLRC4 and CASP11 signaling.

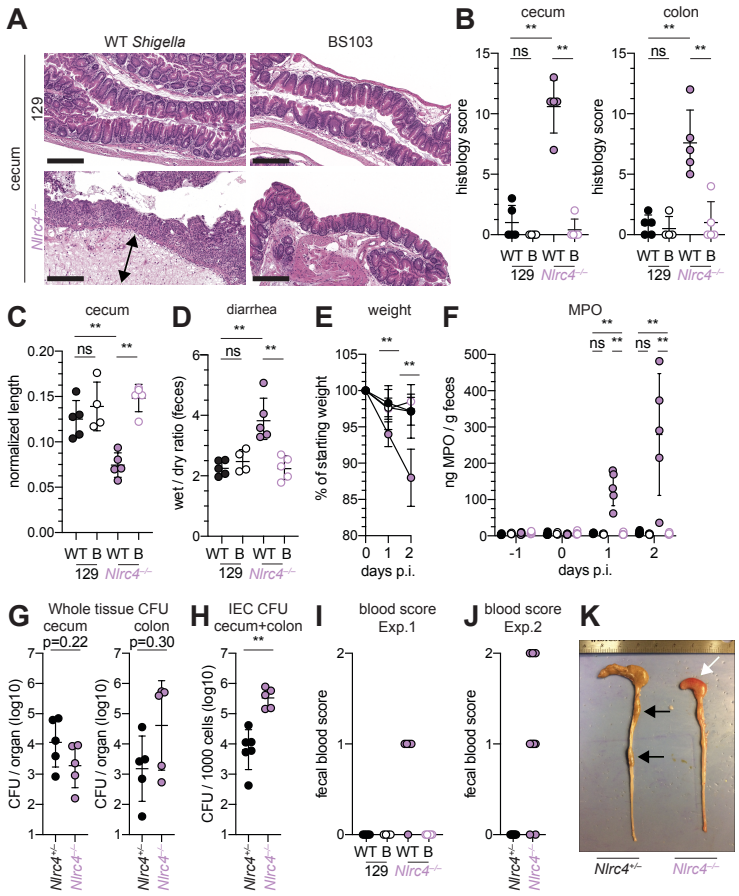

Figure 2.6. *Shigella*-infected 129.*Nlrc4*$^{-/-}$ mice exhibit hallmarks of severe human shigellosis.
(**A–H**) 129.*Nlrc4*$^{+/-}$ and 129.*Nlrc4*$^{-/-}$ littermates were infected as described for **Figure 2**. Endpoint harvests were performed at 48 hours post-infection (p.i.). (**A**) Representative images of H&E stained cecum and colon tissue from infected mice. Scale bar, 200μm. (**B**) Blinded quantification of histology score (cumulative) for tissues in (**A**). Edema, hyperplasia, inflammatory infiltrate, and epithelial cell death were scored from 0-4. The final score is the sum of individual scores from each category. (**C**) Quantification of cecum and colon lengths. Values were normalized to mouse weight prior to infection; cecum length (cm) / mouse weight (g). (**D**) Quantification of feces weights before and after dehydration at two days p.i. A larger ratio indicates diarrhea. (**E**) Mouse weights at 0 through 2 days p.i. Each symbol represents the mean for all mice of the indicated condition. Statistics refer to both WT *Shigella*-infected 129.*Nlrc4*$^{+/-}$ and 129.*Nlrc4*$^{-/-}$ mice and WT versus BS103 *Shigella*-infected 129.*Nlrc4*$^{-/-}$ mice at both 1 and 2 days p.i. All other comparisons were non-significant. (**F**) MPO levels measured by ELISA from feces of 129.*Nlrc4*$^{+/-}$ and 129.*Nlrc4*$^{-/-}$ mice collected -1 through 2 days p.i. (**G**) CFU determination from gentamicin-treated whole tissue homogenates from the cecum or colon. (**H**) CFU determination from the IEC enriched fraction of gentamicin-treated cecum and colon tissue (combined). (**I,J**) Fecal blood scores from feces at two days p.i. 1 = occult blood, 2 = macroscopic blood. (**I**) and (**J**) show scores from two representative experiments. (**K**) Representative images of the cecum and colon dissected from 129.*Nlrc4*$^{+/-}$ and 129.*Nlrc4*$^{-/-}$ mice. Note the cecum tissue thickening (size reduction), macroscopic edema, and loose stool (absence of arrows), and vascular lesions and bleeding. (**B–D,F–J)** Each symbol represents one mouse. Filled symbols, WT *Shigella*; open symbols, BS103. Data are representative of three independent experiments. Mean ± SD is shown in (**B**, **C**, **D, E**, **F**). Geometric mean ± SD is shown in (**G** and **H)**. Mann-Whitney test, **P* < 0.05, ***P* < 0.01, ****P* < 0.001.

Similar to the B6 genetic background, antibiotic-pretreated 129.*Nlrc4*$^{-/-}$ but not 129.*Nlrc4*$^{+/-}$ littermates challenged with WT (or BS103) *Shigella* exhibited severe signs of shigellosis, including pronounced edema, epithelial cell hyperplasia, and disruption of the columnar epithelium of infected tissues (Figure 2.6A, B). 129.*Nlrc4*$^{-/-}$ mice also exhibited dramatic cecum shrinkage and diarrhea (Figure 2.6C, D, K), lost between eight and 18 percent of their starting weight within two days of infection (Figure 2.6E),

and exhibited a massive increase in fecal MPO following infection (Figure 2.6F). We found no significant difference in the bacterial colonization of the whole cecum and colon tissue between 129.*Nlrc4*$^{+/-}$ and 129.*Nlrc4*$^{-/-}$ mice (Figure 2.6G). However, IECs enriched from infected 129.*Nlrc4*$^{-/-}$ mice again exhibited ~20-fold higher bacterial burdens than IECs enriched from 129.*Nlrc4*$^{+/-}$ mice (Figure 2.6H), despite similar levels of lumenal colonization. A hallmark of severe human shigellosis (dysentery) is the presence of blood in patient stools. Using an assay to detect occult blood (see Methods), we were unable to detect blood in the feces of NAIP–NLRC4-deficient mice on the B6 background (data not shown). However, when we tested 129.*Nlrc4*$^{-/-}$ mouse stools, we found that 4/5 mice infected with WT *Shigella* had occult blood in their feces (Figure 2.6I). In a subsequent infection, 80% (8/10) of 129.*Nlrc4*$^{-/-}$ mice had bloody stool (occult blood only, n=5; macroscopically visible blood, n=3) (Figure 2.6J). In mice with visible blood, we often observed ruptured blood vessels in the cecum or colon (Figure 2.6K). Thus, 129.*Nlrc4*$^{-/-}$ mice recapitulate the bloody stool (dysentery) that is a hallmark of severe human shigellosis.

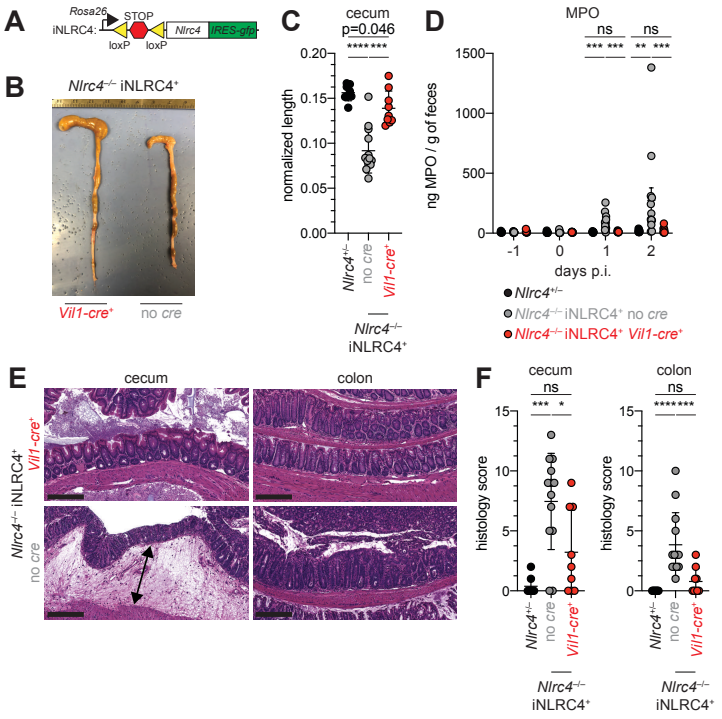

Figure 2.7. *Nlrc4* expression in IECs is sufficient to prevent shigellosis.
(**A**) Schematic of the B6 *Rosa26* locus containing the iNLRC4 cassette, as described previously [1]. (**B–F**) Vil1-cre positive (+) or negative *Nlrc4*$^{-/-}$ iNlrc4 littermates, or *Nlrc4*$^{+/-}$ mice were orally infected with 5x10^7 CFU of WT *Shigella* 24 hours after oral streptomycin treatment. Endpoint harvests were done 48 hours post-infection (p.i.). (**B**) Representative images of the cecum and colon dissected from iNLRC4 *Nlrc4*$^{-/-}$ Vil1-cre positive or negative mice. (**C**) Quantification of cecum length reduction normalized to the weight of the animal prior to infection; cecum length (cm) / mouse weight (g). (**D**) MPO levels measured by ELISA of feces collected -1 through 2 days p.i. (**E**) Representative images of H&E stained cecum and colon tissue from infected mice. Scale bar, 200μm. (**F**) Blinded quantification of histology score (cumulative) for cecum and colon tissue. Data are representative of two independent experiments. Mean ± SD is shown in (**C**,**D**,**F**), Mann-Whitney test, **P* < 0.05, ***P* < 0.01, ****P* < 0.001. (**C**,**D**,**F**) Each symbol represents one mouse.

2.3.4 Epithelial NLRC4 is sufficient to protect mice from shigellosis

Given the difference in *Shigella* colonization of IECs between WT and NAIP–NLRC4-deficient mice, we next sought to determine if IEC-specific expression of the NAIP–NLRC4 inflammasome is sufficient to protect mice from *Shigella* infection. We thus infected B6 mice that selectively express NLRC4 in IECs. These mice encode a Cre-inducible *Nlrc4* gene on an otherwise *Nlrc4*$^{-/-}$ background and are referred to as iNLRC4 mice (Figure 2.7A) [1]. Crosses of iNLRC4 and *Vil1-Cre* mice generated animals with selective expression of NLRC4 in Villin^{+} IECs. *Shigella* infected *Vil1-Cre*$^{+}$ iNLRC4 mice, but not *Cre*$^{-}$ littermate controls, were protected from intestinal inflammation to a similar extent as co-housed *Nlrc4*$^{+/-}$ mice (Figure 2.7B–F). Thus, NLRC4 expression in IECs is sufficient to prevent shigellosis.

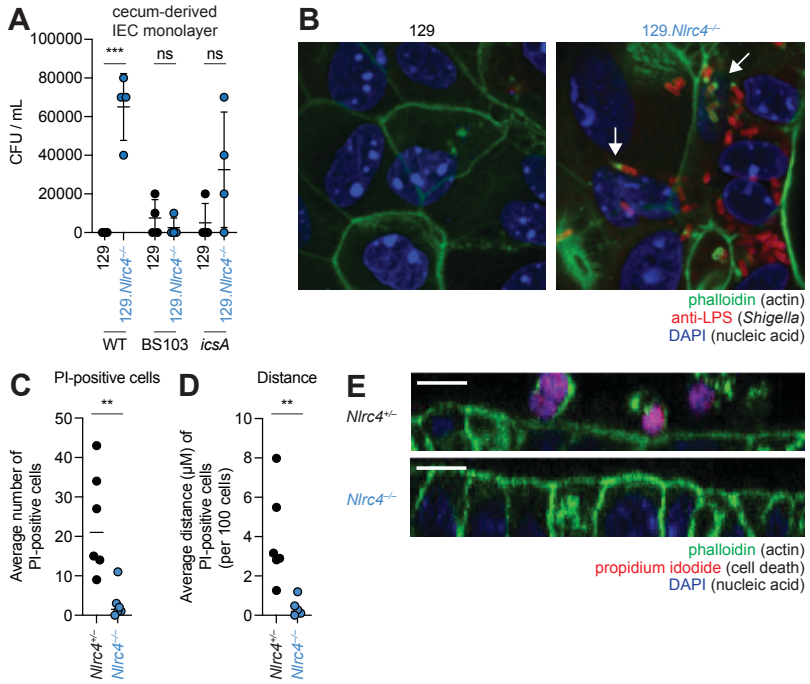

Figure 2.8. NLRC4 prevents *Shigella* colonization via cell expulsion in IEC monolayer cultures.
(**A**) *Shigella* (WT, BS103, or *icsA*) CFU from transwell culture of WT or 129.*Nlrc4*$^{-/-}$ cecum-derived IEC monolayers. CFU was determined 8 hours p.i. Each symbol represents one infected monolayer. (**B**) Immunofluorescent staining of WT *Shigella*-infected transwell cultures of WT or 129.*Nlrc4*$^{-/-}$ cecum-derived IEC monolayers: green, fluorescent phalloidin (actin); red, anti-*Shigella* LPS, blue, DAPI (nucleic acid). (**C**,**D**) Quantification of the number and position of PI-positive cells in *Shigella*-infected 129.*Nlrc4*$^{+/-}$ or 129.*Nlrc4*$^{-/-}$ cecum-derived IEC monolayers. In (**C**) each symbol represents the average number of PI-positive cells within an imaged field. In (**D**) each symbol represents the average distance of PI-positive cells from the lower boundary of the z-stack, per 100 cells. Two fields were counted for three independent slides. (**E**) A representative slice of *Shigella*-infected transwell cultures of 129.*Nlrc4*$^{+/-}$ or 129.*Nlrc4*$^{-/-}$ cecum-derived IEC monolayers. green, fluorescent phalloidin (actin); red, PI (cell death), blue, DAPI (nucleic acid). Mann-Whitney test, $^{**}P < 0.01$, $^{***}P < 0.001$.

To further characterize the role of the NAIP–NLRC4 inflammasome during *Shigella* infection of IECs, we generated intestinal epithelial stem cell-derived organoids from the ceca of 129.WT and 129.*Nlrc4*$^{-/-}$ mice and established a trans-well monolayer infection assay (see Methods).To further characterize the role of the NAIP–NLRC4 inflammasome during *Shigella* infection of IECs, we generated intestinal epithelial stem cell-derived organoids from the ceca of 129.WT and 129.*Nlrc4*$^{-/-}$ mice and established a transwell monolayer infection assay (see Methods). We were unable to recover CFUs

from WT IEC monolayers infected with WT *Shigella* (Figure 2.8A). In contrast, 129.*Nlrc4*$^{-/-}$ IEC monolayers supported replication of WT *Shigella*. The avirulent non-invasive BS103 strain was detected sporadically at low levels, independent of NAIP–NLRC4, while a strain lacking IcsA, a protein essential for *Shigella* actin tail formation and cell-to-cell spread [139, 140], colonized 129.*Nlrc4*$^{-/-}$ IEC monolayers to a lesser extent than WT *Shigella*, consistent with loss of IcsA-mediated cell-to-cell spread. Immunostaining for *Shigella* in infected IEC organoid cultures also revealed intracellular replication and actin tail formation (detected by fluorescent phalloidin) exclusively in *Nlrc4*$^{-/-}$ IEC monolayers infected with WT *Shigella* (Figure 2.8B). Thus, IEC organotypic infections faithfully recapitulate the NAIP–NLRC4-dependent differences in *Shigella* replication observed *in vivo*. Our results suggest that NAIP–NLRC4 can provide resistance in a cell-type (IEC) intrinsic manner, though additional non-IEC intrinsic functions of NAIP–NLRC4 may also contribute to protection *in vivo*. In addition, our results demonstrate that key *Shigella* virulence factors are functional within mouse cells and can initiate invasion and actin-based motility in mouse IECs, as long as the NAIP–NLRC4 inflammasome is absent.

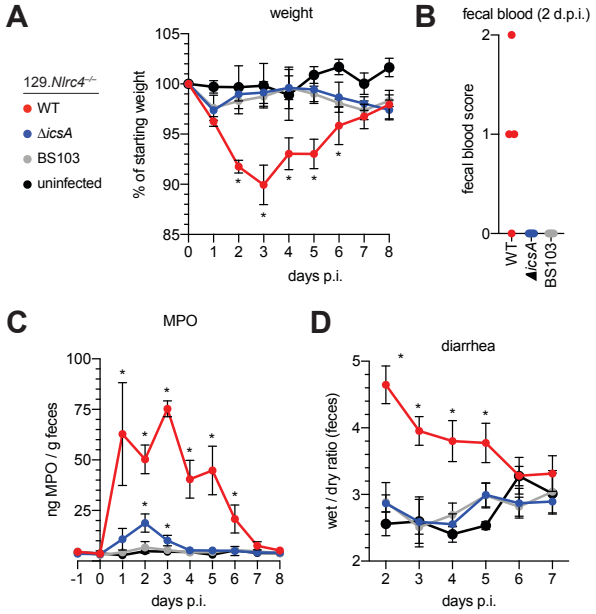

Figure 2.9. 129.*Nlrc4*$^{-/-}$ mice are resistant to attenuated *Shigella* strains.
(**A–D**) 129.*Nlrc4*$^{-/-}$ littermates were uninfected (black) or inoculated orally with 5x10^7 CFU of WT (red), *icsA* mutant (blue), or BS103 (grey) *Shigella* 24 hours after oral streptomycin treatment and monitored for 8 days post-infection (p.i.). (**A**) Mouse weights. (**B**) Fecal blood scores from feces at two days post-infection (d.p.i.). 1 = occult blood, 2 = macroscopic blood. Each symbol represents feces from one mouse. (**C**) MPO levels measured by ELISA from feces collected -1 through 8 days p.i. (**D**) Quantification of diarrhea comparing weight of feces before and after dehydration. A larger ratio indicates diarrhea. (**A–C**) Each symbol represents the mean at a specific time point for four individual mice per infection condition. Data are representative of two independent experiments. Mean ± SEM is shown in (**A–C**) Mann-Whitney test, **P* < 0.05. In (**A**,**B**) significance was determined by independently comparing to Day 0 and to BS103 + uninfected at the same day. In (**C**), significance was determined by comparing to BS103 + uninfected at the same day.

We sought to determine whether the NAIP–NLRC4 inflammasome prevented *Shigella* colonization of the IEC monolayers by mediating expulsion of the infected cells. Using confocal microscopy, we quantified both cell death (the number of PI-positive cells) and cell expulsion (the z-position of PI-positive cells from the monolayer). There were more PI-positive cells in *Shigella*-infected WT versus *Nlrc4*$^{-/-}$ IEC monolayers (Figure 2.8C,E), and the average position of PI-positive cells was significantly above the

monolayer (Figure 2.8D). Thus, data from our *ex vivo* IEC monolayer culture system, as well as from previous work [1], suggest that the NAIP–NLRC4 inflammasome prevents *Shigella* invasion by coordinating the expulsion of infected IECs.

2.3.5 IcsA-dependent cell-to-cell spread is required for pathogenesis

The *Shigella* IcsA protein is required for virulence in humans [160-162]. To test if *icsA* is required for pathogenesis in mice, we infected 129.*Nlrc4*$^{-/-}$ mice with isogenic WT, *icsA* mutant, or BS103 *Shigella* and monitored disease for eight days. Mice infected with WT *Shigella* exhibited weight loss (Figure 2.9A), diarrhea (Figure 2.9B), increases in fecal MPO (Figure 2.9C), and blood in their stool (Figure 2.9D). Signs of disease in WT-infected mice peaked between 2-3 days post-infection with weight loss, stool consistency, and MPO signal returning to baseline levels at approximately seven days post-infection, consistent with the disease progression and resolution of human shigellosis. Interestingly, 129.*Nlrc4*$^{-/-}$ mice infected with *icsA* mutant *Shigella* did not experience weight loss, diarrhea, or fecal blood, and largely phenocopied mice infected with the non-invasive BS103 strain (Figures 2.9A–D). We did observe a slight but significant increase in fecal MPO levels at 1-3 days post-infection in these mice (Figure 2.9B). These results suggest that, as in humans [163, 164], *icsA* mutants can provoke mild inflammation upon initial colonization of the intestinal epithelium, but that dissemination of bacteria among IECs is a critical driver of severe disease.

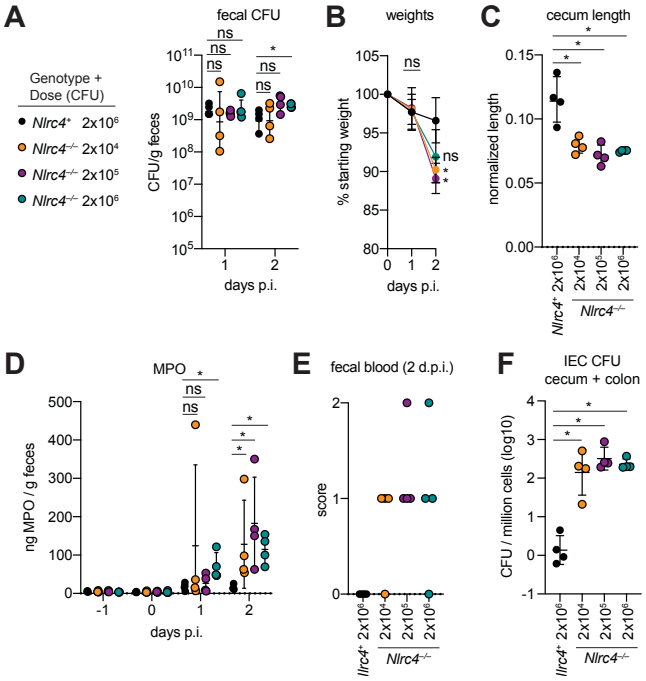

Figure 2.10. Antibiotic treated *Nlrc4*$^{-/-}$ mice are susceptible to modest infectious doses of *Shigella*.
(**A–F**) 129.*Nlrc4*$^{+}$ mice were inoculated orally with 2x10^6 (black) and 129.*Nlrc4*$^{-/-}$ littermates were inoculated with 2x10^6 (teal), 2x10^5 (purple), or 2x10^4 (orange) CFU of WT *Shigella* 24 hours after oral streptomycin treatment. (**A**) CFU determination from feces. (**B**) Mouse weights. Each symbol represents the mean at that time point. (**C**) Quantification of cecum length reduction normalized to the weight of the animal prior to infection; cecum length (cm) / mouse weight (g). (**D**) MPO levels measured by ELISA from feces collected -1 through 2 days p.i. (**E**) Fecal blood scores from feces at two days post-infection (d.p.i.). 1 = occult blood, 2 = macroscopic blood. (**F**) CFU determination from the IEC enriched fraction of gentamicin-treated cecum and colon tissue (combined). (**A, C–F)** Each symbol represents one mouse. Data are representative of two independent experiments. Mean ± SD is shown in (**A**–**D**). Geometric mean ± SD is show in (**F).** Mann-Whitney test, *P < 0.05.

2.3.6 Antibiotic-treated *Nlrc4*$^{-/-}$ mice are susceptible to modest infectious doses

One hallmark of human *Shigella* infection is the low infectious dose relative to other enteric bacterial pathogens. While the reported infectious dose ranges widely from person to person, ingestion of as few as 10-100 bacteria are sufficient to cause dysentery in some humans, though infection of some individuals requires higher doses [142]. To determine the infectious dose in our NAIP–NLRC4-deficient mouse model, streptomycin pretreated 129.*Nlrc4*$^{-/-}$ mice were infected with either $2x10^6$, $2x10^5$, or $2x10^4$ CFU of WT *Shigella* and compared to *Nlrc4*$^{+}$ littermates infected with $2x10^6$ CFU. Regardless of the inoculum, all mice showed similar levels of lumenal colonization (>10^8 CFU/g feces) at one and two days post-infection (Figure 2.10A). This suggests that even a relatively small bacterial population can rapidly expand within the intestines of antibiotic treated mice. As expected, *Nlrc4*$^{+}$ mice were largely resistant to disease (Figure 2.10B-E). In contrast, we observed robust disease, including weight loss, cecum shrinkage, elevated fecal MPO, and occult blood in *Nlrc4*$^{-/-}$ mice regardless of the infectious dose (Figure 2.10B-E). The rise in fecal MPO in mice receiving smaller inoculums was delayed relative to previous infections with $5x10^7$ CFU (Figure 2.10D, Figure 2.10F), suggesting that infectious dose correlates with disease onset. Importantly, there was a 100-fold difference in bacterial colonization of IECs between *Nlrc4*$^{-/-}$ mice and *Nlrc4*$^{+}$ mice, regardless of infectious dose, but no difference in IEC colonization among *Nlrc4*$^{-/-}$ mice inoculated with $2x10^4$ – $2x10^6$ CFU (Figure 2.10F). These results indicate that in antibiotic treated mice, disease is fully penetrant at $2x10^4$ CFU, a dose that recapitulates the infectious dose observed in at least some human patients.

2.4 Discussion

Here we demonstrate that the NAIP–NLRC4 inflammasome is a formidable species-specific barrier to *Shigella* invasion of the intestinal epithelium. *Shigella* infection of antibiotic pre-treated, NAIP–NLRC4-deficient mice recapitulates key features of human shigellosis, including bacterial invasion of and replication in IECs, severe inflammatory disease at relevant sites (e.g., colon, cecum), and bloody diarrhea. While ocular, pulmonary, and intraperitoneal *Shigella* infections have been used to assess bacterial virulence in mice, these models do not feature bacterial colonization of intestinal epithelial cells, a key event required for pathogenesis in humans. Thus, inflammasome-deficient mice provide the first physiologically relevant mouse model of bacillary dysentery. The genetic and immunological tractability of this system relative to other small animal oral infection models (rabbit, guinea pigs) should pave the way for detailed genetic and mechanistic *in vivo* studies of the host factors underlying *Shigella* pathogenesis that have long been elusive.

There remain key differences between orogastric *Shigella* infection of NAIP–NLRC4-deficient mice and human infection. First, even genetically susceptible mice require oral antibiotic treatment to alter the mouse microbiome and allow *Shigella* to establish a replicative niche in the gut. However, this limitation is not unique to our *Shigella* model, as antibiotic pretreatment is a common practice in studying many mouse models of enteric bacterial infections [165-167]. Interestingly, *S. sonnei* encodes a type VI secretion system that mediates competition with other bacterial species [10]. This finding suggests that interbacterial interactions may also be an important selective

pressure acting on *Shigella* in the human gut. An important next step will be to identify interactions between *Shigella* and the human versus mouse microbiome that define the species-specific differences in colonization resistance.

In our model we were able to achieve shigellosis in mice inoculated with as few as $2x10^4$ CFU. Although much is made of the low infectious dose of *Shigella* required to cause disease in humans, we note that experimental human infection studies did not routinely achieve disease with 100 CFU (14%) [141] and even higher inoculums failed to cause disease in some individuals 10^5-10^8 CFU (68-88%) [142]. We also note that *Shigella* rapidly expands in the antibiotic-treated mouse gut regardless of starting inoculum, such that the concept of infectious dose may not be a wholly meaningful metric for *Shigella* pathogenesis. Ultimately, infectious dose during natural infections likely varies depending on a multitude of environmental and host factors. While many questions remain, our model now provides a means by which to dissect these key questions, which will allow future refinement and greater utility of the model to understand human infection and disease.

A long-held belief is that *Shigella* exploits inflammasomes to induce pyroptosis. Pyroptotic cell death is presumed to allow bacteria to escape macrophages and invade the basolateral surface of polarized enterocytes [8, 154, 155]. Although we do not directly address this possibility, our experiments suggest that *Shigella* has instead evolved to inhibit or evade the human NAIP–NLRC4 inflammasome to limit intestinal epithelial cell death. Indeed, we find that the NAIP–NLRC4 inflammasome plays a critical role in host defense by restricting *Shigella* replication and spread in IECs. Further supporting this notion, only *Nlrc4*$^{-/-}$ but not WT IEC organoid monolayers are permissive to *Shigella* infection. Our data are consistent with the NAIP–NLRC4 inflammasome providing defense by coordinating the expulsion of *Shigella*-infected cells. Similarly, *Salmonella* infected IECs are expelled from the intestinal epithelial barrier in an NLRC4-dependent manner [1, 81]. Thus, epithelial inflammasomes coordinate the expulsion of infected IECs as a general defense strategy against enteric bacterial pathogens. A non-mutually exclusive possibility is that NAIP–NLRC4 (or other inflammasomes) are required for *Shigella* invasion and or pathogenesis in non-IECs, including macrophages. Interestingly, in *Nlrc4*$^{-/-}$ mice IL-1β and KC levels in target tissues are elevated, indicating that *Shigella* may encounter multiple inflammasomes at distinct stages of infection with opposing consequences for bacterial replication and host pathogenesis.

We seem to observe more severe shigellosis in *Nlrc4*$^{-/-}$ mice generated on the 129 genetic background. 129 mice naturally harbor a null *Casp11* allele [114]. Although other genetic differences may contribute to the variation in susceptibility to *Shigella* between B6 and 129 NAIP–NLRC4-deficient mice, we speculate that both the NAIP–NLRC4 and the CASP11 inflammasomes mediate protection in IECs against *Shigella* invasion. However, the susceptibility of B6 NAIP–NLRC4-deficient (but CASP11^{+}) mice, as well as the resistance of *Casp1/11*$^{-/-}$ mice, suggest that these inflammasomes are not strictly redundant and that NAIP–NLRC4 alone is sufficient to confer resistance to shigellosis in mice. The *Shigella* effector OspC3 antagonizes the human LPS sensor CASP4 [115], and IEC-expressed CASP4 provides protection against other human bacterial pathogens [89, 92], underscoring the importance of the LPS sensing pathway during human infection.

There is currently no licensed *Shigella* vaccine, and very limited knowledge of what vaccine-induced immune responses would be desirable to elicit to mediate protection [161, 168]. Our new shigellosis model will finally allow the field to leverage the outstanding genetic and immunological tools and reagents in the mouse to address fundamental questions about the immune response to *Shigella*. Our finding that NAIP–NLRC4 inflammasome-deficient mice clear the attenuated *Shigella icsA* strain, derivatives of which are currently deployed in human vaccine trials [147, 160, 163], speaks to the readiness of our model to support testing and development of *Shigella* therapeutics. More broadly, our results also provide a striking example of how inflammasomes provide an important species-specific barrier against infection.

Chapter Three. A hierarchy of cell death pathways confers layered resistance to shigellosis in mice

3.1 Summary

Bacteria of the genus *Shigella* cause shigellosis, a severe gastrointestinal disease driven by bacterial colonization of colonic intestinal epithelial cells. Vertebrates have evolved programmed cell death pathways that sense invasive enteric pathogens and eliminate their intracellular niche. The genetic removal of one such pathway, the NAIP–NLRC4 inflammasome, is sufficient to convert mice from resistant to susceptible to oral *Shigella flexneri* challenge [112]. Here, we investigate the protective role of additional cell death pathways during oral mouse *Shigella* infection. We find that the Caspase-11 inflammasome, which senses *Shigella* LPS, restricts *Shigella* colonization of the intestinal epithelium in the absence of NAIP–NLRC4. However, this protection is limited when *Shigella* expresses OspC3, an effector that antagonizes Caspase-11 activity. TNFα, a cytokine that activates Caspase-8-dependent apoptosis, also provides protection from *Shigella* colonization of the intestinal epithelium, but only in the absence of both NAIP–NLRC4 and Caspase-11. The combined genetic removal of Caspases-1,-11, and -8 renders mice hyper-susceptible to oral *Shigella* infection. Our findings uncover a layered hierarchy of cell death pathways that limit the ability of an invasive gastrointestinal pathogen to cause disease.

3.2 Introduction

Shigella is a genus of enteric bacterial pathogens that causes ~270 million yearly cases of shigellosis, with ~200,000 of these resulting in death [4]. Shigellosis manifests as an acute inflammatory colitis resulting in abdominal cramping, fever, and in severe cases, bloody diarrhea (dysentery) [5]. Bacterial invasion of the colonic intestinal epithelium and subsequent dissemination between adjacent intestinal epithelial cells (IECs) is believed to drive inflammation and disease. *Shigella* pathogenesis is mediated by a virulence plasmid which encodes a type three secretion system (T3SS) and more than 30 virulence factors or effectors [3]. The T3SS injects effectors into the host cell that facilitate bacterial uptake, escape into the cytosol, and actin–based motility, which is essential for bacterial spread to neighboring epithelial cells [139, 140, 169]. The T3SS also secretes several effectors that disarm the host innate immune response to make the cell a more hospitable niche for replicating *Shigella* [170].

The innate immune system can counteract intracellular bacterial pathogens by inducing programmed cell death [171]. Programmed cell death eliminates the intracellular pathogen niche, maintains epithelial barrier integrity, promotes clearance of damaged cells, and enhances presentation of foreign antigens to cells of the adaptive immune response [72, 172-175]. Three main modes of programmed cell death are common to mammalian cells: pyroptosis, apoptosis, and necroptosis. Each is controlled by distinct sensors and conserved downstream executors which together provide a formidable barrier that pathogens must subvert for successful intracellular replication. Of particular relevance to *Shigella* and other gastrointestinal pathogens, cell death of IECs is accompanied by a unique cellular expulsion process that rapidly and selectively ejects dying or infected cells from the epithelial layer, thereby potently limiting pathogen invasion into deeper tissue [1, 84, 89, 176].

Shigella is an example of a pathogen in intense conflict with host cell death pathways [177]. *Shigella* encodes multiple effectors to prevent cell death in human cells, including OspC3 to block Caspase-4 inflammasome activation [55, 115, 120, 121], IpaH7.8 to inhibit Gasdermin D-dependent pyroptosis [56], OspC1 to suppress Caspase-8-dependent apoptosis [138], and OspD3 to block necroptosis [138]. The antagonism of these pathways (and perhaps others that are yet undiscovered) and the resulting maintenance of the epithelial niche appears sufficient to render humans susceptible to *Shigella* infection. Mice, however, are resistant to oral *Shigella* challenge because *Shigella* is unable to counteract epithelial NAIP–NLRC4-dependent cell death and expulsion [71, 112]. Removal of the NAIP–NLRC4 inflammasome renders mice susceptible to shigellosis, providing a tractable genetic model to dissect *Shigella* pathogenesis after oral infection *in vivo* [112].

Here, we use the NAIP–NLRC4-deficient mouse model of shigellosis to investigate the role of programmed cell death in defense against *Shigella in vivo.* We find that Caspase-11 (CASP11), a cytosolic sensor of LPS and the mouse ortholog of Caspase-4 [116], provides modest protection from *Shigella* infection in the absence of NAIP–NLRC4. Like in humans, this pathway is antagonized by the *Shigella* effector OspC3, and genetic removal of *ospC3* from *Shigella* results in a significant reduction in bacterial colonization of IECs and virulence which depends on CASP11. We also find that TNFα, a cytokine that can induce TNF receptor 1 (TNFRI)-dependent extrinsic apoptosis [101], defends mouse IECs from bacterial colonization and limits subsequent disease. TNFα-dependent protection, however, was only observed when mice lack both NAIP–NLRC4 and CASP11, revealing a hierarchal program of cell death pathways that counteract *Shigella in vivo*. *Casp1/11*$^{-/-}$*Ripk3*$^{-/-}$ and *Casp8*$^{-/-}$*Ripk3*$^{-/-}$ mice, which lack some but not all key components of pyroptosis, apoptosis, and necroptosis are largely protected from disease, revealing redundancies between these pathways. *Casp1/11/8*$^{-/-}$ *Ripk3*$^{-/-}$ mice, however, are hyper-susceptible to shigellosis, indicating that programmed cell death is a predominant host defense mechanism against *Shigella* infection. Furthermore, neither Interleukin-1 receptor (IL-1R)-mediated signaling nor myeloid-restricted NAIP–NLRC4 have an apparent effect on *Shigella* pathogenesis, suggesting that it is cell death of IECs that primarily protects mice from shigellosis. Our findings underscore the importance of cell death in defense against intracellular bacterial pathogens and provide an example of how layered and hierarchical immune pathways can provide robust defense against pathogens that have evolved a broad arsenal of virulence factors.

3.3 Results

3.3.1 CASP11 contributes to resistance of B6 versus 129 *Nlrc4*$^{-/-}$ mice to shigellosis

We previously generated NLRC4 deficient mice on the 129S1/SvImJ (129) background (129.*Nlrc4*$^{-/-}$) and observed that these mice appeared more susceptible to oral *Shigella flexneri* challenge than C57BL/6J (B6) NLRC4 deficient mice (B6.*Nlrc4*$^{-/-}$) [112]. We reasoned that the apparent difference between the strains might be due to genetic and/or microbiota differences. To address these possibilities, we infected co-housed B6.*Nlrc4*$^{-/-}$ and 129.*Nlrc4*$^{-/-}$ mice and directly compared disease severity

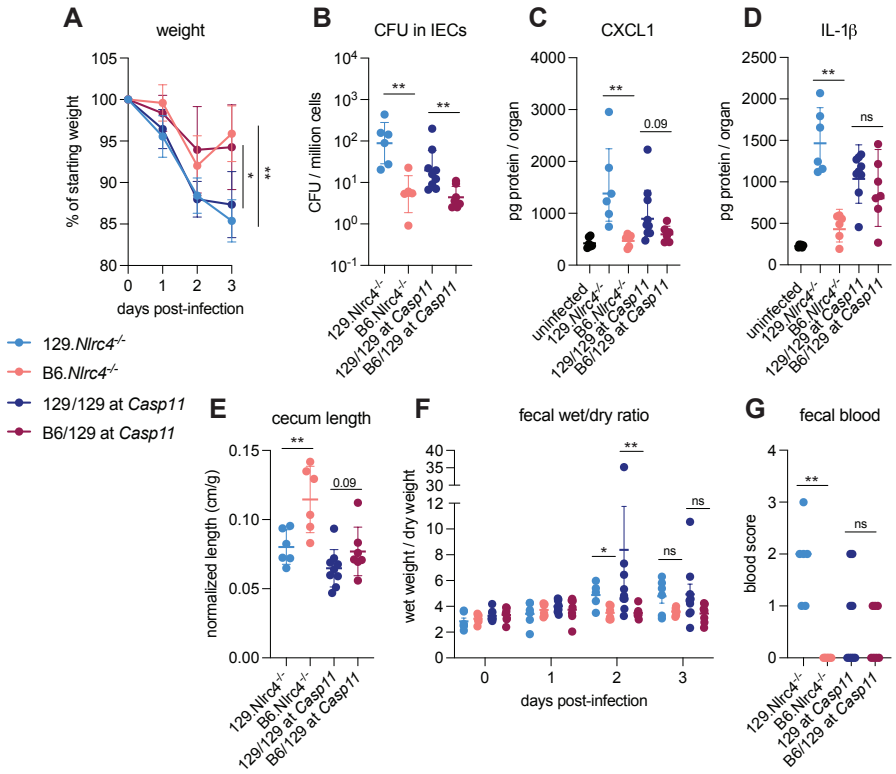

Figure 3.1. CASP11 contributes to resistance of B6 versus 129 *Nlrc4*$^{-/-}$ mice to shigellosis.
(**A-G**) B6.*Nlrc4*$^{-/-}$ (pink), 129.*Nlrc4*$^{-/-}$ (light blue), backcrossed littermates that are homozygous 129/129 at *Casp11* (dark blue), and backcrossed littermates that are heterozygous B6/129 at *Casp11* (maroon) were co-housed for 3 weeks, treated orally with 25 mg streptomycin sulfate in water, and orally challenged the next day with 10^7 CFU of WT *Shigella flexneri.* Mice were sacrificed at three days post-infection. (**A**) Mouse weights from 0 through 3 days post-infection. Each symbol represents the mean for all mice of the indicated genotype. (**B**) *Shigella* colony forming units (CFU) per million cells from the combined intestinal epithelial cell (IEC) enriched fraction of gentamicin-treated cecum and colon tissue. (**C**, **D**) CXCL1 and IL-1β levels measured by ELISA from homogenized cecum and colon tissue of infected mice. (**E**) Quantification of cecum lengths normalized to mouse weight prior to infection; cecum length (cm) / mouse weight (g). (**F**) The ratio of fecal pellet weight when wet (fresh) divided by the fecal pellet weight after overnight drying. A larger wet/dry ratio indicates increased diarrhea. Pellets were collected daily from 0-3 days post-infection. (**G**) Additive blood scores from feces collected at two and three days post-infection. 1 = occult blood, 2 = macroscopic blood for a given day, maximum score is 4. (**B-G**) Each symbol represents one mouse. Mean ± SD is shown in (**A, C- E**). Geometric mean ± SD is shown in (**B**). Mean ± SEM is shown in (**F**). Mann-Whitney test, *p < 0.05, **p < 0.01, ***p < 0.001, ****p < 0.0001, ns = not significant (p > 0.05).

between the two strains (Figure 3.1). The B6.*Nlrc4*$^{-/-}$ mice exhibited only modest weight-loss (5-10% of starting weight) through two days and began to recover by day three (Figure 3.1A). The 129.*Nlrc4*$^{-/-}$ mice, however, continued to lose weight through day three (10-15% of starting weight) (Figure 3.1A). Upon sacrifice at day three, we harvested the intestinal epithelial cell fraction from the cecum and colon of each mouse, washed this fraction in gentamicin to eliminate any extracellular *Shigella*, and lysed these cells to enumerate intracellular bacterial colonization of IECs. IECs from 129.*Nlrc4*$^{-/-}$ mice harbored >10-fold higher intracellular *Shigella* burdens than those from B6.*Nlrc4*$^{-/-}$ mice (Figure 3.1B). We also found that 129.*Nlrc4*$^{-/-}$ mice had higher levels of inflammatory cytokines CXCL1 and IL-1β in their intestinal tissue, as measured by ELISA (Figure 1C, D) and exhibited significantly more gross cecum shrinkage than B6.*Nlrc4*$^{-/-}$ mice (Figure 3.1E). The 129.*Nlrc4*$^{-/-}$ mice also exhibited more pronounced diarrhea (as measured by the wet weight to dry weight ratio of mouse feces) relative to the B6.*Nlrc4*$^{-/-}$ mice at two days post-infection (Figure 3.1F). We scored mouse feces

for the presence of occult blood (score = 1) or macroscopic blood (score = 2) at day two and three, the sum of which represents a blood score from zero to four (Figure 3.1G). All 129.*Nlrc4*$^{-/-}$ mice had occult blood in their feces on at least one of these days, with many having occult or macroscopic blood on both days. In contrast, B6.*Nlrc4*$^{-/-}$ mice did not exhibit fecal blood.

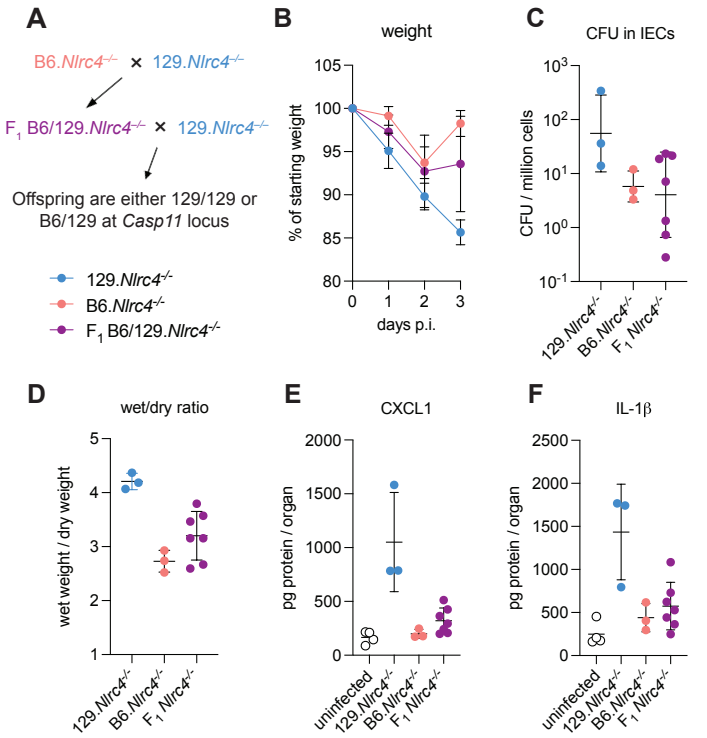

Figure 3.2. B6/129.*Nlrc4*$^{-/-}$ F_1 hybrids are modestly susceptibility to *Shigella*
(**A**) Crossing scheme to generate B6/129.*Nlrc4*$^{-/-}$ F_1 mice and backcrossed *Nlrc4*$^{-/-}$ mice that are heterozygous B6/129 or homozygous 129/129 at *Casp11*. (**B-E**) B6.*Nlrc4*$^{-/-}$ (pink), 129.*Nlrc4*$^{-/-}$ (light blue), and 129/B6.*Nlrc4*$^{-/-}$ F_1 (plum) mice were treated orally with 25 mg streptomycin sulfate in water and orally challenged the next day with 10^7 CFU of WT *Shigella flexneri.* Mice were sacrificed at three days post-infection. (**B**) Mouse weights from 0 through 3 days post-infection. Each symbol represents the mean for all mice of the indicated group. (**C**) *Shigella* colony forming units (CFU) per million cells from the combined intestinal epithelial cell (IEC) enriched fraction of gentamicin-treated cecum and colon tissue. (**D**) The ratio of fecal pellet weight when wet (fresh) divided by the fecal pellet weight after overnight drying. A larger wet/dry ratio indicates increased diarrhea. Pellets were collected at day two post-infection. (**E**, **F**) CXCL1 and IL-1β levels measured by ELISA from homogenized cecum and colon tissue of infected mice. (**C-F**) Each symbol represents one mouse. Mean ± SD is shown in (**B, D-F**). Geometric mean ± SD is shown in (**C**).

The persistence of this difference in disease severity between co-housed 129 and B6 *Nlrc4*$^{-/-}$ mice suggested that genetic rather than microbiota differences might explain the differential susceptibility of the strains. The mouse non-canonical inflammasome Caspase-11 (CASP11) and its human orthologs Caspases-4 and -5 sense cytosolic *Shigella* LPS to initiate pyroptosis [113-116]. Notably, 129 mice are naturally deficient for Caspase-11 [114]. To determine if Caspase-11 contributes to the difference in susceptibility between these strains, we crossed B6.*Nlrc4*$^{-/-}$ and 129.*Nlrc4*$^{-/-}$ mice to generate B6/129.*Nlrc4*$^{-/-}$ F_1 hybrids (Figure 3.2A). We infected these F_1 hybrids and found that they were relatively resistant to *Shigella* challenge and resembled the parental B6.*Nlrc4*$^{-/-}$ mice (Figure 3.2B-F). These results are consistent with the possibility that a dominant gene on the C57BL/6J background provides protection from *Shigella*. Next, we backcrossed these hybrids to the 129.*Nlrc4*$^{-/-}$ parental strain to generate littermate *Nlrc4*$^{-/-}$ mice that were mixed homozygous 129/129 or heterozygous B6/129 at all loci (Figure 3.2A). We co-housed these *Nlrc4*$^{-/-}$ backcrossed mice with their parental 129.*Nlrc4*$^{-/-}$ and B6.*Nlrc4*$^{-/-}$ strains for >3 weeks, infected them with *Shigella*, and genotyped each at the *Casp11* locus to determine whether a functional B6 *Casp11* allele would correlate with reduced disease severity.

Indeed, backcrossed *Nlrc4*$^{-/-}$ mice that were heterozygous B6/129 at *Casp11* were more resistant to shigellosis than backcrossed *Nlrc4*$^{-/-}$ mice that were 129/129 at *Casp11* (Figure 3.1). Mice that were heterozygous B6/129 at *Casp11* showed a similar weight-loss pattern to the parental B6.*Nlrc4*$^{-/-}$ mice and began to recover by day three while the weight-loss in mice that were homozygous 129/129 at *Casp11* phenocopied that of the parental 129.*Nlrc4*$^{-/-}$ mice (Figure 3.1A). Consistent with these results, mice that were homozygous 129/129 at *Casp11* exhibited enhanced bacterial colonization of the intestinal epithelium (Figure 3.1B), modest increases in inflammatory cytokines (Figure 3.1C, D) and cecum shrinkage (Figure 3.1E), and more pronounced diarrhea (Figure 3.1F). Despite these differences, there was no strong correlation between fecal blood score and *Casp11* genotype (Figure 3.1G), suggesting that while *Casp11* contributes to resistance, there are additional genetic modifiers present on the 129 or B6 background that affect susceptibility to shigellosis. As these additional modifiers appear to be relatively weak compared to *Casp11*, we did not attempt to map them

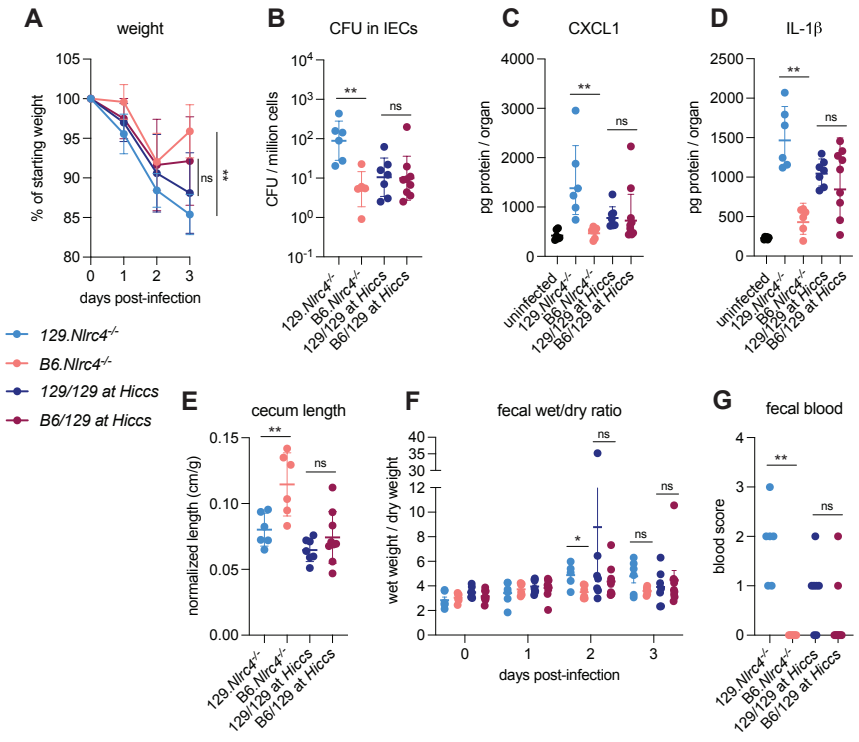

Figure 3.3. *Hiccs* does not contributes to resistance of B6 versus 129 *Nlrc4*$^{-/-}$ mice to shigellosis
(**A-G**) B6.*Nlrc4*$^{-/-}$ (pink), 129.*Nlrc4*$^{-/-}$ (light blue), backcrossed littermates that are homozygous 129/129 at *Hiccs* (dark blue), and backcrossed littermates that are heterozygous B6/129 at *Hiccs* (maroon) were co-housed for 3 weeks, treated orally with 25 mg streptomycin sulfate in water, and orally challenged the next day with 10^7 CFU of WT *Shigella flexneri*. Mice were sacrificed at three days post-infection. (**A**) Mouse weights from 0 through 3 days post-infection. Each symbol represents the mean for all mice of the indicated genotype. (**B**) *Shigella* colony forming units (CFU) per million cells from the combined intestinal epithelial cell (IEC) enriched fraction of gentamicin-treated cecum and colon tissue. (**C**, **D**) CXCL1 and IL-1β levels measured by ELISA from homogenized cecum and colon tissue of infected mice. (**E**) Quantification of cecum lengths normalized to mouse weight prior to infection; cecum length (cm) / mouse weight (g). (**F**) The ratio of fecal pellet weight when wet (fresh) divided by the fecal pellet weight after overnight drying. A larger wet/dry ratio indicates increased diarrhea. Pellets were collected daily from 0-3 days post-infection. (**G**) Additive blood scores from feces collected at two and three days post-infection. 1 = occult blood, 2 = macroscopic blood for a given day. (**B-G**) Each symbol represents one mouse. Mean ± SD is shown in (**A, C-E**). Geometric mean ± SD is shown in (**B**). Mean ± SEM is show in (**F**). Mann-Whitney test, *p < 0.05, **p < 0.01, ***p < 0.001, ****p < 0.0001, ns = not significant (p > 0.05)

genetically. However, we did specifically test for a contribution of *Hiccs*, a genetic locus in 129 mice that associates with increased susceptibility to *Helicobacter hepaticus*-dependent colitis [178]. In contrast to *Casp11*, we found that *Hiccs* did not significantly associate with increased susceptibility to shigellosis in 129 mice (Figure 3.3).

3.3.2 CASP11 prevents IEC colonization and disease in B6.*Nlrc4*$^{-/-}$ mice

To define the role of mouse Caspase-11 in a uniform genetic background, we generated *Casp11*$^{-/-}$ mice on the B6.*Nlrc4*$^{-/-}$ background using CRISPR-Cas9 editing (Figure 3.4). We previously found that *Casp1/11*$^{-/-}$ mice are largely resistant to oral WT *Shigella flexneri* infection, likely because NLRC4-dependent Caspase-8 activation is sufficient to prevent bacterial colonization of IECs (Figure 2.2) [1, 112]. Thus, Caspase-11 is dispensable for protection from WT *Shigella* challenge when mice express functional NLRC4, but Caspase-11 could still be critical as a backup pathway in the absence of NLRC4. We therefore challenged B6.*Nlrc4*$^{-/-}$ and B6.*Nlrc4*$^{-/-}$*Casp11*$^{-/-}$ littermates with WT *Shigella* and assessed pathogenicity for two days following infection.

We observed a modest increase in susceptibility to *Shigella* infection in B6.*Nlrc4*$^{-/-}$*Casp11*$^{-/-}$ mice relative to B6.*Nlrc4*$^{-/-}$ mice (Figure 3.5). While B6.*Nlrc4*$^{-/-}$*Casp11*$^{-/-}$ mice did not experience more weight loss (Figure 3.5A), cecum shrinkage (Figure 3.5B), or diarrhea (Figure 3.5C) than B6.*Nlrc4*$^{-/-}$ mice, there was a 5-fold increase in *Shigella* burdens in IECs from B6.*Nlrc4*$^{-/-}$*Casp11*$^{-/-}$ mice (Figure 3.5D), indicating that Caspase-11 protects the mouse epithelium from bacterial colonization in the absence of NLRC4. Intestinal tissue from B6.*Nlrc4*$^{-/-}$*Casp11*$^{-/-}$ mice also expressed higher levels of inflammatory cytokines CXCL1 and IL-1β than tissue from B6.*Nlrc4*$^{-/-}$ mice (Figure 3.5E, F). Consistent with these findings, B6.*Nlrc4*$^{-/-}$ mice did not exhibit blood in their feces but two of the nine B6.*Nlrc4*$^{-/-}$*Casp11*$^{-/-}$ did present with occult blood (Figure 3.5G). These results suggest that Caspase-11 has a relatively modest contribution to defense against wild-type *Shigella.* Indeed, a minor role for Caspase-11 is expected given that

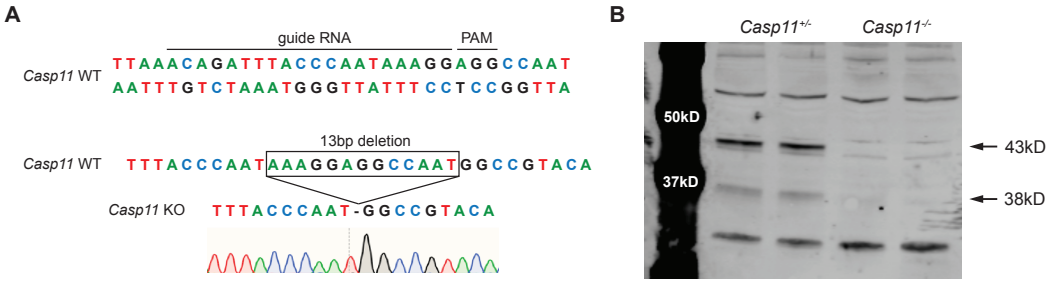

Figure 3.4. B6/129.*Nlrc4*$^{-/-}$ F$_1$ hybrids are modestly susceptibility to *Shigella* Crossing scheme to generate B6/129.*Nlrc4*$^{-/-}$ F$_1$ mice and backcrossed *Nlrc4*$^{-/-}$ mice that are heterozygous B6/129 or homozygous 129/129 at *Casp11*. (**B-E**) B6.*Nlrc4*$^{-/-}$ (pink), 129.*Nlrc4*$^{-/-}$ (light blue), and 129/B6.*Nlrc4*$^{-/-}$ F$_1$ (plum) mice were treated orally with 25 mg streptomycin sulfate in water and orally challenged the next day with 10^7 CFU of WT *Shigella flexneri.* Mice were sacrificed at three days post-infection. (**B**) Mouse weights from 0 through 3 days post-infection. Each symbol represents the mean for all mice of the indicated group. (**C**) *Shigella* colony forming units (CFU) per million cells from the combined intestinal epithelial cell (IEC) enriched fraction of gentamicin-treated cecum and colon tissue. (**D**) The ratio of fecal pellet weight when wet (fresh) divided by the fecal pellet weight after overnight drying. A larger wet/dry ratio indicates increased diarrhea. Pellets were collected at day two post-infection. (**E**, **F**) CXCL1 and IL-1β levels measured by ELISA from homogenized cecum and colon tissue of infected mice. (**C-F**) Each symbol represents one mouse. Mean ± SD is shown in (**B, D-F**). Geometric mean ± SD is shown in (**C**).

Shigella is known to encode an effector called OspC3 that inhibits Caspase-11 (see below). Nevertheless, taken together, our results in mixed 129/B6.*Nlrc4*$^{-/-}$ and B6.*Nlrc4*$^{-/-}$*Casp11*$^{-/-}$ mice indicate that Caspase-11 contributes to defense against *Shigella in vivo* as a backup pathway in the absence of NLRC4.

3.3.3 *Shigella* effector OspC3 is critical for virulence in oral *Shigella* infection

Shigella flexneri protein OspC3 is a T3SS-secreted effector that inhibits both human Caspase-4 and mouse Caspase-11 to suppress pyroptosis [55, 115, 120, 121]. While OspC3 has been shown to be required for virulence during intraperitoneal mouse infection [120, 121] and for intestinal lumenal colonization in wild-type mice [179], the role of this effector has not been studied in an oral mouse model of infection where *Shigella* invades and replicates within the intestinal epithelium. Indeed, our results indicating a role for Caspase-11 in defense against wild-type *Shigella* (see above, Figures 1 and 2) suggested that the inhibition of Caspase-11 by OspC3 could be incomplete in epithelial cells. To test the role of OspC3 in shigellosis, we orally infected

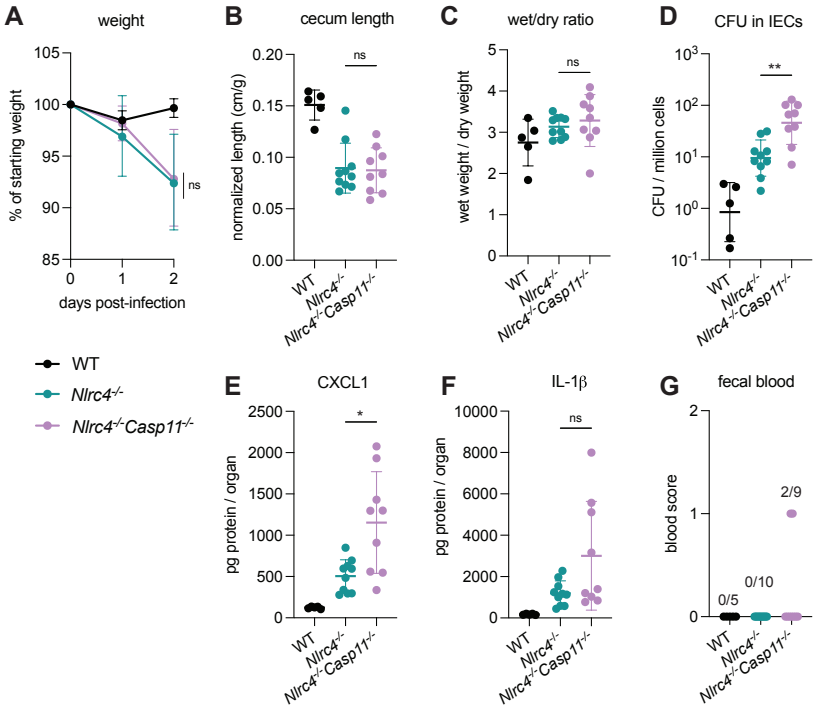

Figure 3.5. *Shigella* effector OspC3 is critical for virulence in oral *Shigella* infection
(**A-H**) Mice were treated orally with 25 mg streptomycin sulfate in water and infected one day later. B6.WT mice were orally challenged with 10^7 CFU of WT *Shigella flexneri* (black) and B6.*Nlrc4*$^{-/-}$ co-housed/littermate mice were challenged with WT (green) or *ΔospC3 Shigella flexneri* (blue). Mice were sacrificed at two days post-infection. (**A**) Representative images of the cecum and colon from B6.*Nlrc4*$^{-/-}$ mice infected with WT or *ΔospC3 Shigella flexneri.* The white arrow indicates clear but reduced inflammation in mice infected with the *ΔospC3* strain. (**B**) Mouse weights from 0 through 2 days post-infection. Each symbol represents the mean for all mice of the indicated genotype. (**C**) *Shigella* colony forming units (CFU) per million cells from the combined intestinal epithelial cell (IEC) enriched fraction of gentamicin-treated cecum and colon tissue. (**D**) Quantification of cecum lengths normalized to mouse weight prior to infection; cecum length (cm) / mouse weight (g). (**E**) The ratio of fecal pellet weight when wet (fresh) divided by the fecal pellet weight after overnight drying. Pellets were collected at day two post-infection. (**F, G**) CXCL1 and IL-1β levels measured by ELISA from homogenized cecum and colon tissue of infected mice. (**H**) Blood scores from feces collected at two days post-infection. 1 = occult blood, 2 = macroscopic blood. (**C-H**) Each symbol represents one mouse. Data collected from two independent experiments. Mean ± SD is shown in (**B, D-G**). Geometric mean ± SD is shown in (**C**). Mann-Whitney test, *p < 0.05, **p < 0.01, ***p < 0.001, ****p < 0.0001, ns = not significant (p > 0.05).

Figure 3.6. *Shigella* effector OspC3 is critical for virulence in oral *Shigella* infection
(**A-H**) Mice were treated orally with 25 mg streptomycin sulfate in water and infected one day later. B6.WT mice were orally challenged with 10^7 CFU of WT *Shigella flexneri* (black) and B6.*Nlrc4*$^{-/-}$ co-housed/littermate mice were challenged with WT (green) or *ΔospC3 Shigella flexneri* (blue). Mice were sacrificed at two days post-infection. (**A**) Representative images of the cecum and colon from B6.*Nlrc4*$^{-/-}$ mice infected with WT or *ΔospC3 Shigella flexneri.* The white arrow indicates clear but reduced inflammation in mice infected with the *ΔospC3* strain. (**B**) Mouse weights from 0 through 2 days post-infection. Each symbol represents the mean for all mice of the indicated genotype. (**C**) *Shigella* colony forming units (CFU) per million cells from the combined intestinal epithelial cell (IEC) enriched fraction of gentamicin-treated cecum and colon tissue. (**D**) Quantification of cecum lengths normalized to mouse weight prior to infection; cecum length (cm) / mouse weight (g). (**E**) The ratio of fecal pellet weight when wet (fresh) divided by the fecal pellet weight after overnight drying. Pellets were collected at day two post-infection. (**F, G**) CXCL1 and IL-1β levels measured by ELISA from homogenized cecum and colon tissue of infected mice. (**H**) Blood scores from feces collected at two days post-infection. 1 = occult blood, 2 = macroscopic blood. (**C-H**) Each symbol represents one mouse. Data collected from two independent experiments. Mean ± SD is shown in (**B, D-G**). Geometric mean ± SD is shown in (**C**). Mann-Whitney test, *p < 0.05, **p < 0.01, ***p < 0.001, ****p < 0.0001, ns = not significant (p > 0.05).

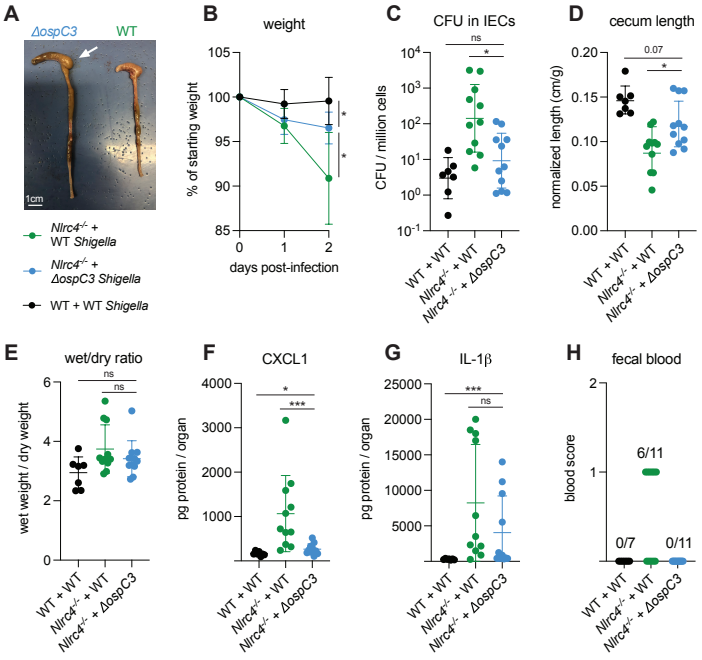

Figure 3.7. OspC3-driven virulence in B6.*Nlrc4*$^{-/-}$ mice depends on Caspase-11
(**A-G**) Mice were treated orally with 25 mg streptomycin sulfate in water and then infected one day later. B6.WT mice were orally challenged with 10^7 CFU of WT *Shigella flexneri* (black), B6.*Nlrc4*$^{-/-}$ mice were challenged with WT (blue) or *ΔospC3 Shigella flexneri* (pink), and B6.*Nlrc4*$^{-/-}$*Casp11*$^{-/-}$ mice were challenged with WT (teal) or *ΔospC3 Shigella flexneri* (maroon). Mice were littermates or were co-housed for 3 weeks prior to infection and were sacrificed at two days post-infection. (**A**) Mouse weights from 0 through 2 days post-infection. Each symbol represents the mean for all mice of the indicated group. (**B**) *Shigella* colony forming units (CFU) per million cells from the combined intestinal epithelial cell (IEC) enriched fraction of gentamicin-treated cecum and colon tissue. (**C**) Quantification of cecum lengths normalized to mouse weight prior to infection; cecum length (cm) / mouse weight (g). (**D**) The ratio of fecal pellet weight when wet (fresh) divided by the fecal pellet weight after overnight drying. Pellets were collected at day two post-infection. (**E, F**) CXCL1 and IL-1β levels measured by ELISA from homogenized cecum and colon tissue of infected mice. (**G**) Blood scores from feces collected at two days post-infection. 1 = occult blood, 2 = macroscopic blood. (**B-G**) Each symbol represents one mouse. Data collected from two independent experiments. Mean ± SD is shown in (**A, C-F**). Geometric mean ± SD is shown in (**B**). Mann-Whitney test, *p < 0.05, **p < 0.01, ***p < 0.001, ****p < 0.0001, ns = not significant (p > 0.05).

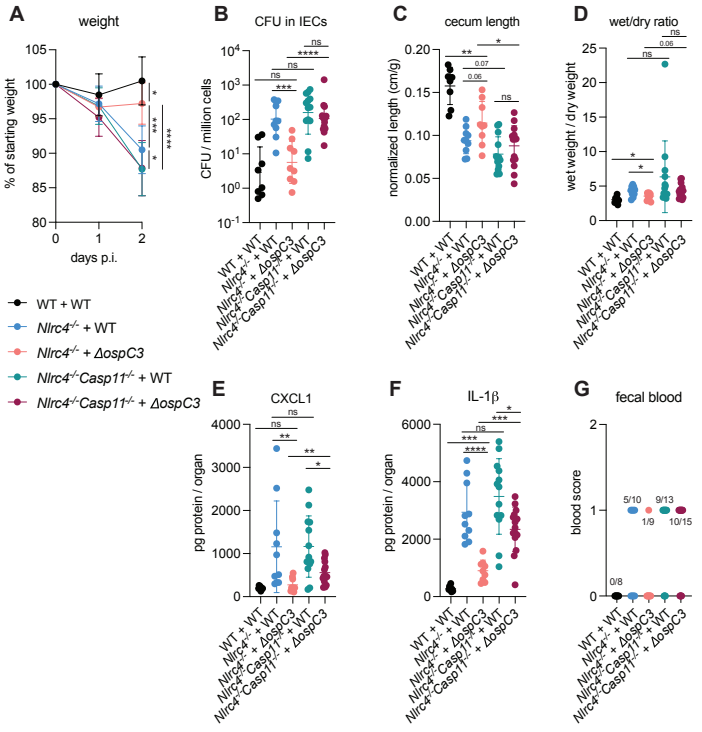

B6.*Nlrc4*$^{-/-}$ mice with WT S*higella flexneri* or a mutant stain that lacks OspC3 (*ΔospC3*)

(Figure 3.6). Consistent with our previous experiments, B6.*Nlrc4*$^{-/-}$ mice challenged with WT *Shigella* developed shigellosis characterized by weight-loss, increases in bacterial colonization of the intestinal epithelium, cecum shrinkage, diarrhea, and inflammatory cytokines (Figure 3.6A-G). However, B6.*Nlrc4*$^{-/-}$ mice challenged with *ΔospC3 Shigella flexneri* were almost fully resistant to infection (Figure 3.6). *ΔospC3*-infected B6.*Nlrc4*$^{-/-}$ mice still experienced some weight-loss (Figure 3.6B) and cecum shrinkage (Figure 3.6A, D), but exhibited a >10-fold decrease in IEC colonization (Figure 3.6C) and reduced levels of inflammatory cytokines relative to WT-infected B6.*Nlrc4*$^{-/-}$ mice (Figure 3.6F, G). Importantly, B6.*Nlrc4*$^{-/-}$ mice infected with *ΔospC3 Shigella* did not display fecal blood while, in this experiment, six of the eleven B6.*Nlrc4*$^{-/-}$ mice infected with WT *Shigella* did present with fecal blood (Figure 3.6H). These results indicate that *ΔospC3 Shigella* is attenuated in our B6.*Nlrc4*$^{-/-}$ mouse model of shigellosis.

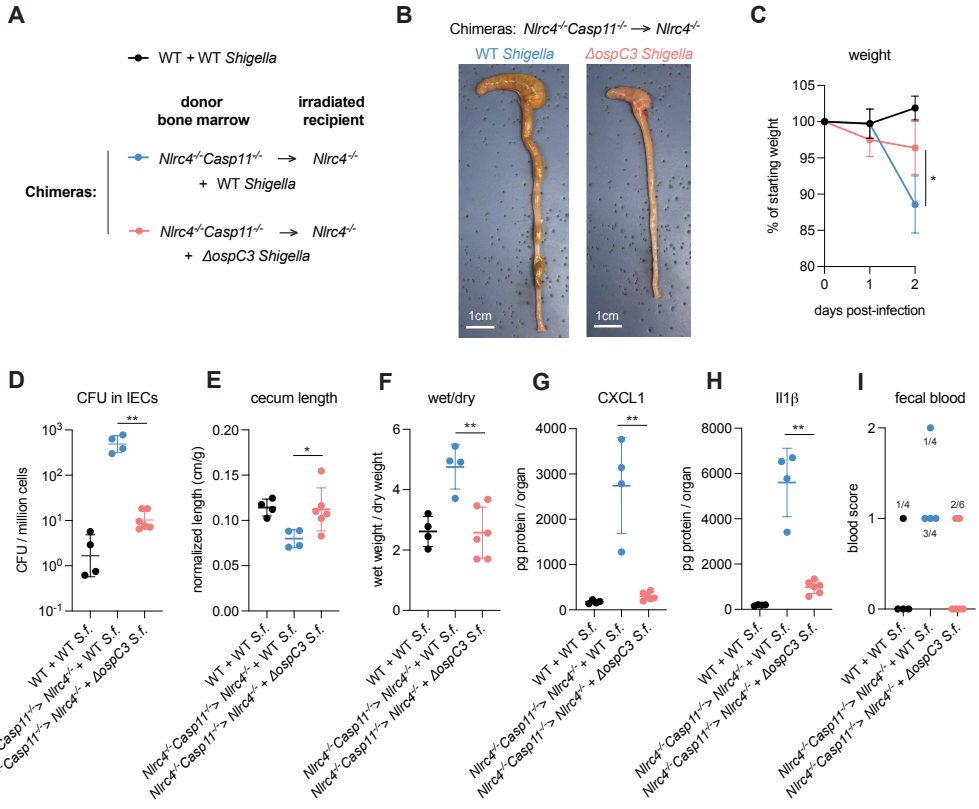

Figure 3.8. OspC3-driven virulence in B6.*Nlrc4*$^{-/-}$ mice depends on Caspase-11 in non-hematopoetic cells
(**A-G**) B6.*Nlrc4*$^{-/-}$ recipient mice were lethally irradiated and reconstituted with bone marrow from B6.*Nlrc4*$^{-/-}$*Casp11*$^{-/-}$ donor mice to generate chimeras. Mice were treated orally with 25 mg streptomycin sulfate in water and then infected one day later. B6.WT mice were orally challenged with 10^7 CFU of WT *Shigella flexneri* (black) and knockout chimeric mice were challenged with WT (blue) or *ΔospC3 Shigella flexneri* (pink). Mice were littermates or were co-housed for 3 weeks prior to infection and were sacrificed at two days post-infection. (**A**) Legend showing experimental setup. (**B**) Images of the cecum and colon from chimeric mice infected with the indicated strains. (**C**) Mouse weights from 0 through 2 days post-infection. Each symbol represents the mean for all mice of the indicated group. (**D**) *Shigella* colony forming units (CFU) per million cells from the combined intestinal epithelial cell (IEC) enriched fraction of gentamicin-treated cecum and colon tissue. (**E**) Quantification of cecum lengths normalized to mouse weight prior to infection; cecum length (cm) / mouse weight (g). (**F**) The ratio of fecal pellet weight when wet (fresh) divided by the fecal pellet weight after overnight drying. Pellets were collected at day two post-infection. (**G, H**) CXCL1 and IL-1β levels measured by ELISA from homogenized cecum and colon tissue of infected mice. (**I**) Blood scores from feces collected at two days post-infection. 1 = occult blood, 2 = macroscopic blood. (**D-I**) Each symbol represents one mouse. Data collected from two independent experiments. Mean ± SD is shown in (**C, E-H**). Geometric mean ± SD is shown in (**D**). Mann-Whitney test, *p < 0.05, **p < 0.01, ***p < 0.001, ****p < 0.0001, ns = not significant (p > 0.05).

OspC3 directly inactivates mouse Caspase-11 [120] but has also been reported to modulate other signaling pathways, including interferon signaling [179]. To test if the effect of OspC3 on virulence is dependent on inhibition of mouse Caspase-11, we infected both B6.*Nlrc4*$^{-/-}$ and B6.*Nlrc4*$^{-/-}$*Casp11*$^{-/-}$ mice with either WT or *ΔospC3 Shigella* strains. We again observed that the *ospC3* mutant was attenuated relative to WT *Shigella* in B6.*Nlrc4*$^{-/-}$ mice (Figure 3.7). However, both WT and *ΔospC3 Shigella* caused severe disease in B6.*Nlrc4*$^{-/-}$*Casp11*$^{-/-}$ mice, with comparable weight-loss, bacterial colonization of the intestinal epithelium, cecum lengths, diarrhea, and fecal blood (Figure 3.7A-D, G). These results suggest that Caspase-11 is the primary physiological target of OspC3 *in vivo*. We did observe a significant increase in inflammatory cytokines in WT-infected B6.*Nlrc4*$^{-/-}$*Casp11*$^{-/-}$ mice relative to *ΔospC3*-infected B6.*Nlrc4*$^{-/-}$*Casp11*$^{-/-}$ mice (Figure 3.7E, F), indicating that OspC3 might also affect immune pathways independent of Caspase-11. Again, we only observed a modest difference in disease severity between B6.*Nlrc4*$^{-/-}$ and B6.*Nlrc4*$^{-/-}$*Casp11*$^{-/-}$ mice infected with WT *Shigella* (Figure 3.7), consistent with the ability of OspC3 to significantly reduce Caspase-11 activity. These results confirm prior reports that OspC3

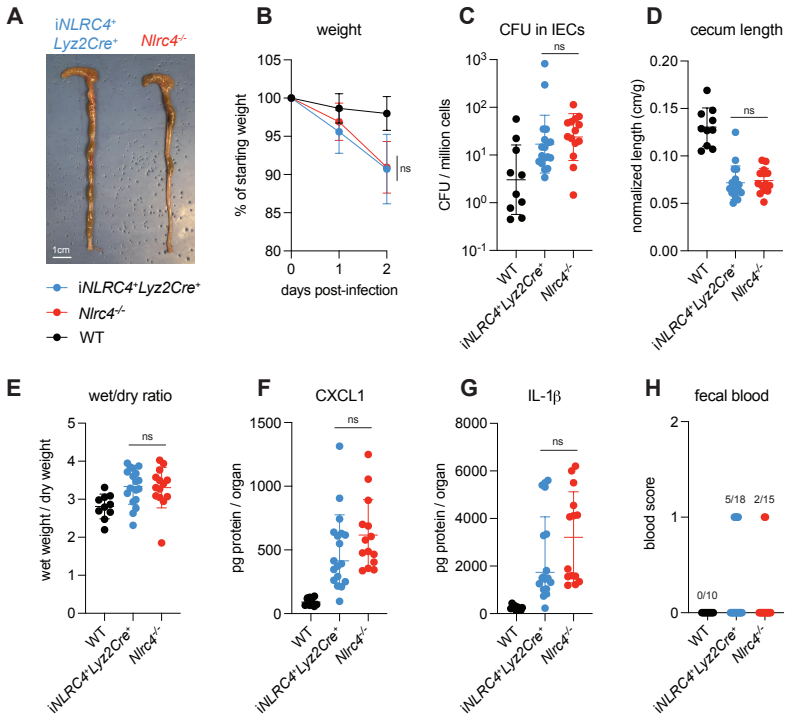

Figure 3.9. NLRC4 in myeloid-derived cells does not affect *Shigella* pathogenesis
(**A-H**) WT (black) mice and B6.*Nlrc4*$^{-/-}$ (Cre^{-}) (red) and i*Nlrc4Lyz2Cre* (blue) littermates were treated orally with 25 mg streptomycin sulfate in water and orally challenged the next day with 10^7 CFU of WT *Shigella flexneri*. Mice were sacrificed at two days post-infection. (**A**) Representative images of the cecum and colon from i*Nlrc4Lyz2Cre* and B6.*Nlrc4*$^{-/-}$ mice. Note the similarity in gross pathology between the two genotypes. (**B**) Mouse weights from 0 through 2 days post-infection. Each symbol represents the mean for all mice of the indicated group. (**C**) *Shigella* colony forming units (CFU) per million cells from the combined intestinal epithelial cell (IEC) enriched fraction of gentamicin-treated cecum and colon tissue. (**D**) Quantification of cecum lengths normalized to mouse weight prior to infection; cecum length (cm) / mouse weight (g). (**E**) The ratio of fecal pellet weight when wet (fresh) divided by the fecal pellet weight after overnight drying. Pellets were collected at day two post-infection. (**F**, **G**) CXCL1 and IL-1β levels measured by ELISA from homogenized cecum and colon tissue of infected mice. (**H**) Blood scores from feces collected at two days post-infection. 1 = occult blood, 2 = macroscopic blood. (**C-H**) Each symbol represents one mouse. Data collected from two independent experiments. Mean ± SD is shown in (**B, D-G**). Geometric mean ± SD is shown in (**C**). Mann-Whitney test, *p < 0.05, **p < 0.01, ***p < 0.001, ****p < 0.0001, ns = not significant (p > 0.05).

inhibits Caspase-11 *in vivo* [55, 115, 120, 121] and further show that OspC3-dependent inhibition of Caspase-11 is required for *Shigella* virulence. Nonetheless, this inhibition is likely incomplete, as Caspase-11 still provides a degree of protection in B6.*Nlrc4*$^{-/-}$ mice even when *Shigella* expresses OspC3 (Figures 3.5, 3.6).

The *Shigella* cycle of pathogenesis likely involves bacterial invasion of both macrophages and IECs [8] and thus, OspC3 might drive virulence by inhibiting Caspase-11 in either or both cell types. To test if OspC3 acts on Caspase-11 in IECs, we generated mouse bone marrow chimeras in which B6.*Nlrc4*$^{-/-}$ mice were used as irradiated recipients and B6.*Nlrc4*$^{-/-}$*Casp11*$^{-/-}$ were used as bone marrow donors (Figure 3.8A). The reconstituted chimeras mice should lack NLRC4 in their IECs and both NLRC4 and CASP11 in their hematopoietic compartment, which includes macrophages. Thus, the only physiologically relevant target of OspC3 in these chimeras should be CASP11 within in the intestinal epithelium. We infected these chimeras with either WT or *ΔospC3 Shigella* and found, similar to the results in B6.*Nlrc4*$^{-/-}$ mice, that *ΔospC3 Shigella* was significantly attenuated relative to WT *Shigella* (Figure 3.8B-I).

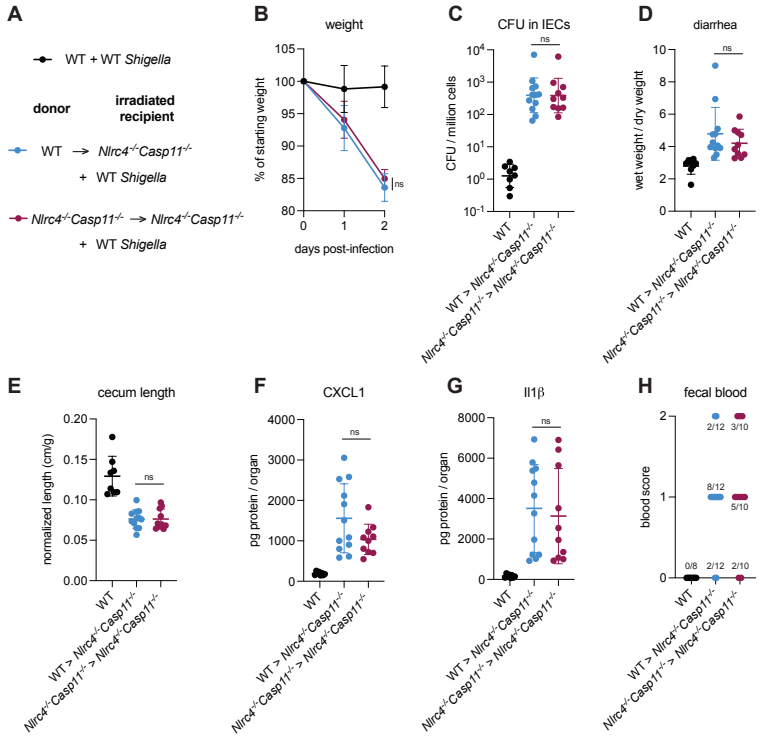

Figure 3.10. Hematopoietic NLRC4 and CASP11 are dispensable for protection against *Shigella* and do not affect *Shigella* pathogenesis

(**A-G**) B6.*Nlrc4*$^{-/-}$*Casp11*$^{-/-}$ recipient mice were lethally irradiated and reconstituted with bone marrow from B6.WT (blue) or B6.*Nlrc4*$^{-/-}$*Casp11*$^{-/-}$ (maroon) donor mice to generate chimeras. Chimeras and B6.WT mice (black) were treated orally with 25 mg streptomycin sulfate in water and then infected one day later with 10^7 CFU of WT *Shigella flexneri.* Mice were littermates or were co-housed for 3 weeks prior to infection and were sacrificed at two days post-infection. (**A**) Legend showing experimental setup. (**B**)) Mouse weights from 0 through 2 days post-infection. Each symbol represents the mean for all mice of the indicated group. (**C**) *Shigella* colony forming units (CFU) per million cells from the combined intestinal epithelial cell (IEC) enriched fraction of gentamicin-treated cecum and colon tissue. (**D**) The ratio of fecal pellet weight when wet (fresh) divided by the fecal pellet weight after overnight drying. Pellets were collected at day two post-infection. (**E**) Quantification of cecum lengths normalized to mouse weight prior to infection; cecum length (cm) / mouse weight (g). (**F**, **G**) CXCL1 and IL-1β levels measured by ELISA from homogenized cecum and colon tissue of infected mice. (**H**) Blood scores from feces collected at two days post-infection. 1 = occult blood, 2 = macroscopic blood. (**C**-**H**) Each symbol represents one mouse. Data collected from two independent experiments. Mean ± SD is shown in (**B, D**-**G**). Geometric mean ± SD is shown in (**C**). Mann-Whitney test, *p < 0.05, **p < 0.01, ***p < 0.001, ****p < 0.0001, ns = not significant (p > 0.05).

These results indicate that OspC3-dependent virulence is driven by inhibition of Caspase-11 specifically in intestinal epithelial cells and not macrophages and further suggest that the protective effect of CASP11 during infection is due to its expression in IECs and not other cell types.

3.3.4 Neither myeloid inflammasomes nor IL-1 affect *Shigella* pathogenesis

The generally accepted model of *Shigella* pathogenesis proposes that *Shigella* cross the colonic epithelium via transcytosis through M-cells [3, 8]. After transcytosis, *Shigella* is then believed to be phagocytosed by macrophages, followed by two additional steps: (1) the inflammasome-dependent lysis of infected macrophages to release bacteria to facilitate epithelial invasion [8, 111, 180, 181], and (2) the concomitant processing and release of IL-1β, a pro-inflammatory cytokine, that drives inflammation [48, 182, 183]. However, the roles of these particular steps during mammalian oral infection have never been addressed experimentally.

To evaluate the role of NLRC4 inflammasome activation in myeloid cells, we utilized i*Nlrc4Lyz2Cre* mice [1]. These mice harbor a germline null mutation in *Nlrc4*, but encode a *Lyz2Cre*-inducible *Nlrc4* cDNA transgene that restores NLRC4 expression selectively in myeloid cells (primarily macrophages, monocytes, and neutrophils). We infected wild-type B6, i*Nlrc4Lyz2Cre,* and B6.*Nlrc4*$^{-/-}$ (*Cre*$^{-}$) mice and compared disease outcomes across genotypes (Figure 3.9). Surprisingly, i*Nlrc4Lyz2Cre* mice phenocopied B6.*Nlrc4*$^{-/-}$ mice, and did not exhibit significant differences in weight-loss, bacterial colonization of the intestinal epithelium, cecum length, or diarrhea (Figure 3.9A-E). There was a modest but insignificant increase in inflammatory cytokines CXCL1 and IL-1β in i*Nlrc4Lyz2Cre* mice (Figure 3.9F, G), but fewer of these mice displayed fecal blood compared to B6.*Nlrc4*$^{-/-}$ mice (Figure 3.9H). These results provide a striking contrast to our previous results with *iNlrc4VilCre* mice in which NLRC4 is selectively expressed in IECs [112]. Unlike *iNlrc4Lyz2Cre* mice, *iNlrc4VilCre* mice were strongly protected from oral *Shigella* infection, implying that epithelial but not myeloid cell NLRC4 is protective. We conclude that NLRC4-dependent pyroptosis in macrophages is neither a major driver of disease pathogenesis nor bacterial colonization in our oral mouse model of infection.

Myeloid cells express multiple inflammasomes including Caspase-11, which plays a modest role in protection against *Shigella* infection in *Nlrc4*$^{-/-}$ mice and is inhibited by OspC3 (see above Figures 3.5-3.7). To evaluate the role of both myeloid NLRC4 and myeloid CASP11 during *in vivo* infection, we generated bone marrow chimeras with B6.*Nlrc4*$^{-/-}$*Casp11*$^{-/-}$ mice as irradiated recipients and either B6.*Nlrc4*$^{-/-}$ *Casp11*$^{-/-}$ and B6.WT mice as bone marrow donors (Figure 3.10A). Following streptomycin treatment, we infected B6.WT mice and these chimeric mice with WT *Shigella* and assessed disease through two days. Consistent with the results in *iNlrc4Lyz2Cre* mice, we observed no significant differences in pathogenesis and disease between reconstituted B6.*Nlrc4*$^{-/-}$*Casp11*$^{-/-}$ mice that received WT bone marrow and reconstituted B6.*Nlrc4*$^{-/-}$*Casp11*$^{-/-}$ mice that received B6.*Nlrc4*$^{-/-}$*Casp11*$^{-/-}$ bone marrow (Figure 3.10B-H). These results refute the generally accepted hypothesis that inflammasome-dependent pyroptosis of macrophages contributes to pathogenesis and indicate that the key role for inflammasomes during *Shigella* infection is in defense of the intestinal epithelial cell niche.

IL-1α and IL-1β are related cytokines that are produced downstream of inflammasome activation in myeloid cells and that signal via the common IL-1 receptor. IL-1 cytokines have been implicated in driving inflammation in the context of mouse intranasal *Shigella* challenge [182] and rabbit ligated intestinal loop infection [48]. To better address the role of IL-1 in shigellosis, we crossed B6.*Nlrc4*$^{-/-}$ mice to B6.*Il1r1*$^{-/-}$

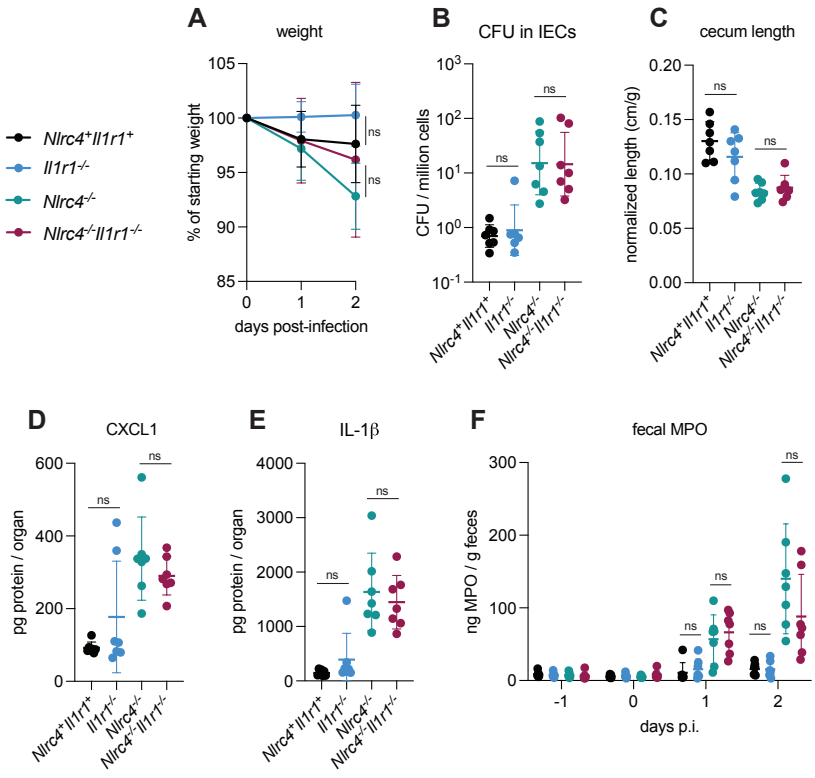

Figure 3.11. IL-1 signaling does not affect *Shigella* pathogenesis
(**A-F**) WT or *Nlrc4*$^{+/-}$*Il1r1*$^{+/-}$ (black), *Il1r1*$^{-/-}$ (blue), *Nlrc4*$^{-/-}$ (teal), and *Nlrc4*$^{-/-}$ *Il1r1*$^{-/-}$ (maroon) littermates were treated orally with 25 mg streptomycin sulfate in water and orally challenged the next day with 10^7 CFU of WT *Shigella flexneri*. Mice were sacrificed at two days post-infection. (**A**) Mouse weights from 0 through 2 days post-infection. Each symbol represents the mean for all mice of the indicated group. (**B**) *Shigella* colony forming units (CFU) per million cells from the combined intestinal epithelial cell (IEC) enriched fraction of gentamicin-treated cecum and colon tissue. (**C**) Quantification of cecum lengths normalized to mouse weight prior to infection; cecum length (cm) / mouse weight (g). (**D, E**) CXCL1 and IL-1β levels measured by ELISA from homogenized cecum and colon tissue of infected mice. (**F**) Myeloperoxidase enzyme levels in mouse feces collected each day prior to and during infection and measured by ELISA. (**B-F**) Each symbol represents one mouse. Data are representative of two independent experiments. Mean ± SD is shown in (**A**, **C-F**). Geometric mean ± SD is shown in (**B**). Mann-Whitney test, *p < 0.05, **p < 0.01, ***p < 0.001, ****p < 0.0001, ns = not significant (p > 0.05).

mice to generate B6.*Nlrc4*$^{-/-}$*Il1r1*$^{-/-}$ double-deficient mice that are susceptible to *Shigella* infection but fail to respond to IL-1. We infected *Nlrc4*$^{+/-}$*Il1r1*$^{+/-}$, *Il1r1*$^{-/-}$, *Nlrc4*$^{-/-}$, and *Nlrc4*$^{-/-}$*Il1r1*$^{-/-}$ littermates and again assessed disease outcomes (Figure 3.11). Surprisingly, *Nlrc4*$^{-/-}$*Il1r1*$^{-/-}$ mice phenocopied *Nlrc4*$^{-/-}$ mice, and we did not observe significant differences in weight-loss, colonization of the intestinal epithelium, normalized cecum lengths, or inflammatory cytokines (Figure 3.11A-E). In many bacterial infections, IL-1 signaling initiates the recruitment of neutrophils to sites of infection. However, we did not observe a significant difference in the amount of the neutrophil marker myeloperoxidase (MPO) in the feces of *Nlrc4*$^{-/-}$*Il1r1*$^{-/-}$ versus *Nlrc4*$^{-/-}$ mice, suggesting that IL-1 might not be essential for neutrophilic inflammation during *Shigella* infection (Figure 3.11F). We also found that *Nlrc4*-sufficient *Il1r1*$^{-/-}$ mice

phenocopy WT mice and are resistant to infection. Overall, these results indicate that, despite the increases in IL-1β consistently seen in susceptible mice, IL-1 signaling is not a primary driver of pathogenesis or protection during oral *Shigella* infection. NLRC4-dependent resistance to shigellosis is therefore likely due to the initiation of pyroptosis and expulsion in IECs and not myeloid cell pyroptosis nor IL-1 signaling. Our results

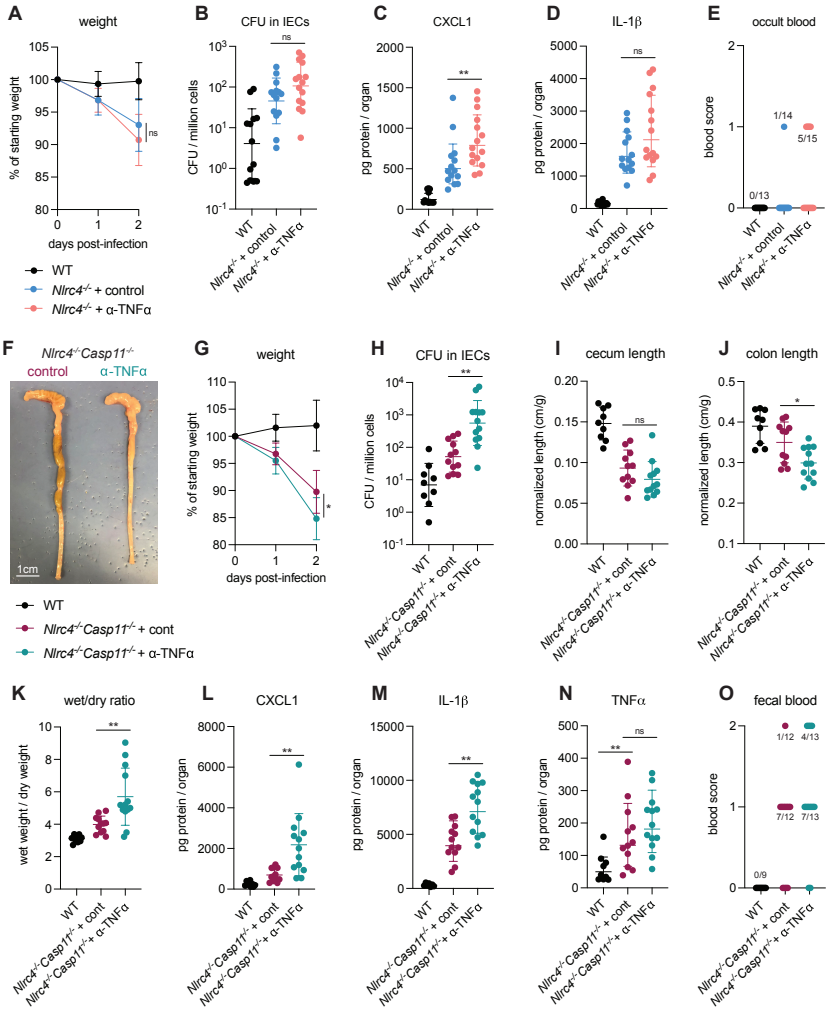

Figure 3.12. TNFα contributes to resistance to *Shigella* when mice lack NLRC4 and CASP11
B6.WT (black), B6.*Nlrc4*$^{-/-}$, and B6.*Nlrc4*$^{-/-}$*Casp11*$^{-/-}$ mice were treated orally with 25 mg streptomycin sulfate in water and orally challenged the next day with 10^7 CFU of WT *Shigella flexneri*. In (**A-E**), B6.*Nlrc4*$^{-/-}$ mice received 200 μg of either TNFα neutralizing antibody (pink) or isotype control antibody (light blue) by intraperitoneal injection daily from one day before infection through sacrifice at two days post-infection. In (**F-O**), B6.*Nlrc4*$^{-/-}$*Casp11*$^{-/-}$ mice received 200 μg of either TNFα neutralizing antibody (teal) or isotype control antibody (maroon) by intraperitoneal injection daily from one day before infection through sacrifice at two days post-infection. (**A, G**) Mouse weights from 0 through 2 days post-infection. Each symbol represents the mean for all mice of the indicated group. (**B, H**) *Shigella* colony forming units (CFU) per million cells from the combined intestinal epithelial cell (IEC) enriched fraction of gentamicin-treated cecum and colon tissue. (**C, D, L-N**) CXCL1, IL-1β, and TNFα levels measured by ELISA from homogenized cecum and colon tissue of infected mice. (**E, O**) Blood scores from feces collected at two days post-infection. 1 = occult blood, 2 = macroscopic blood. (**F**) Representative images of the cecum and colon from B6.*Nlrc4*$^{-/-}$ *Casp11*$^{-/-}$ mice receiving either isotype control or TNFα neutralizing antibody. (**I, J**) Quantification of cecum and colon lengths normalized to mouse weight prior to infection; cecum or colon length (cm) / mouse weight (g). (**K**) The ratio of fecal pellet weight when wet (fresh) divided by the fecal pellet weight after overnight drying. Pellets were collected at day two post-infection. (**B-E, H-O**) Each symbol represents one mouse. Data collected from three independent experiments (**A-E**) and two independent experiments (**F-O**). Mean ± SD is shown in (**A, C, D, G, I-N**). Geometric mean ± SD is shown in (**B, H**). Mann-Whitney test, *p < 0.05, **p < 0.01, ***p < 0.001, ****p < 0.0001, ns = not significant (p > 0.05).

leave open a possible role for another inflammasome-dependent cytokine, IL-18, which unlike IL-1β, is highly expressed in IECs.

3.3.5 TNFα contributes to resistance to *Shigella*

Given that both NLRC4 and CASP11 protect the mouse epithelium from *Shigella* colonization, we reasoned that additional mechanisms of cell death might function in this niche to counteract *Shigella* invasion and spread. Another cell death initiator in the intestine is TNFα, which has been shown to promote *Salmonella*-induced IEC death and dislodgement [84]. TNFα initiates Caspase-8 dependent apoptosis through TNFRI engagement particularly when NF-κB signaling is altered or blocked [98, 99, 101, 184]. *Shigella* encodes several effectors reported to inhibit NF-κB signaling [131-137], and thus, we hypothesized that TNFα might restrict *Shigella* by inducing death of infected IECs.

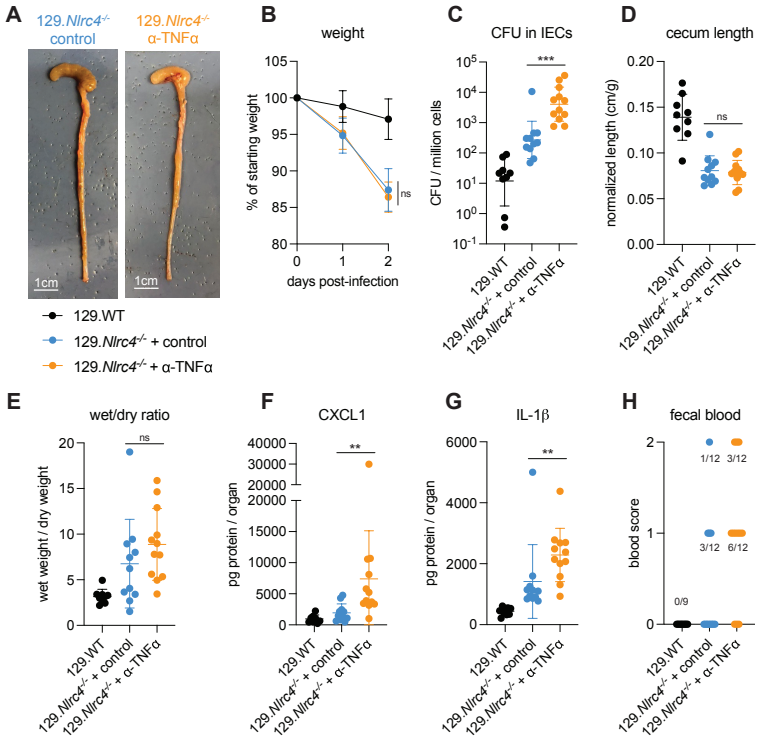

Figure 3.13. TNFα neutralization renders 129.*Nlrc4*$^{-/-}$ mice more susceptible to *Shigella*
(**A-H**) 129.WT (black) and 129.*Nlrc4*$^{-/-}$ mice were treated orally with 25 mg streptomycin sulfate in water and orally challenged the next day with 10^7 CFU of WT *Shigella flexneri*. 129.*Nlrc4*$^{-/-}$ mice also received 200 μg of either TNFα neutralizing antibody (orange) or isotype control antibody (blue) by intraperitoneal injection daily from one day before infection through sacrifice at two days post-infection. (**A**) Representative images of the cecum and colon from 129.*Nlrc4*$^{-/-}$ mice receiving either isotype control or TNFα neutralizing antibody. (**B**) Mouse weights from 0 through 2 days post-infection. Each symbol represents the mean for all mice of the indicated group. (**C**) *Shigella* colony forming units (CFU) per million cells from the combined intestinal epithelial cell (IEC) enriched fraction of gentamicin-treated cecum and colon tissue. (**D**) Quantification of cecum lengths normalized to mouse weight prior to infection; cecum length (cm) / mouse weight (g). (**E**) The ratio of fecal pellet weight when wet (fresh) divided by the fecal pellet weight after overnight drying. Pellets were collected at day two post-infection. (**F**, **G**) CXCL1 and IL-1β levels measured by ELISA from homogenized cecum and colon tissue of infected mice. (**H**) Blood scores from feces collected at two days post-infection. 1 = occult blood, 2 = macroscopic blood. (**C-H**) Each symbol represents one mouse. Data collected from two independent experiments. Mean ± SD is shown in (**B, D-G**). Geometric mean ± SD is shown in (**C**). Mann-Whitney test, *p < 0.05, **p < 0.01, ***p < 0.001, ****p < 0.0001, ns = not significant (p > 0.05).

To assess the *in vivo* role of TNFα during shigellosis, we first infected B6.*Nlrc4*$^{-/-}$ mice treated with an antibody that neutralizes TNFα or with an isotype control antibody (Figure 3.12). B6.*Nlrc4*$^{-/-}$ mice that underwent TNFα neutralization were slightly more susceptible to shigellosis than B6.*Nlrc4*$^{-/-}$ mice treated with control antibody and displayed modest increases in weight-loss, bacterial burdens in IECs, inflammatory cytokines, and fecal blood (Figure 3.12A-E). B6.*Nlrc4*$^{-/-}$ mice express a functional Caspase-11 inflammasome and given the redundancy we observed between NLRC4 and Caspase-11 (Figures 3.1, 3.5, 3.7) [112]), we hypothesized that a protective role for TNFα during *Shigella* infection might be most evident in the absence of both of these cell death pathways. To test this, we repeated the experiment in B6.*Nlrc4*$^{-/-}$*Casp11*$^{-/-}$ mice and, indeed, found that TNFα neutralization on this genetic background significantly increased susceptibility to *Shigella* infection. Mice treated with antibody to TNFα experienced a ~5% increase in weight-loss, a 10-fold increase in bacterial colonization of the intestinal epithelium, and increases in cecal and colonic shrinkage, diarrhea, inflammatory cytokines, and fecal blood (Figure 3.12F-O). TNFα levels were elevated significantly in B6.*Nlrc4*$^{-/-}$*Casp11*$^{-/-}$ mice, indicating that expression of this cytokine is induced in susceptible mice (Figure 3.12N). The anti-TNFα antibody did not decrease the levels of TNFα measured by ELISA because the antibody neutralizes signaling by the cytokine without interfering with its ability to be detected by ELISA.

Importantly, we could also observe a significant protective role for TNFα in similar experiments performed in 129.*Nlrc4*$^{-/-}$ mice that are naturally deficient in Caspase-11 (Figure 3.13), confirming that TNFα-dependent protection is redundant with both NLRC4 and Caspase-11. These results suggest that a hierarchy of cell death pathways protect the intestinal epithelium from *Shigella* infection. NLRC4 appears to be both necessary and sufficient to protect mice from disease, but in the absence of NLRC4, functional CASP11 can provide compensatory protection. However, in the absence of both NLRC4 and Caspase-11, a critical role for TNFα is revealed.

3.3.6 Loss of multiple cell death pathways renders mice hyper-susceptible to *Shigella*

To directly test the role of Caspase-8-dependent cell death during *Shigella* infection, we generated mice lacking either Caspases-1 and 11 (B6.*Casp1/11*$^{-/-}$*Ripk3*$^{-/-}$), Caspase-8 (B6.*Casp8*$^{-/-}$*Ripk3*$^{-/-}$), or Caspases-1, 11, and 8 (B6.*Casp1/11/8*$^{-/-}$*Ripk3*$^{-/-}$). Since loss of Caspase-8 results in Ripk3-depedent embryonic lethality, all three genotypes also lack *Ripk3*. *Casp1/11*$^{-/-}$*Ripk3*$^{-/-}$ mice retain Caspase-8 function downstream of both NLRC4 and TNFα (Figure 3.15) and based on our previous experiments with *Casp1/11*$^{-/-}$ mice [112], we expected that these mice would be resistant to infection. Similarly, *Casp8*$^{-/-}$*Ripk3*$^{-/-}$ mice retain the ability to recruit Caspase-1 to NLRC4 and to initiate cell death via Caspase-11 (Figure 3.15) and should also thus be resistant to infection. *Casp1/11/8*$^{-/-}$*Ripk3*$^{-/-}$ mice, however, should lack the cell death pathways initiated by NLRC4 (via Caspase-1 or Caspase-8), Caspase-11, and TNFα (Figure 3.15), and our results above suggest that these mice might be highly susceptible to infection.

We infected wild-type B6 mice as well as *Casp1/11*$^{-/-}$*Ripk3*$^{-/-}$, *Casp8*$^{-/-}$*Ripk3*$^{-/-}$, and *Casp1/11/8*$^{-/-}$*Ripk3*$^{-/-}$ littermates and assessed disease phenotypes across all four genotypes (Figure 3.14). We found that *Casp8*$^{-/-}$*Ripk3*$^{-/-}$ mice largely phenocopied wild-

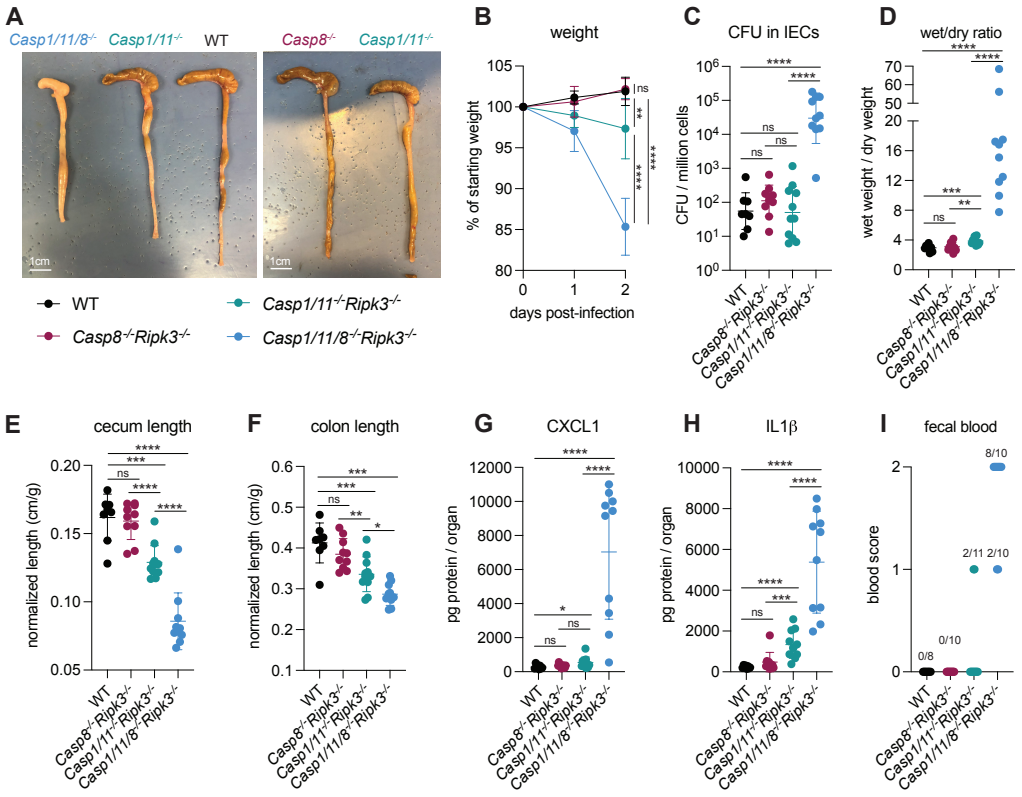

Figure 3.14. Loss of multiple cell death pathways renders mice hyper-susceptible to *Shigella*
(**A-I**) B6.WT mice (black), and B6.*Casp8*$^{-/-}$*Ripk3*$^{-/-}$ (maroon), B6.*Casp1/11*$^{-/-}$*Ripk3*$^{-/-}$ (teal), and B6.*Casp1/11/8*$^{-/-}$*Ripk3*$^{-/-}$ (light blue) littermates were treated orally with 25 mg streptomycin sulfate in water and orally challenged the next day with 10^7 CFU of WT *Shigella flexneri*. Mice were sacrificed at two days post-infection. (**A**) Representative images of the cecum and colon of infected B6.WT, B6.*Casp8*$^{-/-}$*Ripk3*$^{-/-}$, B6.*Casp1/11*$^{-/-}$*Ripk3*$^{-/-}$, and *Casp1/11/8*$^{-/-}$*Ripk3*$^{-/-}$ mice. Note the severe inflammation in the *Casp1/11/8*$^{-/-}$*Ripk3*$^{-/-}$ mice (left-most organs). (**B**) Mouse weights from 0 through 2 days post-infection. Each symbol represents the mean for all mice of the indicated group. (**C**) *Shigella* colony forming units (CFU) per million cells from the combined intestinal epithelial cell (IEC) enriched fraction of gentamicin-treated cecum and colon tissue. (**D**) The ratio of fecal pellet weight when wet (fresh) divided by the fecal pellet weight after overnight drying. Pellets were collected at day two post-infection. (**E, F**) Quantification of cecum and colon lengths normalized to mouse weight prior to infection; cecum or colon length (cm) / mouse weight (g). (**G**, **H**) CXCL1 and IL-1β levels measured by ELISA from homogenized cecum and colon tissue of infected mice. (**I**) Blood scores from feces collected at two days post-infection. 1 = occult blood, 2 = macroscopic blood. (**C-I**) Each symbol represents one mouse. Data collected from two independent experiments. Mean ± SD is shown in (**B, D-H**). Geometric mean ± SD is shown in (**C**). Mann-Whitney test, *p < 0.05, **p < 0.01, ***p < 0.001, ****p < 0.0001, ns = not significant (p > 0.05).

type B6 mice, and were resistant to infection, exhibiting minimal weight-loss, diarrhea, cecal or colonic shrinkage, and fecal blood (Figure 3.14A, B, D, E, F, I). Furthermore, we could not detect significant increases in bacterial burdens in the epithelium (Figure 8C) nor inflammatory cytokines (Figure 3.14G, H) in *Casp8*$^{-/-}$*Ripk3*$^{-/-}$ mice. These results suggest that Caspase-8 alone is not necessary for resistance to *Shigella* in the presence of functional NLRC4–CASP1 and CASP11 inflammasomes. Interestingly, *Casp1/11*$^{-/-}$*Ripk3*$^{-/-}$ mice were not fully resistant to disease and experienced modest weight-loss (~5% relative to WT), diarrhea, cecal and colonic shrinkage, and a small but significant increase in inflammatory cytokines CXCL1 and IL-1β (Figure 3.14A, B, D-H). Two of the eleven *Casp1/11*$^{-/-}$*Ripk3*$^{-/-}$ mice also exhibited occult fecal blood (Figure 3.14I). Despite the modest susceptibility of this genotype, we were unable to detect an increase in bacterial colonization of the intestinal epithelium relative to WT or *Casp8*$^{-/-}$*Ripk3*$^{-/-}$ (Figure 3.14C).

The most striking observation was that *Casp1/11/8*$^{-/-}$*Ripk3*$^{-/-}$ mice were highly susceptible to *Shigella* infection, exhibiting severe weight-loss (~15% of starting weight), diarrhea, and cecal and colonic shrinkage (Figure 3.14A, B, D-F). These mice also exhibited a massive (>500×) increase in bacterial colonization of the epithelium (Figure 3.14C) and elevated levels of inflammatory cytokines (Figure 3.14G, H). All *Casp1/11/8*$^{-/-}$*Ripk3*$^{-/-}$ mice presented with blood in their feces (Figure 3.14I) and one of the ten mice also died of shigellosis within 2 days of infection. The ceca and colons of *Casp1/11/8*$^{-/-}$ *Ripk3*$^{-/-}$ mice were highly inflamed – the tissue thickened, turned white, and sections of the epithelium appeared to have been shed into the lumen, which was completely devoid of feces and filled instead with neutrophilic pus (Figure 3.14A). While the most significant inflammation in B6.*Nlrc4*$^{-/-}$ mice is typically seen in the cecum [112], we noted that the colon of *Casp1/11/8*$^{-/-}$*Ripk3*$^{-/-}$ mice was highly inflamed as well (Figure 3.14A, F), suggesting that a protective role for Caspase-8 might be most important in this organ. Taken together, our results imply that redundant cell death pathways protect mice from disease upon oral *Shigella* challenge. Genetic removal of three caspases essential to this response leads to severe disease and even death. However, removal of one or two caspases critical to this response does not lead to severe disease because of significant compensation from the other pathway(s). We observe a hierarchical importance of the cell death pathways, namely, NLRC4 > CASP11 > TNFα–CASP8 (Figure 3.15). We speculate that this hierarchy may be established by the timing by which a pathway can sense invasive *Shigella* within the epithelium.

3.4 Discussion

We have previously shown that intestinal epithelial cell expression of the NAIP–NLRC4 inflammasome is sufficient to confer resistance to shigellosis in mice [112]. Activation of NAIP–NLRC4 by *Shigella* drives pyroptosis and expulsion of infected IECs. Genetic removal of NAIP–NLRC4 from IECs allows *Shigella* to colonize the intestinal epithelium, an event which drives intestinal inflammation and disease. Mouse IECs, however, deploy additional initiators of programmed cell death [185] and it remained an open question whether these cell death pathways might also counteract *Shigella*.
We utilized the natural variation in 129.*Nlrc4*$^{-/-}$ mice, which lack functional CASP11 [114], to show that CASP11 partially controls the difference in susceptibility between 129.*Nlrc4*$^{-/-}$ and B6.*Nlrc4*$^{-/-}$ mice (Figure 3.1, 3.2). In F_1 129/B6.*Nlrc4*$^{-/-}$ × 129.*Nlrc4*$^{-/-}$ backcrossed mice, which were either 129/129 or B6/129 at the *Casp11* locus, increased disease severity and colonization of the intestinal epithelium was associated with a homozygous null *Casp11*^{129} locus. We also investigated the role of *Hiccs*, a locus present in 129 mice that confers increased susceptibility to *Helicobacter hepaticus*-induced colitis [178]. The 129 *Hiccs* locus contains polymorphisms in the *Alpk1* gene which encodes alpha-kinase 1 (ALPK1), an activator of NF-κB which has been show to sense *Shigella*-derived ADP-heptose in human cells [14]. However, we did not find that *Hiccs* contributed to differences in susceptibility between the two strains (Figure 3.3)

We observed that *ΔospC3 Shigella* is significantly attenuated in B6.*Nlrc4*$^{-/-}$ mice but not in B6.*Nlrc4*$^{-/-}$*Casp11*$^{-/-}$, indicating by a “genetics squared” analysis [186] that *Shigella* effector OspC3 inhibits CASP11 during oral mouse infection (Figures 3.6, 3.7). The striking decrease in colonization of the intestinal epithelium in *ΔospC3*-infected B6.*Nlrc4*$^{-/-}$ mice relative to *ΔospC3*-infected B6.*Nlrc4*$^{-/-}$*Casp11*$^{-/-}$ mice suggests that

CASP11-dependent protection is epithelial intrinsic. *Shigella* also deploys an effector, IpaH7.8, which degrades human (but not mouse) GSDMD to block pyroptosis, further underscoring the importance of this axis in defense [56]. We note that CASP11-dependent protection is not sufficient to render *ΔospC3*-infected B6.*Nlrc4*$^{-/-}$ mice fully resistant to disease symptoms, perhaps because the priming required to induce CASP11 expression might delay its protective response [121].

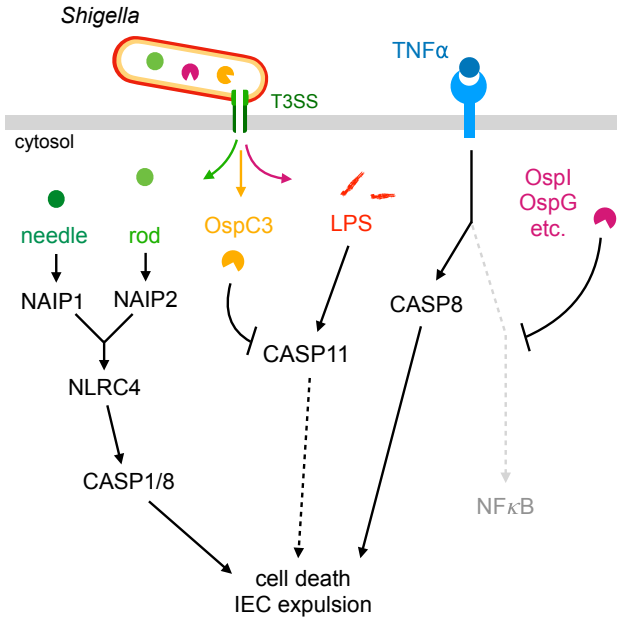

Figure 3.15. *Shigella* activates mouse cell death pathways
Mouse NAIP–NLRC4, CASP11, and CASP8 respond to *Shigella* pathogen associated molecular patterns or activities to initiate cell death. NAIP1 and NAIP2 receptors bind cytosolic needle and rod proteins (green), respectively, that are secreted through the *Shigella* type three secretion system (T3SS) leading to NLRC4 inflammasome formation and CASP1- or CASP8-dependent pyroptosis. CASP11 recognizes cytosolic *Shigella* LPS (read), leading to non-canonical inflammasome formation and pyroptosis which is partially inhibited when *Shigella* expresses effector OspC3 (yellow). TNFα (blue) initiates CASP8-dependent apoptosis through TNFRI when NF-κB signaling is suppressed by *Shigella* effectors (magenta). All three pathways also lead to cell expulsion when activated in intestinal epithelial cells.

Despite its role as a key cell death initiator in the gut [98, 101, 185], TNFα has not yet been shown to play a major role in defense against pathogens that colonize the intestinal epithelium. Indeed, its role is usually detrimental to the host. For example, TNFα is a major driver of pathology during Crohn's Disease [187]. In the context of *Salmonella* infection, TNFα appears to drive widespread pathological death and dislodgement of IECs at 72 hours post-infection [84]. Here, we show that TNFα is protective during oral *Shigella* infection, providing a rationale for why this cytokine is produced in the intestine. In both B6.*Nlrc4*$^{-/-}$*Casp11*$^{-/-}$ and 129.*Nlrc4*$^{-/-}$ mice, TNFα neutralization lead to an increase in severity of infection and a 10-fold increase in bacterial colonization of the intestinal epithelium, suggesting that TNFα-dependent IEC apoptosis restricts colonization of this niche by *Shigella* (Figure 3.12, 3.13). NF-κB-dependent cytokines IL-1β and CXCL1 increase after TNFα neutralization, indicating that protection is not likely driven by the TNFα-dependent activation of NF-κB. An important next step will be to assess whether there is a link between the *Shigella*-dependent inhibition of NF-κB [131-137] and CASP8-dependent apoptosis in IECs.

However, existing reports that *Shigella* suppresses CASP8–dependent apoptosis in human epithelial cells further implicate this pathway in defense [128, 138]. Interestingly, TNFα neutralization in B6.*Nlrc4*$^{-/-}$ mice had only a modest effect on disease susceptibility and colonization of IECs, indicating that TNFα-dependent protection is only fully revealed in the absence of both NLRC4 and CASP11. The protective cell death pathway hierarchy (NLRC4 > CASP11 > TNFα–CASP8) established by these experiments highlights the importance of redundant layers of immunity as a strategy to counteract pathogen evolution (Figure 3.15).

We find that *Casp1/11/8*$^{-/-}$*Ripk3*$^{-/-}$ mice, which lack the pathways to execute pyroptosis, extrinsic apoptosis, and necroptosis, experience severe *Shigellosis* with a 500-fold increase in colonization of the intestinal epithelium relative to B6 wild-type mice (Figure 3.14). Although we did not directly compare the two mouse strains, *Casp1/11/8*$^{-/-}$*Ripk3*$^{-/-}$ mice (Figure 8) experienced more severe disease and epithelial colonization than *Nlrc4*$^{-/-}$*Casp11*$^{-/-}$ mice (Figure 3.5, 3.7). We speculate that the additional susceptibility of *Casp1/11/8*$^{-/-}$*Ripk3*$^{-/-}$ mice partially results from the absence of TNFRI–CASP8-dependent apoptosis and possibly from the absence of RIPK3-dependent necroptosis. However, there likely exist other roles for CASP8 during *Shigella* infection which might further account for its importance [106, 188-192]. Interestingly, *Casp1/11*$^{-/-}$*Ripk3*$^{-/-}$ mice experience modest susceptibility to *Shigella* relative to *Casp8*$^{-/-}$*Ripk3*$^{-/-}$ mice, which are fully protected (Figure 3.14), potentially because NLRC4–CASP8-dependent cell death is delayed relative to NLRC4–CASP1-dependent cell death [1, 193]. Furthermore, CASP8 might be both protective and partially inhibited by a *Shigella* effector [138], thus implicating RIPK3-dependent IEC necroptosis in protection [194]. In the future, a comparison of *Casp1/11*$^{-/-}$ and *Casp1/11*$^{-/-}$*Ripk3*$^{-/-}$ mice could test whether RIPK3-dependent necroptosis provides an additional layer of protection during *Shigella* infection.

Despite the commonly held belief that macrophage pyroptosis and IL-1β release drive *Shigella* pathogenesis [3, 8], we find no major protective or pathogenic role for either during *Shigella* infection (Figure 3.9, 3.10, 3.11). These data suggest that epithelial-specific cell death and expulsion may be the key mechanism that protects mice from *Shigella.* Infections in IL-18 deficient mice will further clarify the role of inflammasome-dependent cytokines in protection. Additional studies in bone marrow chimeric mice or tissue specific knockout mice are required to genetically confirm whether the protective effects of CASP11 and TNFα are epithelial intrinsic.

Here, we illustrate the existence of a layered cell death pathway hierarchy that is essential in defense against oral *Shigella* infection in mice. Our work highlights the significant evolutionary steps required by *Shigella* to overcome these pathways and cause disease in humans. We observed a correlation between bacterial burdens in IECs and pathogenicity in our experiments, indicating that the extent to which *Shigella* can colonize the intestinal epithelium dictates the severity of disease during infection. However, the sensors within IECs that initiate inflammation and drive pathogenicity *in vivo* have yet to be uncovered and might present an ideal pharmacological target to limit pathological inflammation during acute *Shigella* infection.

Chapter Four. Future directions and conclusions

Despite decades of research, the development of an oral mouse model of *Shigella* infection that faithfully recapitulates human shigellosis has remained elusive. In my thesis work, I have identified the genetic and molecular basis of mouse resistance to oral infection with *Shigella*. By challenging mice that lack key inflammasomes and cell death pathways with *Shigella*, I have revealed that cell death and expulsion in the intestinal epithelium dictates resistance to infection. In wild-type mice with a competent NAIP-NLRC4 inflammasome, *Shigella* cannot colonize the intestinal epithelium because of rapid pyroptosis and expulsion of infected IECs. However, in the absence of NAIP–NLRC4-dependent intestinal epithelial cell death and expulsion, *Shigella* can invade, replicate, and disseminate within the intestinal epithelium – a key hallmark of human disease that, until now, has not yet been observed in mice. The removal of additional cell death pathways on the NAIP–NLRC4 knockout background allows for increased *Shigella* colonization of the intestinal epithelium and renders mice more susceptible to infection, indicating that multiple redundant and layered cell death pathways work together to defend this niche against this (and other) intracellular bacteria pathogens. Thus, NAIP–NLRC4 deficient mice serve as the first physiologically relevant mouse model of infection.

The development of this mouse model of shigellosis will allow the field to test several important questions about bacterial virulence, disease progression and pathogenesis, and the immune response to *Shigella* – questions that were much more difficult, if not impossible, to address in previous animal models of shigellosis. Here, I outline the most pressing questions in the field that might be answered using this novel *in vivo* model.

4.1 Why are humans susceptible to infection while mice are resistant?

While it is now clear that both colonization resistance (provided by the host microbiome) and NAIP–NLRC4 dictate mouse resistance to infection, it is not yet clear why humans remain acutely susceptible to natural *Shigella* infection. One hypothesis is that *Shigella* has evolved to compete with and survive within the natural human microbiome but not the mouse microbiome. This hypothesis can be readily tested in the NAIP–NLRC4 knockout mouse model of shigellosis by generating germ-free *Nlrc4*$^{-/-}$ mice, reconstituting their microbiome with defined species from the human microbiome, and infecting these “chimeric” mice to assess if *Shigella* can persist in the gut and establish an infection. By changing individual microbial species within this defined microbiome, one could establish which human-specific microbes are key to resistance and susceptibility in the mouse – studies that could be later extended to humans.

Another pressing questions regarding the differential susceptibility between mice and humans is the role of human NAIP–NLRC4 in protection in the human intestine. While hNAIP–NLRC4 is activated by *Shigella* rod and needle (see chapter one, section four and five and [76, 77]) in human macrophage cell lines and human-derived PBMCs, is not clear whether this inflammasome is active in the intestinal epithelium. Indeed, the high susceptibility of humans to shigellosis would indicate that NAIP–NLRC4 does not provide defense against *Shigella* in human IECs. But whether this is because *Shigella* actively blocks or inhibits human epithelial NAIP–NLRC4 or because NAIP–NLRC4

simply is not expresses in human IECs is not clear. Studies in our lab are addressing these questions, and, despite extensive efforts, we have not yet been able to definitively say that *Shigella* can inhibit the NAIP–NLRC4 pathway or that NAIP–NLRC4 is expressed in human IECs. There is significant evidence, however, that CASP11 is active in human intestinal epithelial cells [82] and that *Shigella* effector OspC3 [115, 120, 121] blocks its activation, indicating that this cell death pathway might instead be the most critical for defense against *Shigella* in the human intestinal epithelium.

4.2 What key events lead to *Shigella* tissue invasion and dissemination?

Numerous *in vitro* studies have established that *Shigella* does not effectively invade the apical surface of intestinal epithelial cells [3, 8] and, thus, must access the basolateral side of cells to establish an infection in the epithelium. How *Shigella* reaches the underside of the epithelium *in vivo* remains an open question. Early studies in primate, rabbit, and guinea pig infection models associated the follicle associated epithelium with sites of epithelial invasion and dissemination (see chapter one, section three and [8]), suggesting that M-cells might serve as a portal for *Shigella* to reach the lamina propria and basolateral epithelium. However, the precise role of M-cells in these processes has never been tested and the experimental depletion of M-cells in mice [195] offers the first opportunity to do so *in vivo*. These experiments would involve the serial administration of RANK-ligand neutralizing antibody to *Nlrc4*$^{-/-}$ mice, which significantly reduces the number of M-cells in the intestine, and the subsequent infection of these mice after confirming that the depletion was effective.

Another open question regarding the progression of *Shigella* infection *in vivo* is the extent to which bacterial colonization of the intestinal epithelium is the result of a small number of initial invasion events and extensive dissemination or a large number of initial invasion events and relatively limited dissemination between adjacent cells. One way to address these questions and test the bacterial population dynamics within a host is to employ an isogenic barcoded labelling technique of the *Shigella* infectious inoculum. STAMP, or sequence tag-based analysis of microbial population dynamics, is a bacterial barcoding technique recently used in *Vibrio cholerae*, *Escherichia coli*, and *Listeria monocytogenes* to quantify population bottlenecks and infer the founding population sizes of events during infection [196-198]. Infecting susceptible *Nlrc4*$^{-/-}$ mice with STAMP labelled *Shigella* would identify key bottlenecks *in vivo* and establish the number of founding invasion events that occur during the colonization of the intestinal epithelium. An understanding of these *in vivo* dynamics would allow for a more precise identification of which events during infection are most important in driving pathogenesis and disease.

4.3 What other innate immune factors limit *Shigella* replication in IECs?

While my thesis work defines cell death and expulsion as critical mediators of resistance to *Shigella* infection, there likely exist other cell intrinsic immune pathways and mediators important for limiting *Shigella* replication and spread within IECs. While studies in other systems have identified autophagy, septin caging, GBP-dependent bacterial coating, and bactericidal GSDMB activity as antimicrobial in the context of *Shigella* infection (see chapter one), these host factors have not yet been tested in a physiological *in vivo* model, and thus, their importance during animal infection remains

to be determined. Indeed, the removal of specific genes within these pathways via CRISPR-Cas9 editing allows for the testing of each in our *Nlrc4*$^{-/-}$ model of infection.

One method to discern the epithelial-intrinsic innate immune responses to *Shigella* infection is to perform RNA sequencing on transcripts from intestinal epithelial cells isolated from resistant wild-type mice and susceptible *Nlrc4*$^{-/-}$ mice. To further increase the precision of these experiments, one could also infect mice with a fluorescently labelled *Shigella* inoculum and sort specifically for cells that are infected or uninfected. Analysis of the expression profiles of these epithelial cells should reveal which key innate immune pathways and components are induced during infection, either directly or indirectly, and begin to establish which additional factors are important for bacterial restriction in this niche.

4.4 What are the drivers of pathogenesis during *Shigella* infection?

One consistent observation from our studies of *Shigella* pathogenesis in susceptible mice is that increases in colonization of the intestinal epithelium correlate with increases in disease. This observation would indicate that the extent to which this niche is colonized dictates the extent of inflammation *in vivo* and further suggests that there are specific innate sensors and pathways within IECs that initiate the inflammatory response to *Shigella.* It has long been assumed that inflammation and pathogenesis during *Shigella* infection is driven by the inflammasome-dependent release of IL-1β from pyroptotic macrophages in concert with the NF-κB-dependent expression and release of CXCL1 and other cytokines from infected or bystander IECs [8]. Our results in *Nlrc4*$^{-/-}$ *Il1r*$^{-/-}$ mice (Figure 3.11), however, indicate that IL-1 is largely dispensable for the initiation of inflammation, and thus, we speculate that IEC-intrinsic inflammatory pathways alone might be sufficient to induce inflammation and pathogenesis.

NOD1, NOD2, and ALPK1 are sensors of *Shigella* PAMPs peptidoglycan and ADP-heptose that have been implicated in the initiation of inflammation during shigellosis (see chapter one and [12-15]). Each sensor is present in the cytosol of IECs and leads to the activation of the NF-κB signaling pathway and the expression and secretion of CXCL1. However, the role of these sensors during *in vivo* infection has not yet been addressed. In chapter three, I provide data on our attempt to map the differences in pathogenesis between 129 and B6 *Nlrc4*$^{-/-}$ mice to the *Hiccs* locus present in the 129 strain. *Hiccs* is associated with colitis during to *helicobacter hepaticus* infection and contains an allele of the *Alpk1* gene with numerous single nucleotide polymorphisms [179]. These observations tentatively implicate *Alpk1* in a hyperactive immune response to *Shigella* which might drive pathogenesis during infection. Our results (Figure 3.3), however, indicate that *Hiccs* is not associated with pathogenesis during shigellosis. A comprehensive investigation of the role of ALPK1 in sensing and inflammation during mouse infection, however, requires the generation of *Alpk1*$^{-/-}$ mice on the B6.*Nlrc4*$^{-/-}$ background.

To study the role of NOD1 and NOD2 in inflammation and pathogenesis during shigellosis, we crossed B6.*Nod1*$^{-/-}$*Nod2*$^{-/-}$ double knockout mice to susceptible B6.*Nlrc4*$^{-/-}$ mice to generate B6.*Nod1*$^{-/-}$*Nod2*$^{-/-}$*Nlrc4*$^{-/-}$ triple knockout mice that are susceptible to *Shigella* infection and are deficient in cytosolic peptidoglycan sensing. We infected these mice with wild-type *Shigella flexneri* and assessed disease phenotypes through two days following infection (Figure 4.1). We hypothesized that in

the absence of NOD1 and NOD2 sensing in susceptible *Nod1*$^{-/-}$*Nod2*$^{-/-}$*Nlrc4*$^{-/-}$ mice, there would be reduced NF-κB signaling from IECs and a subsequent reduction in inflammation and pathogenesis. Despite the proposed role for the NOD1/NOD2 sensors in initiating inflammation via CXCL1, however, we observed only modest decreases in disease severity in *Nod1*$^{-/-}$*Nod2*$^{-/-}$*Nlrc4*$^{-/-}$ mice relative to *Nlrc4*$^{-/-}$ mice. The triple knockouts experienced less cecum shrinkage (Figure 4.1C) than *Nlrc4*$^{-/-}$ mice but there were no significant differences in weight-loss, bacterial burdens in IECs, diarrhea, and inflammatory cytokines, including CXCL1, between the two genotypes (Figure 4.1A, B, D-F). B6.*Nod1*$^{-/-}$*Nod2*$^{-/-}$ were resistant to infection and did not exhibit significant bacterial colonization of IECs, weight-loss, diarrhea, nor makers of inflammation in their tissue, indicating that neither NOD1 nor NOD2 are essential for mouse resistance to shigellosis when mice express NLRC4 (Figure 4.1A-F).

Taken together, these results indicate that NOD1/NOD2-dependent inflammatory signaling is not necessary for initiating the expression of CXCL1 nor the initiation of inflammation *in vivo*. It is possible and perhaps likely that these sensors do typically contribute to inflammation but that there is significant compensation from other pathways that activate NF-κB signaling during infection. A study of the IEC-specific initiators of inflammation *in vivo* would again benefit from a comprehensive RNA-sequencing study on expression transcripts from infected and uninfected intestinal epithelial cells. These experiments and analyses might reveal the specific inflammatory pathways activated in these cells and provide insight into which of these most contribute to inflammation and subsequent disease.

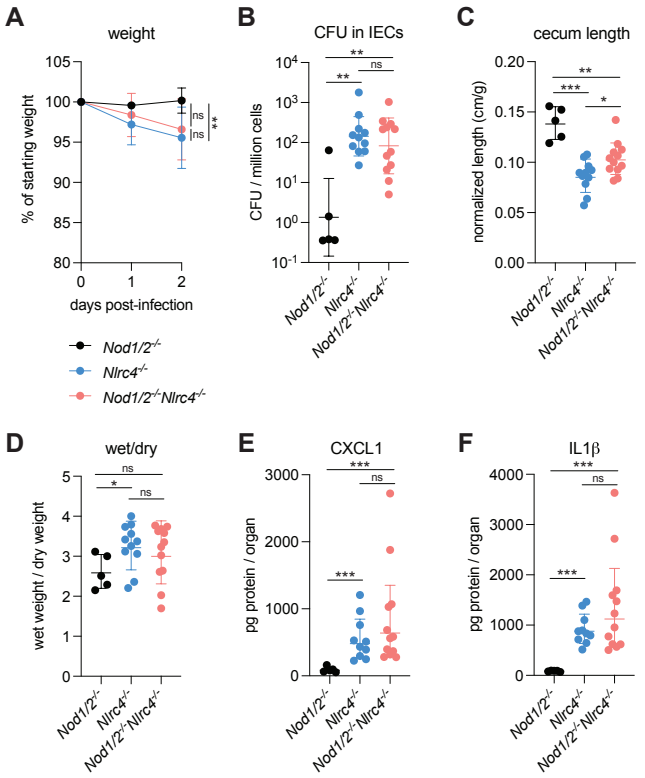

Figure 4.1 — NOD1 and NOD2 deficiency in mice does not affect *Shigella* pathogenesis
(**A-F**) B6.*Nod1*$^{-/-}$*Nod2*$^{-/-}$ (black) and B6.*Nlrc4*$^{-/-}$ (blue) and B6.*Nod1*$^{-/-}$*Nod2*$^{-/-}$*Nlrc4*$^{-/-}$ (pink) mice were treated orally with 25 mg streptomycin sulfate in water and orally challenged the next day with 10^7 CFU of WT *Shigella flexneri.* Mice were sacrificed at two days following infection. (**A**) Mouse weights from 0 through 2 days post-infection. Each symbol represents the mean for all mice of the indicated group. (**B**) *Shigella* colony forming units (CFU) per million cells from the combined intestinal epithelial cell (IEC) enriched fraction of gentamicin-treated cecum and colon tissue. (**C**) Quantification of cecum lengths normalized to mouse weight prior to infection; cecum length (cm) / mouse weight (g). (**D**) The ratio of fecal pellet weight when wet (fresh) divided by the fecal pellet weight after overnight drying. Pellets were collected at day two post-infection. (**E**, **F**) CXCL1 and IL-1β levels measured by ELISA from homogenized cecum and colon tissue of infected mice. (**B-F**) Each symbol represents one mouse. Data collected from one experiment. Mean ± SD is shown in (**A, C-F**). Geometric mean ± SD is shown in (**B**). Mann-Whitney test, *p < 0.05, **p < 0.01, ***p < 0.001, ****p < 0.0001, ns = not significant (p > 0.05). Materials and methods used in this experiment can be found in the "Materials and Methods, Chapter Three" entry of this dissertation.

4.5 What are the role of innate immune cells during infection?

Our results (Figure 2.3), as well as results from studies in humans and other animal models indicate that several innate immune cell subtypes are recruited to the gut or are activated locally during *Shigella* infection. These include macrophages, dendritic cells, NK-cells, innate lymphoid cells, gamma-delta T-cells, and neutrophils [3, 8]. While each cell type has been implicated in defense against *Shigella*, some cell types might be detrimental to the host in the context of infection by contributing to pathological inflammation. The precise role of each cell type in limiting infection or contributing to pathogenesis *in vivo* has not yet been thoroughly investigated. A comprehensive study of innate immune cells during shigellosis would involve the *in vivo* depletion of each cell type by utilizing cell-specific antibody depletions, global and conditional genetic knockouts, and diphtheria toxin dependent depletions – tools that are readily available and effective in mice. Surprisingly, our preliminary studies in infected *Nlrc4*$^{-/-}$ mice receiving anti-Ly6G antibody, which should eliminate neutrophils, indicate that neutrophils do not contribute to inflammation and disease nor to bacterial clearance and disease resolution (data not shown). Indeed, further studies are warranted to understand the role of neutrophils and other cell types during infection.

4.6 What are the adaptive immune correlates of protection?

Perhaps the largest impact of our new oral mouse model of shigellosis is that it allows for the *in vivo* study of the adaptive immune response to *Shigella* in a highly tractable system. As reviewed in chapter one, there is no licensed vaccine to *Shigella* and a poor understanding of the immune correlates of protection [5, 8]. In fact, there remains little consensus on whether the adaptive immune response elicited by natural *Shigella* infection is even effective at preventing re-infection. Massive T and B-cell death has been observed in rectal biopsies of shigellosis patients and many humans experience poor long-lived B-cell immunity and require multiple infections to establish sufficient resistance to further infection [8]. These observations indicate that *Shigella* is effective at subverting or dampening the host adaptive immune response, perhaps to facilitate re-infection and transmission in endemic areas. However, detailed *in vivo* studies of how this occurs are lacking.

A study of the adaptive immune response to *Shigella* and the immune correlates of adaptive protection requires establishing a system of initial infection and rechallenge to establish if there is protection upon secondary infection. Our preliminary results suggest that protection upon secondary infection does occur in mice (data not shown). A dissection of the cellular mechanisms of this immunity might involve the antibody-mediated depletion of $CD4^+$ and $CD8^+$ T-cells upon rechallenge to establish which arms of the T-cell response are important for protection. Furthermore, the establishment of *Igha*$^{-/-}$*Nlrc4*$^{-/-}$ and μ*MT*$^{-/-}$*Nlrc4*$^{-/-}$ double knockout mice, which lack IgA antibody production or are deficient in B-cell maturation (and thus lack all antibody classes), respectively, would provide a valuable means to test the role of antibodies in protection during primary *Shigella* infection and secondary re-challenge. Our lab is currently developing these tools to begin to dissect the correlates of immunity to *Shigella.*

4.7 Concluding remarks

The future directions and experiments that I have outlined above provide only a glimpse of what this new NAIP–NLRC4-defienct mouse model of infection can bring to the field of *Shigella* research. Indeed, using this model, our lab continues to expand our knowledge of the immune response to *Shigella* and the mediators of pathogenesis and defense *in vivo*. We hope and anticipate that other researchers in the field will adopt and employ our mouse model to test the key questions they have been investigating in their own labs. Ultimately, we expect that the wide-spread use of this model will invigorate the state of *Shigella* research and lead to a rigorous testing of many of the fields most pressing question for the first time *in vivo*.

Materials and Methods

Chapter Two

Cell culture

293T cells were cultured in DMEM supplemented with 10% FBS and 2mM L-glutamine. THP1 cells were cultured in RPMI supplemented with 10% FBS and 2mM L-glutamine. B6 primary BMMs were cultured in RPMI supplemented with 10% FBS, 5% mCSF, 100U/ml penicillin, 100mg/ml Streptomycin and 2mM L-glutamine. THP1 cells were a gift from Veit Hornung, and generated as previously described [199]. Cells were grown in media without antibiotics for infection experiments.

Bacterial strains

All experiments were conducted with the *S. flexneri* serovar 2a WT 2457T strain, or the WT-derived virulence plasmid-cured strain BS103 [200] or *icsA* mutant [140, 201]. The *icsA* mutant strain was a gift from Marcia Goldberg. Natural streptomycin resistant strains of 2457T and BS103 were generated by plating cultured bacteria on tryptic soy broth (TSB) plates containing 0.01% Congo Red (CR) and increasing concentrations of streptomycin sulfate. Streptomycin-resistant strains were confirmed to grow indistinguishably from parental strains in TSB broth lacking antibiotics, indicating an absence of streptomycin-dependence.

Toxins

Recombinant proteins for cytosolic delivery of *Shigella* MxiH were produced using the BD BaculoGOLD system for protein expression in insect cells. The MxiH coding sequence was subcloned into pAcSG2-6xHIS-LFn using the primers: PSMpr943 F (BamHI) 5' - GAAAGG GGATCC ATG AGT GTT ACA GTA CCG GAT AAA GAT TGG ACT CTG - 3' and PSMpr944 R (NotI) 5' - GAAAGG GCGGCCGC TTA TCT GAA GTT TTG AAT AAT TGC AGC ATC AAC ATC C - 3'. The PA-6xHIS coding sequence was subcloned from pET22b-PA-6xHIS[158] into pAcSG2 using the primers: PSMpr896 F (XhoI) 5' - GAAAGG CTCGAG ATG GAA GTT AAA CAG GAG AAC CGG TTA TTA AAT GAA TC - 3' and PSMpr897 R (NotI) 5' - GAAAGG GCGGCCGC TCA GTG GTG GTG GTG GTG GTG T - 3'. Constructs were co-transfected with BestBac linearized baculovirus DNA (Expression Systems) into SF9 cells following the manufacturer's protocol to generate infectious baculovirus. Primary virus was amplified in SF9 cells. Recombinant proteins were produced by infecting 2L of High Five cells with 1ml of amplified virus/L cells. Cells were harvested ~60 hours after infection by centrifugation at 500x*g* for 15 minutes. Cell pellets were resuspended in lysis buffer (50mM Tris pH7.4, 150mM NaCl, 1% NP-40 with protease inhibitors) and lysed on ice using a dounce homogenizer. Samples were then clarified at 24,000x*g* for 30 minutes and supernatants were batch bound to 1ml nickel resin for 2 hours at 4^{o}C. Samples were column purified by gravity. Resin was washed with 100ml of wash buffer (20mM Tris pH7.4, 400mM NaCl, 20mM imidizole). Sample was eluted with 1ml fractions of elution buffer (20mM Tris pH7.4, 150mM NaCl, 250mM imidizole). Peak elutions were pooled and buffer exchanged into 20mM Tris pH7.4.

Infection of cells in culture

S. flexneri was grown at 37°C on tryptic soy agar plates containing 0.01% Congo red (CR), supplemented with 100µg/ml spectinomycin and 100 µg/ml carbenicillin for growth of the *icsA* strain. For infections, a single CR-positive colony was inoculated into 5ml TSB and grown shaking overnight at 37°C. Saturated cultures were back-diluted 1:100 in 5ml fresh TSB shaking for ~2 hours at 37°C. THP1 and BMM cells were seeded at 100,000 cells per well of a Nunc F96 MicroWell white polystyrene plate. Bacteria were washed three times in cell culture media, then spinfected onto cells for 10 minutes at 500x*g*. Bacterial invasion was allowed to proceed for an additional 20 minutes at 37°C, followed by three washes in with cell culture media containing 25mg/ml gentamicin. Cells were then maintained in cell culture media containing 2.5mg/ml gentamicin with propidium iodide (Sigma, diluted 1:100 from stock) at 37°C for the duration of the assay (30 minutes to 4 hours). A MOI of 10 was used unless otherwise specified. For suppression assays, PMA-differentiated THP1 cells were infected as described above for 1 hour. Media was then replaced with cell culture media containing 2.5mg/ml gentamicin and propidium iodide (1:100) and either 10µg/ml PA only, PA with 1.0µg/ml LFn-MxiH, or 10µM nigericin. PI uptake was measured using a SpectraMax M2 plate reader, and 100% cell death was set by normalizing values of infected wells to cells lysed with 1% Triton X-100 after background subtraction based on media only controls.

Establishment, propagation and infection of IECs

Primary intestinal epithelial stem cell-derived organoids from the cecum were isolated and maintained in culture as previously described [202]. Each transwell monolayer culture was established 1:1 from a confluent enteroid Matrigel (Corning, 356255) 'dome.' Enteroids were disassociated from Matrigel with 0.25% trypsin for 10 minutes, manually disrupted, resuspended in monolayer culture wash media (ADMEM/F12 supplemented with 20% FBS, 1% L-glutamine) and plated on polycarbonate transwells (Corning, 3413) that had been pre-coated for >1 hour at 37°C with 1:30 Matrigel:wash media. Monolayer cultures were differentiated for 12-14 days in complete monolayer culture media (monolayer culture wash media mixed 1:1 with LWRN-conditioned media supplemented with 10µM Y27632 (Stem Cell), and RANKL (BioLegend) in the absence of SB431542). Two days prior to infection, cells were cultured in antibiotic-free monolayer culture media. Monolayers were treated with 20µM EGTA for 15 minutes prior to *Shigella* infection (MOI=10). Bacterial invasion was allowed to proceed for 2 hours, followed by gentamicin washes as described above to both upper and lower compartments, then maintained in monolayer culture media containing 2.5mg/ml gentamicin with propidium iodide (Sigma, diluted 1:100 from stock) at 37°C for the duration of the assay (1 hour for IF and 8 hours for CFU determination). For IF, cells were washed in PBS, fixed in 4% paraformaldehyde for 15 minutes, permeabilized in 0.1% Triton X-100 for 15 minutes, blocked in PBS with 2% BSA, 0.1% Tween-20 for 1 hour. Primary antibodies were incubated overnight, followed by a one hour incubation with fluorophore-conjugated secondary antibodies and a 10 minute incubation with DAPI and fluorophore-conjugated phalloidin. Slides were analyzed on a Zeiss LSM710. The number and z-axis position of PI-positive cells was performed using Imaris. Antibodies: anti-*Shigella* (Abcam, ab65282), 488 phalloidin (PHDG1-A, Cytoskeleton Inc.), Alexfluor conjugated secondary antibodies (Invitrogen). To determine bacterial

replication in IECs, 8h post-infection monolayers were washed three times with PBS, lysed in 1% Triton X-100, and bacteria were plated for CFU determination.

Reconstituted NAIP–NLRC4 inflammasome activity assays

To reconstitute inflammasome activity in 293T cells, constructs (100ng of each) producing human NAIP, NLRC4, CASP1 and IL-1β were co-transfected with constructs (200ng of each) producing *Shigella* MxiI, MxiH or empty vector (pcDNA3) using Lipofectamine 2000 (Invitrogen) following the manufacturer's protocol and harvested 24 hours post-transfection. For experiments using recombinant proteins, fresh media containing 10μg/ml PA and 1.0μg/ml LFn-MxiH was added to cells for 3-4 hours. In all experiments, cells were lysed in RIPA buffer with protease inhibitor cocktail (Roche).

Immunoblot and antibodies

Lysates were clarified by spinning at 16,100x*g* for 10 minutes at 4^{o}C. Clarified lysates were denatured in SDS loading buffer. Samples were separated on NuPAGE Bis-Tris 4-12% gradient gels (ThermoFisher) following the manufacturer's protocol. Proteins were transferred onto Immobilon-FL PVDF membranes at 375mA for 90 minutes and blocked with Odyssey blocking buffer (Li-Cor). Proteins were detected on a Li-Cor Odyssey Blot Imager using the following primary and secondary antibodies: anti-IL-1β (R&D systems, AF-201-NA), anti-GFP (Clontech, JL8), anti-TUBULIN (Sigma, clone TUB 2.1), Alexfluor-680 conjugated secondary antibodies (Invitrogen).

Animal Procedures

All mice were maintained in a specific pathogen free colony until 1-2 weeks prior to infection, maintained under a 12 hour light-dark cycle (7am to 7pm), and given a standard chow diet (Harlan irradiated laboratory animal diet) ad libitum. Wild-type C57BL/6J and 129S1/SvImJ mice were originally obtained from the Jackson Laboratories. 129.*Nlrc4*$^{-/-}$ animals were generated by targeting *Nlrc4* via CRISPR-Cas9 mutagenesis. CRISPR/Cas9 targeting was performed by pronuclear injection of Cas9 mRNA and sgRNA into fertilized zygotes, essentially as described previously[203]. Founder mice were genotyped by PCR and sequencing using the primers: JLR035 F 5' CAGGTCACAGAAG AAGACCTGAATG 3' and JLR036 R 5' CACCTGGACTCCTGGATTTGG 3'. Founders carrying mutations were bred one generation to wild-type mice to separate modified haplotypes. Homozygous lines were generated by interbreeding heterozygotes carrying matched haplotypes. B6.Δ*Naip* mice were generated as described previously [158]. B6.*Nlrc4*$^{-/-}$ [204] and iNLRC4 [1] mice were previously described. iNLRC4 mice were crossed to the *Nlrc4*$^{-/-}$ line and then further crossed to *Vil1*-cre (Jax strain 004586) transgenic lines on a *Nlrc4*$^{-/-}$ background. Animals used in infection experiments were littermates or, if not possible, were co-housed upon weaning. In rare cases when mice were not co-housed upon weaning, mice were co-housed for at least one week prior to infection. Animals were transferred from a SPF colony to an ABSL2 facility at least one weeks prior to infection. All animal experiments complied with the regulatory standards of, and were approved by, the University of California, Berkeley Animal Care and Use Committee.

***In vivo Shigella* infections**

Mouse infections were performed in 6-16 week old mice. Initially, mice deprived of food and water for 4-6 hours were orally gavaged with 100µL of 250 mg/mL streptomycin sulfate dissolved in water (25 mg/mouse) and placed in a cage with fresh bedding. 24 hours later, mice again deprived of food and water for 4-6 hours were orally gavaged with 100µL of $5x10^8$ CFU ($5x10^7$ CFUs per mouse) of log-phase, streptomycin resistant *Shigella flexneri* 2457T, BS103, or *icsA* mutant 2457T prepared as above and resuspended in PBS. Mouse weights and fecal pellets were recorded or collected daily from one day prior to infection to the day of euthanasia and harvest (usually 2 days post-infection) to assess the severity of disease and biomarkers of inflammation. Infection inputs were determined by serially diluting a fraction of the initial inoculum and plating on TSB plates containing 0.01% CR and 100µg/mL streptomycin.

Fecal CFUs, fecal MPO ELISAs, wet/dry ratio, fecal occult blood

Fecal pellets were collected in 2mL tubes, suspended in 2% FBS in 1mL of PBS containing protease inhibitors, and homogenized. For CFU enumeration, serial dilutions were made in PBS and plated on TSB plates containing 0.01% CR and 100 µg/mL streptomycin sulfate. For MPO ELISAs, fecal homogenates were spun at 2,000*g* and supernatants were plated in triplicate on absorbent immunoassay 96-well plates. Recombinant mouse MPO standard, MPO capture antibody, and MPO sandwich antibody were purchased from R&D. Wet/dry ratios were determined by weighing fecal pellets before and after they had been dried in a fume hood. The presence or absence of fecal occult blood in fresh pellets was determined using a Hemoccult blood testing kit (Beckman Coulter).

Tissue ELISAs

The cecum and colon were isolated from mice at two days post infection and rinsed 5x in PBS to removal fecal contents. Organs were then homogenized in 1mL of 2% FBS in PBS + protease inhibitors, spun down at 2,000*g*, and supernatants were plated in duplicate on absorbent immunoassay 96-well plates. Recombinant mouse IL-1β and KC standards, capture antibodies, and sandwich antibodies were purchased from R&D. IL-18 paired antibodies were purchased from BD Biosciences and eBioscience and recombinant IL-18 standard from eBiosciene.

Histology

Mice were euthanized at two days post-infection by CO_2 inhalation and cervical dislocation. Ceca and colons from mice were isolated, cut longitudinally, removed of lumenal contents, swiss-rolled, and fixed in methacarn followed by transfer to 70% ethanol. Samples were processed by routine histologic methods on an automated tissue processor (TissueTek, Sakura), embedded in paraffin, sectioned at 4µm thickness on a rotary microtome, and mounted on glass slides. Sections were stained with hematoxylin and eosin on an automated histostainer and coverslipped. Histopathological evaluation was performed by light microscopy (Olympus BX45, Olympus Corporation) at magnifications ranging from x20 to x600 by a board-certified veterinary pathologist (I.L.B.) who was blinded to the experimental groups at the time of evaluation. Representative images were generated as Tiff files from digitized histology slides scanned on a digital slide scanner (Leica Aperio AT2, Leica Biosystems). Images were taken using freely downloadable software (Image Scope, Leica Aperio, Leica Biosystems) and processed in Adobe Photoshop. Photo processing was confined to global adjustments of image size, white balance, contrast, brightness, sharpness, or

correction of lens distortion and did not alter the interpretation of the image. Sample preparation, imaging, and histology scoring was conducted by the Unit for Laboratory Animal Medicine at the University of Michigan.

Intestinal CFU determination

To enumerate whole tissue intestinal CFU, ceca and colons from mice were isolated, cut longitudinally and removed of lumenal contents, placed in culture tubes containing 400μg/mL gentamicin antibiotic in PBS, vortexed, and incubated in this solution for 1-2 hours. Organs were washed 5 times in PBS to dilute the gentamicin, homogenized in 1mL of PBS, serially diluted, and plated on TSB agar plates containing 0.01% CR and 100μg/mL streptomycin. To enumerate intracellular CFU from the intestinal epithelial cell fraction of the cecum and colon, organs prepared as above were incubated in RPMI with 5% FBS, 2mM L-glutamine, and 400μg/ml of gentamicin for 1-2 hours. Tissues were then washed 5 times in PBS, cut into 1cm pieces, placed in 15mL of stripping solution (HBSS, 10mM HEPES, 1mM DTT, 2.6mM EDTA), and incubated at 37°C for 25 minutes with gentle agitation. Supernatants were passed through a 100 μm filter and the remaining pieces of tissue were shaken in a 50mL conical with 10 mL of PBS and passed again through the 100μm filter. This enriched epithelial cell fraction was incubated in 50μg/mL gentamicin for 25 minutes on ice, spun at 300x*g* at 4°C for 8 minutes, and washed twice by aspirating the supernatant, resuspending in PBS, and spinning at 300x*g* at 4°C for 5 minutes. After the first wash, a fraction of cells were set aside to determine the cell count. After the second wash, the pellet was resuspended and lysed in 1mL of 1% Triton X-100. Serial dilutions were made from this solution and plated on TSB agar plates containing 0.01% CR and 100μg/ml streptomycin and CR+ positive colonies were counted following overnight incubation at 37°C.

Chapter Three

Animal Procedures

All mice were maintained in a specific pathogen free colony until 1–8 weeks prior to infection, maintained under a 12 hr light-dark cycle (7 am to 7 pm), and given a standard chow diet (Harlan irradiated laboratory animal diet) ad libitum. Animals used in infection experiments were littermates or, if not possible, were generally cohoused upon weaning. In cases when mice were not co-housed upon weaning, mice were cohoused for at least three week prior to infection. Different experimental treatments (comparing disease across different *Shigella* genotypes or antibody treatments) were stratified within mouse genotypes of the same litter, where possible, to ensure that phenotypes were not the result of the differences in different litter microbiomes. Mice were transferred from a SPF colony to an ABSL2 facility at least one week prior to infection. All mouse infections complied with the regulatory standards of, and were approved by, the University of California, Berkeley Animal Care and Use Committee. B6.*Nlrc4*$^{-/-}$ and 129.*Nlrc4*$^{-/-}$ mice were generated as previously described [112, 204]. F_1 129/B6.*Nlrc4*$^{-/-}$ were generated by crossing parental 129.*Nlrc4*$^{-/-}$ and B6.*Nlrc4*$^{-/-}$ mice. F_1 129/B6.*Nlrc4*$^{-/-}$ mice were crossed to parental 129.*Nlrc4*$^{-/-}$ mice to generate backcrossed mice that were either B6/129 or 129/129 at all loci. 129 and B6 *Casp11* alleles were distinguished by PCR and sequencing using the primers B6.129_Casp11_F 5’ GTTATCTATCAGTAGGAAGTGG 3’ and B6.129_Casp11_R 5’ AAACTAATACTTCTTATGAGAGC 3’. 129 mice have a distinguishable 5-bp deletion

encompassing the exon 7 splice acceptor junction [114]. The *Hiccs* locus was genotyped by PCR using the primers D3Mit348_F 5' CATCATGCATACTTTTTTCCTCA 3', D3Mit348_R 5' GCCAAATCATTCACAGCAGA 3', D3Mit319_F 5' TCTCCCTCACTTTTTCCTTCC 3', and D3Mit319_R 5' AACAGCCAGTCCAGCAAATC 3' to distinguish polymorphisms between the B6 and 129 alleles. B6.*Nlrc4*$^{-/-}$*Casp11*$^{-/-}$ animals were generated by targeting *Casp11* via CRISPR-Cas9 mutagenesis in existing B6.*Nlrc4*$^{-/-}$ mice. CRISPR/Cas9 targeting was performed by electroporation of Cas9 protein and sgRNA into fertilized zygotes, essentially as described previously [205]. Founder mice were genotyped by PCR and sequencing using the primers: Casp4_F 5' GTCTTTAGCCCTTGAGAAGGACAC 3' and Casp4_R 5' CACCCCTTCACTTGAGTTTCTCC 3'. Founders carrying mutations were bred one generation to B6.*Nlrc4*$^{-/-}$ mice to separate modified haplotypes. Homozygous lines were generated by interbreeding heterozygotes carrying matched haplotypes. i*Nlrc4* mice [1] were previously described. i*Nlrc4* mice were crossed to the B6.*Nlrc4*$^{-/-}$ line and then further crossed to *Lyz2Cre* (Jax strain 004781) transgenic lines on a B6.*Nlrc4*$^{-/-}$ background to generate i*Nlrc4Lyz2Cre* mice. *Nlrc4*$^{-/-}$*Il1r1*$^{-/-}$ mice were generated by crossing B6.*Nlrc4*$^{-/-}$ mice to B6.*Il1r1*$^{-/-}$ mice (Jax strain 003245). B6.*Casp8*$^{-/-}$*Ripk3*$^{-/-}$, B6.*Casp1/11*$^{-/-}$*Ripk3*$^{-/-}$, and B6.*Casp1/11/8*$^{-/-}$*Ripk3*$^{-/-}$ mice were generated as previously described [1]. For bone marrow chimeras, wild-type donor bone marrow was derived from WT B6.CD45.1 mice (Jax strain 002014). To generate chimeras, 6-12 week old B6.*Nlrc4*$^{-/-}$ and B6.*Nlrc4*$^{-/-}$*Casp11*$^{-/-}$ recipient mice were lethally irradiated (two doses of 500 rads on consecutive days) and received 2x10^6 bone marrow cells via retro-orbital injection from the indicated donor mice. Mice were infected 8–12 weeks after reconstitution. Blood was drawn and flow cytometry was performed to confirm chimerism.

Shigella Strains

Mouse infections were conducted with the *Shigella flexneri* serovar 2a 2457T strain, WT or *ΔospC3* (Mou et al., 2018). Natural streptomycin resistant strains of WT and *ΔospC3* were generated by plating cultured bacteria on tryptic soy broth (TSB) plates containing 0.01% Congo Red (CR) and increasing concentrations of streptomycin sulfate. Streptomycin-resistant strains were confirmed to grow indistinguishably from parental strains in TSB broth lacking antibiotics, indicating an absence of streptomycin-dependence.

In Vivo Shigella Infections and Treatments

Streptomycin resistant *Shigella flexneri* was grown at 37˚C on tryptic soy agar plates containing 0.01% Congo red (CR), supplemented with 100 μg/mL of streptomycin sulfate. For infections, a single CR-positive colony was inoculated into 5 mL TSB and grown shaking overnight at 37˚C. Saturated cultures were back-diluted 1:100 in 5 mL fresh TSB shaking for 2-3 hours at 37˚C. The approximate infectious dose was determined by spectrophotometry (OD_{600} of 1 = 10^8 CFU/mL). Bacteria were pelleted at 5000×*g*, washed twice in PBS, and suspended in PBS for infection by oral gavage. Actual infectious dose was determined by serially diluting a fraction of the initial inoculum and plating on TSB plates containing 0.01% CR and 100 μg/mL streptomycin. Mouse infections were performed in 6–22 week old mice. Initially, mice deprived of food

and water for 4–6 hours were orally gavaged with 100 μL of 250 mg/mL streptomycin sulfate dissolved in water (25 mg/mouse) and placed in a cage with fresh bedding. One day later, mice again deprived of food and water for 4–6 hours were orally gavaged with 100 μL of log-phase, streptomycin resistant *Shigella flexneri* suspended in PBS at a dose of 10^8 CFU/mL (10^7 CFU/mouse). Mouse weights and fecal pellets were recorded or collected daily from 1 day prior to infection to the day of euthanasia and harvest to assess the severity of disease and biomarkers of inflammation. Fecal colonization (CFU/gram of feces) and successful challenge were determined by homogenizing feces collected one day post-infection and plating (see below). In rare cases when mouse feces were not colonized with *Shigella*, mice were omitted from analysis. For each mouse infection experiment, at least three mice were included in each experimental group. All mouse infection experiments were repeated at least one time (with the exception of Figure 1 and Figure 1 – figure supplement 2). Blinding and randomization were applied when co-housing mice and where possible and ARRIVE guidelines were applied when applicable. Each mouse had a unique numbered ear-tag identifier that was only associated with a treatment group or genotype following data collection. For *in vivo* antibody treatments, 200 μg of anti-TNFα antibody (Bio X Cell, clone TN3–19.12) and polyclonal Armenian hamster IgG isotype control antibody (Bio X Cell) were administered by intraperitoneal injection daily starting one day prior to infection.

Fecal CFUs, fecal MPO ELISAs, wet/dry ratio, fecal blood

Fecal pellets were collected in 2 mL tubes, suspended in 1 mL of 2% FBS in PBS containing protease inhibitors, and homogenized using a polytron homogenizer at 18,000 rpm. For CFU enumeration, serial dilutions were made in PBS and plated on TSB plates containing 0.01% CR and 100 mg/mL streptomycin sulfate. For MPO ELISAs, fecal homogenates were spun at 2000×*g* and supernatants were plated in duplicate on absorbent immunoassay 96-well plates. Recombinant mouse MPO standard, MPO capture antibody, and MPO sandwich antibody were purchased from R&D Systems. Wet/dry ratios were determined by weighing fecal pellets before and after they had been dried in a fume hood. The presence or absence of fecal blood in fresh pellets was determined by macroscopic observation or by applying wet fecal samples to detection tabs from a Hemoccult blood testing kit (Beckman Coulter).

Intestinal CFU determination

To enumerate intracellular *Shigella* CFU from the intestinal epithelial cell fraction of mouse ceca and colons, organs were removed from mice upon sacrifice, cut longitudinally and removed of luminal contents by washing in PBS. Tissues were place in 14 mL culture tubes, incubated in RPMI with 5% FBS, 2 mM L-glutamine, 25 mM HEPES, and 400 μg/mL of gentamicin for 1–2 hours, and vortexed briefly. Tissues were then washed five times in PBS, cut into 1 cm pieces, placed in 15 mL of stripping solution (HBSS, 10 mM HEPES, 1 mM DTT, 2.6 mM EDTA), and incubated at 37˚C for 25 min with gentle agitation. Supernatants were passed through a 100 micron filter and the remaining pieces of tissue were shaken vigorously in a 50 mL conical with 10 mL of PBS and passed again through the 100 micron filter. This enriched epithelial cell fraction was incubated in 50 μg/mL gentamicin for 30-40 minutes on ice, spun at 300×*g* at 4˚C for 8 min, and washed twice by aspirating the supernatant, resuspending in PBS,

and spinning at 300×*g* at 4˚C for 5 min. After the first wash, a fraction of cells were set aside to determine the cell count. After the second wash, the pellet was resuspended and lysed in 1 mL of 1% Triton X-100. Serial dilutions were made from this solution and plated on TSB agar plates containing 0.01% CR and 100 μg/ml streptomycin and CR+ positive colonies were counted following overnight incubation at 37˚C.

Tissue ELISAs

After isolating the intestinal epithelial cell fraction (above), the remaining tissue was transferred to a 14 mL culture tube containing 1 mL of PBS containing 2% FBS and protease inhibitors. Organs were homogenized using a polytron homogenizer at 20,000 rpm, centrifuged at 2000×*g*, and supernatants were plated on absorbent immunoassay 96-well plates. Recombinant mouse CXCL1 and IL-1β standards, capture antibodies, and sandwich antibodies were purchased from R and D. TNFα levels were detected using a high sensitivity ELISA from ThermoFisher (order no: BMS607HS).

Immunoblot and antibodies

Lysates were prepared from *Casp11*$^{+/-}$ and *Casp11*$^{-/-}$ mouse bone marrow derived macrophages and clarified by spinning at 16,100×*g* for 10 min at 4˚C. Clarified lysates were denatured in SDS loading buffer. Samples were separated on NuPAGE Bis-Tris 4–12% gradient gels (ThermoFisher) following the manufacturer's protocol. Proteins were transferred onto Immobilon-FL PVDF membranes at 375mA for 90 min and blocked with Odyssey blocking buffer (Li-Cor). Proteins were detected on a Li-Cor Odyssey Blot Imager using an anti-Caspase-11 primary antibody (cone 17D9) and Alexfluor-680 conjugated secondary antibody (Invitrogen).

References

1. Rauch, I., et al., *NAIP-NLRC4 Inflammasomes Coordinate Intestinal Epithelial Cell Expulsion with Eicosanoid and IL-18 Release via Activation of Caspase-1 and -8.* Immunity, 2017. **46**(4): p. 649-659.
2. Hale, T.L., Keusch, G.T., *Chapeter 22: Shigella*, in *Medical Microbiology*, S. Baron, Editor. 1996, University of Texas Medical Branch at Galveston Galveston (TX).
3. Schroeder, G.N. and H. Hilbi, *Molecular pathogenesis of Shigella spp.: controlling host cell signaling, invasion, and death by type III secretion.* Clin Microbiol Rev, 2008. **21**(1): p. 134-56.
4. Khalil, I.A., et al., *Morbidity and mortality due to shigella and enterotoxigenic Escherichia coli diarrhoea: the Global Burden of Disease Study 1990-2016.* Lancet Infect Dis, 2018. **18**(11): p. 1229-1240.
5. Kotloff, K.L., et al., *Shigellosis.* Lancet, 2018. **391**(10122): p. 801-812.
6. Ranjbar, R. and A. Farahani, *Shigella: Antibiotic-Resistance Mechanisms And New Horizons For Treatment.* Infect Drug Resist, 2019. **12**: p. 3137-3167.
7. Phalipon, A. and P.J. Sansonetti, *Shigella's ways of manipulating the host intestinal innate and adaptive immune system: a tool box for survival?* Immunol Cell Biol, 2007. **85**(2): p. 119-29.
8. Schnupf, P. and P.J. Sansonetti, *Shigella Pathogenesis: New Insights through Advanced Methodologies.* Microbiol Spectr, 2019. **7**(2).
9. Freter, R., *Experimental enteric Shigella and Vibrio infections in mice and guinea pigs.* J Exp Med, 1956. **104**(3): p. 411-8.
10. Anderson, M.C., et al., *Shigella sonnei Encodes a Functional T6SS Used for Interbacterial Competition and Niche Occupancy.* Cell Host Microbe, 2017. **21**(6): p. 769-776 e3.
11. McGuire, C.D. and T.M. Floyd, *Studies on experimental shigellosis. I. Shigella infections of normal mice.* J Exp Med, 1958. **108**(2): p. 269-76.
12. Girardin, S.E., et al., *Nod1 detects a unique muropeptide from gram-negative bacterial peptidoglycan.* Science, 2003. **300**(5625): p. 1584-7.
13. Girardin, S.E., et al., *Nod2 is a general sensor of peptidoglycan through muramyl dipeptide (MDP) detection.* J Biol Chem, 2003. **278**(11): p. 8869-72.
14. Zhou, P., et al., *Alpha-kinase 1 is a cytosolic innate immune receptor for bacterial ADP-heptose.* Nature, 2018. **561**(7721): p. 122-126.
15. Girardin, S.E., et al., *CARD4/Nod1 mediates NF-kappaB and JNK activation by invasive Shigella flexneri.* EMBO Rep, 2001. **2**(8): p. 736-42.
16. Lehman, H.K. and B.H. Segal, *The role of neutrophils in host defense and disease.* J Allergy Clin Immunol, 2020. **145**(6): p. 1535-1544.
17. Weinrauch, Y., et al., *Neutrophil elastase targets virulence factors of enterobacteria.* Nature, 2002. **417**(6884): p. 91-4.
18. Schuch, R. and A.T. Maurelli, *Virulence plasmid instability in Shigella flexneri 2a is induced by virulence gene expression.* Infect Immun, 1997. **65**(9): p. 3686-92.
19. SHAUGHNESSY, H.J. and R.C. OLSSON, *Experimental human bacillary dysentery; polyvalent dysentery vaccine in its prevention.* J Am Med Assoc, 1946. **132**: p. 362-8.

20. Porter, C.K., et al., *The Shigella human challenge model.* Epidemiol Infect, 2013. **141**(2): p. 223-32.
21. Kotloff, K.L., et al., *A modified Shigella volunteer challenge model in which the inoculum is administered with bicarbonate buffer: clinical experience and implications for Shigella infectivity.* Vaccine, 1995. **13**(16): p. 1488-94.
22. Cohen, D., R. Slepon, and M.S. Green, *Sociodemographic factors associated with serum anti-Shigella lipopolysaccharide antibodies and shigellosis.* Int J Epidemiol, 1991. **20**(2): p. 546-50.
23. Cohen, D., et al., *Threshold protective levels of serum IgG to Shigella lipopolysaccharide: re-analysis of Shigella vaccine trials data.* Clin Microbiol Infect, 2022.
24. Ferreccio, C., et al., *Epidemiologic patterns of acute diarrhea and endemic Shigella infections in children in a poor periurban setting in Santiago, Chile.* Am J Epidemiol, 1991. **134**(6): p. 614-27.
25. B. A. Lapin, B.A., Yakovleva, L. A., *Sukhumi Primate Studies: Comparative Pathology in Monkeys*. 1963, Science: Translated from the Russian by the U.S. Joint Publications Research Service. Thomas, Springfield, III.
26. Banish, L.D., et al., *Prevalence of shigellosis and other enteric pathogens in a zoologic collection of primates.* J Am Vet Med Assoc, 1993. **203**(1): p. 126-32.
27. Takeuchi, A., *Early colonic lesions in experimental Shigella infection in rhesus monkeys: revisited.* Vet Pathol Suppl, 1982. **7**: p. 1-8.
28. Rout, W.R., et al., *Pathophysiology of Shigella diarrhea in the rhesus monkey: intestinal transport, morphological, and bacteriological studies.* Gastroenterology, 1975. **68**(2): p. 270-8.
29. OGAWA, H., et al., *SHIGELLOSIS IN CYNOMOLGUS MONEKYS (MACACA IRUS). 3. HISTOPATHOLOGICAL STUDIES ON NATURAL AND EXPERIMENTAL SHIGELLOSIS.* Jpn J Med Sci Biol, 1964. **17**: p. 321-32.
30. Ogawa, H., et al., *Shigellosis in cynomolgus monkeys (Macaca irus). IV. Bacteriological and histopathological observations on the earlier stage of experimental infection with Shigella flexneri 2 A.* Jpn J Med Sci Biol, 1966. **19**(1): p. 22-32.
31. Sansonetti, P.J., et al., *OmpB (osmo-regulation) and icsA (cell-to-cell spread) mutants of Shigella flexneri: vaccine candidates and probes to study the pathogenesis of shigellosis.* Vaccine, 1991. **9**(6): p. 416-22.
32. Takeuchi, A., S.B. Formal, and H. Sprinz, *Exerimental acute colitis in the Rhesus monkey following peroral infection with Shigella flexneri. An electron microscope study.* Am J Pathol, 1968. **52**(3): p. 503-29.
33. Sansonetti, P.J. and J. Arondel, *Construction and evaluation of a double mutant of Shigella flexneri as a candidate for oral vaccination against shigellosis.* Vaccine, 1989. **7**(5): p. 443-50.
34. Shipley, S.T., et al., *A challenge model for Shigella dysenteriae 1 in cynomolgus monkeys (Macaca fascicularis).* Comp Med, 2010. **60**(1): p. 54-61.
35. Levine, M.M., et al., *Clinical trials of Shigella vaccines: two steps forward and one step back on a long, hard road.* Nat Rev Microbiol, 2007. **5**(7): p. 540-53.
36. Harding, J.D., *Nonhuman Primates and Translational Research: Progress, Opportunities, and Challenges.* ILAR J, 2017. **58**(2): p. 141-150.

37. Rabbani, G.H., et al., *Development of an improved animal model of shigellosis in the adult rabbit by colonic infection with Shigella flexneri 2a.* Infect Immun, 1995. **63**(11): p. 4350-7.
38. Shim, D.H., et al., *New animal model of shigellosis in the Guinea pig: its usefulness for protective efficacy studies.* J Immunol, 2007. **178**(4): p. 2476-82.
39. Sereny, B., *Experimental shigella keratoconjunctivitis; a preliminary report.* Acta Microbiol Acad Sci Hung, 1955. **2**(3): p. 293-6.
40. Barman, S., et al., *Development of a new guinea-pig model of shigellosis.* FEMS Immunol Med Microbiol, 2011. **62**(3): p. 304-14.
41. Keren, D.F., et al., *Atrophy of villi with hypertrophy and hyperplasia of Paneth cells in isolated (thiry-Vella) ileal loops in rabbits. Light-microscopic studies.* Gastroenterology, 1975. **68**(1): p. 83-93.
42. Arm, H.G., et al., *Use of ligated segments of rabbit small intestine in experimental shigellosis.* J Bacteriol, 1965. **89**: p. 803-9.
43. Yum, L.K., et al., *Critical role of bacterial dissemination in an infant rabbit model of bacillary dysentery.* Nat Commun, 2019. **10**(1): p. 1826.
44. Wassef, J.S., D.F. Keren, and J.L. Mailloux, *Role of M cells in initial antigen uptake and in ulcer formation in the rabbit intestinal loop model of shigellosis.* Infect Immun, 1989. **57**(3): p. 858-63.
45. Arena, E.T., et al., *Bioimage analysis of Shigella infection reveals targeting of colonic crypts.* Proc Natl Acad Sci U S A, 2015. **112**(25): p. E3282-90.
46. Sansonetti, P.J., et al., *Interleukin-8 controls bacterial transepithelial translocation at the cost of epithelial destruction in experimental shigellosis.* Infect Immun, 1999. **67**(3): p. 1471-80.
47. Perdomo, O.J., et al., *Acute inflammation causes epithelial invasion and mucosal destruction in experimental shigellosis.* J Exp Med, 1994. **180**(4): p. 1307-19.
48. Sansonetti, P.J., et al., *Role of interleukin-1 in the pathogenesis of experimental shigellosis.* J Clin Invest, 1995. **96**(2): p. 884-92.
49. Kuehl, C.J., et al., *An Oral Inoculation Infant Rabbit Model for.* mBio, 2020. **11**(1).
50. Duggan, G.M. and S. Mostowy, *Use of zebrafish to study Shigella infection.* Disease Models & Mechanisms, 2018. **11**(2).
51. Howlader, D.R., et al., *An Experimental Adult Zebrafish Model for Shigella Pathogenesis, Transmission, and Vaccine Efficacy Studies.* Microbiology Spectrum, 2022. **10**(3): p. e0034722.
52. Mostowy, S., et al., *The zebrafish as a new model for the in vivo study of Shigella flexneri interaction with phagocytes and bacterial autophagy.* PLoS Pathog, 2013. **9**(9): p. e1003588.
53. Koestler, B.J., C.M. Ward, and S.M. Payne, *Shigella Pathogenesis Modeling with Tissue Culture Assays.* Curr Protoc Microbiol, 2018. **50**(1): p. e57.
54. Freed, N.E., D. Bumann, and O.K. Silander, *Combining Shigella Tn-seq data with gold-standard E. coli gene deletion data suggests rare transitions between essential and non-essential gene functionality.* BMC Microbiol, 2016. **16**(1): p. 203.
55. Mou, X., et al., *Synthetic bottom-up approach reveals the complex interplay of Shigella effectors in regulation of epithelial cell death.* Proc Natl Acad Sci U S A, 2018. **115**(25): p. 6452-6457.

56. Luchetti, G., et al., *Shigella ubiquitin ligase IpaH7.8 targets gasdermin D for degradation to prevent pyroptosis and enable infection.* Cell Host Microbe, 2021. **29**(10): p. 1521-1530.e10.
57. Koestler, B.J., et al., *Human Intestinal Enteroids as a Model System of.* Infect Immun, 2019. **87**(4).
58. Ranganathan, S., et al., *Evaluating Shigella flexneri Pathogenesis in the Human Enteroid Model.* Infect Immun, 2019. **87**(4).
59. Nickerson, K.P., et al., *A Versatile Human Intestinal Organoid-Derived Epithelial Monolayer Model for the Study of Enteric Pathogens.* Microbiol Spectr, 2021. **9**(1): p. e0000321.
60. Singer, M. and P.J. Sansonetti, *IL-8 is a key chemokine regulating neutrophil recruitment in a new mouse model of Shigella-induced colitis.* J Immunol, 2004. **173**(6): p. 4197-206.
61. Medeiros, Q.S.P.H., et al., *A murine model of diarrhea, growth impairment and metabolic disturbances with Shigella flexneri infection and the role of zinc deficiency.* Gut Microbes, 2019. **10**(5): p. 615-630.
62. Fernandez, M.I., et al., *A newborn mouse model for the study of intestinal pathogenesis of shigellosis.* Cell Microbiol, 2003. **5**(7): p. 481-91.
63. Zhang, Z., et al., *Shigella infection in a SCID mouse-human intestinal xenograft model: role for neutrophils in containing bacterial dissemination in human intestine.* Infect Immun, 2001. **69**(5): p. 3240-7.
64. Voino-Yasenetsky, M.V. and M.K. Voino-Yasenetsky, *Experimental pneumonia caused by bacteria of the Shigella group.* Acta Morphol Acad Sci Hung, 1962. **11**: p. 439-54.
65. Phalipon, A., et al., *Monoclonal immunoglobulin A antibody directed against serotype-specific epitope of Shigella flexneri lipopolysaccharide protects against murine experimental shigellosis.* J Exp Med, 1995. **182**(3): p. 769-78.
66. Yang, J.Y., et al., *A mouse model of shigellosis by intraperitoneal infection.* J Infect Dis, 2014. **209**(2): p. 203-15.
67. Xu, D., et al., *Human Enteric α-Defensin 5 Promotes Shigella Infection by Enhancing Bacterial Adhesion and Invasion.* Immunity, 2018. **48**(6): p. 1233-1244.e6.
68. Fukuda, S., K. Hase, and H. Ohno, *Application of a mouse ligated Peyer's patch intestinal loop assay to evaluate bacterial uptake by M cells.* J Vis Exp, 2011(58).
69. Bravo, V., et al., *Distinct mutations led to inactivation of type 1 fimbriae expression in Shigella spp.* PLoS One, 2015. **10**(3): p. e0121785.
70. Xu, D., et al., *Human Enteric Defensin 5 Promotes Shigella Infection of Macrophages.* Infect Immun, 2019. **88**(1).
71. Chang, S.Y., et al., *Autophagy controls an intrinsic host defense to bacteria by promoting epithelial cell survival: a murine model.* PLoS One, 2013. **8**(11): p. e81095.
72. Jorgensen, I., M. Rayamajhi, and E.A. Miao, *Programmed cell death as a defence against infection.* Nat Rev Immunol, 2017. **17**(3): p. 151-164.
73. von Moltke, J., et al., *Recognition of bacteria by inflammasomes.* Annu Rev Immunol, 2013. **31**: p. 73-106.

74. He, W.T., et al., *Gasdermin D is an executor of pyroptosis and required for interleukin-1β secretion.* Cell Res, 2015. **25**(12): p. 1285-98.
75. Kofoed, E.M. and R.E. Vance, *Innate immune recognition of bacterial ligands by NAIPs determines inflammasome specificity.* Nature, 2011. **477**(7366): p. 592-5.
76. Yang, J., et al., *Human NAIP and mouse NAIP1 recognize bacterial type III secretion needle protein for inflammasome activation.* Proc Natl Acad Sci U S A, 2013. **110**(35): p. 14408-13.
77. Reyes Ruiz, V.M., et al., *Broad detection of bacterial type III secretion system and flagellin proteins by the human NAIP/NLRC4 inflammasome.* Proc Natl Acad Sci U S A, 2017. **114**(50): p. 13242-13247.
78. Zhao, Y., et al., *The NLRC4 inflammasome receptors for bacterial flagellin and type III secretion apparatus.* Nature, 2011. **477**(7366): p. 596-600.
79. Lamkanfi, M. and V.M. Dixit, *Mechanisms and functions of inflammasomes.* Cell, 2014. **157**(5): p. 1013-22.
80. Man, S.M., et al., *Salmonella infection induces recruitment of Caspase-8 to the inflammasome to modulate IL-1β production.* J Immunol, 2013. **191**(10): p. 5239-46.
81. Sellin, M.E., et al., *Epithelium-intrinsic NAIP/NLRC4 inflammasome drives infected enterocyte expulsion to restrict Salmonella replication in the intestinal mucosa.* Cell Host Microbe, 2014. **16**(2): p. 237-248.
82. Naseer, N., et al., *Salmonella enterica Serovar Typhimurium Induces NAIP/NLRC4- and NLRP3/ASC-Independent, Caspase-4-Dependent Inflammasome Activation in Human Intestinal Epithelial Cells.* Infect Immun, 2022. **90**(7): p. e0066321.
83. Pereira, M.S., et al., *The Nlrc4 Inflammasome Contributes to Restriction of Pulmonary Infection by Flagellated Legionella spp. that Trigger Pyroptosis.* Front Microbiol, 2011. **2**: p. 33.
84. Fattinger, S.A., et al., *Epithelium-autonomous NAIP/NLRC4 prevents TNF-driven inflammatory destruction of the gut epithelial barrier in Salmonella-infected mice.* Mucosal Immunol, 2021. **14**(3): p. 615-629.
85. Miao, E.A., et al., *Cytoplasmic flagellin activates caspase-1 and secretion of interleukin 1beta via Ipaf.* Nat Immunol, 2006. **7**(6): p. 569-75.
86. Sauer, J.D., et al., *Listeria monocytogenes engineered to activate the Nlrc4 inflammasome are severely attenuated and are poor inducers of protective immunity.* Proc Natl Acad Sci U S A, 2011. **108**(30): p. 12419-24.
87. Miao, E.A., et al., *Caspase-1-induced pyroptosis is an innate immune effector mechanism against intracellular bacteria.* Nat Immunol, 2010. **11**(12): p. 1136-42.
88. Matikainen, S., T.A. Nyman, and W. Cypryk, *Function and Regulation of Noncanonical Caspase-4/5/11 Inflammasome.* J Immunol, 2020. **204**(12): p. 3063-3069.
89. Knodler, L.A., et al., *Noncanonical inflammasome activation of caspase-4/caspase-11 mediates epithelial defenses against enteric bacterial pathogens.* Cell Host Microbe, 2014. **16**(2): p. 249-256.
90. Maltez, V.I. and E.A. Miao, *Reassessing the Evolutionary Importance of Inflammasomes.* J Immunol, 2016. **196**(3): p. 956-62.

91. Crowley, S.M., et al., *Intestinal restriction of Salmonella Typhimurium requires caspase-1 and caspase-11 epithelial intrinsic inflammasomes.* PLoS Pathog, 2020. **16**(4): p. e1008498.
92. Holly, M.K., et al., *Salmonella enterica infection of murine and human enteroid-derived monolayers elicits differential activation of epithelial-intrinsic inflammasomes.* Infect Immun, 2020.
93. D'Arcy, M.S., *Cell death: a review of the major forms of apoptosis, necrosis and autophagy.* Cell Biol Int, 2019. **43**(6): p. 582-592.
94. Webster, J.D. and D. Vucic, *The Balance of TNF Mediated Pathways Regulates Inflammatory Cell Death Signaling in Healthy and Diseased Tissues.* Front Cell Dev Biol, 2020. **8**: p. 365.
95. Ashida, H., et al., *Cell death and infection: a double-edged sword for host and pathogen survival.* J Cell Biol, 2011. **195**(6): p. 931-42.
96. Negroni, A., S. Cucchiara, and L. Stronati, *Apoptosis, Necrosis, and Necroptosis in the Gut and Intestinal Homeostasis.* Mediators Inflamm, 2015. **2015**: p. 250762.
97. Subramanian, S., H. Geng, and X.D. Tan, *Cell death of intestinal epithelial cells in intestinal diseases.* Sheng Li Xue Bao, 2020. **72**(3): p. 308-324.
98. Ruder, B., R. Atreya, and C. Becker, *Tumour Necrosis Factor Alpha in Intestinal Homeostasis and Gut Related Diseases.* Int J Mol Sci, 2019. **20**(8).
99. Leppkes, M., et al., *Pleiotropic functions of TNF-α in the regulation of the intestinal epithelial response to inflammation.* Int Immunol, 2014. **26**(9): p. 509-15.
100. Grabinger, T., et al., *Inhibitor of Apoptosis Protein-1 Regulates Tumor Necrosis Factor-Mediated Destruction of Intestinal Epithelial Cells.* Gastroenterology, 2017. **152**(4): p. 867-879.
101. Piguet, P.F., et al., *TNF-induced enterocyte apoptosis in mice is mediated by the TNF receptor 1 and does not require p53.* Eur J Immunol, 1998. **28**(11): p. 3499-505.
102. Saavedra, P.H.V., et al., *Apoptosis of intestinal epithelial cells restricts Clostridium difficile infection in a model of pseudomembranous colitis.* Nat Commun, 2018. **9**(1): p. 4846.
103. Upton, J.W., W.J. Kaiser, and E.S. Mocarski, *DAI/ZBP1/DLM-1 complexes with RIP3 to mediate virus-induced programmed necrosis that is targeted by murine cytomegalovirus vIRA.* Cell Host Microbe, 2012. **11**(3): p. 290-7.
104. Newton, K. and G. Manning, *Necroptosis and Inflammation.* Annu Rev Biochem, 2016. **85**: p. 743-63.
105. Kaiser, W.J., et al., *RIP3 mediates the embryonic lethality of caspase-8-deficient mice.* Nature, 2011. **471**(7338): p. 368-72.
106. Weng, D., et al., *Caspase-8 and RIP kinases regulate bacteria-induced innate immune responses and cell death.* Proc Natl Acad Sci U S A, 2014. **111**(20): p. 7391-6.
107. Murphy, J.M., et al., *The pseudokinase MLKL mediates necroptosis via a molecular switch mechanism.* Immunity, 2013. **39**(3): p. 443-53.

108. Zhang, D.W., et al., *RIP3, an energy metabolism regulator that switches TNF-induced cell death from apoptosis to necrosis.* Science, 2009. **325**(5938): p. 332-6.
109. Cho, Y.S., et al., *Phosphorylation-driven assembly of the RIP1-RIP3 complex regulates programmed necrosis and virus-induced inflammation.* Cell, 2009. **137**(6): p. 1112-23.
110. Suzuki, S., et al., *Shigella type III secretion protein MxiI is recognized by Naip2 to induce Nlrc4 inflammasome activation independently of Pkcδ.* PLoS Pathog, 2014. **10**(2): p. e1003926.
111. Suzuki, T., et al., *Differential regulation of caspase-1 activation, pyroptosis, and autophagy via Ipaf and ASC in Shigella-infected macrophages.* PLoS Pathog, 2007. **3**(8): p. e111.
112. Mitchell, P.S., et al., *NAIP-NLRC4-deficient mice are susceptible to shigellosis.* Elife, 2020. **9**.
113. Hagar, J.A., et al., *Cytoplasmic LPS activates caspase-11: implications in TLR4-independent endotoxic shock.* Science, 2013. **341**(6151): p. 1250-3.
114. Kayagaki, N., et al., *Non-canonical inflammasome activation targets caspase-11.* Nature, 2011. **479**(7371): p. 117-21.
115. Kobayashi, T., et al., *The Shigella OspC3 effector inhibits caspase-4, antagonizes inflammatory cell death, and promotes epithelial infection.* Cell Host Microbe, 2013. **13**(5): p. 570-583.
116. Shi, J., et al., *Inflammatory caspases are innate immune receptors for intracellular LPS.* Nature, 2014. **514**(7521): p. 187-92.
117. Wandel, M.P., et al., *Guanylate-binding proteins convert cytosolic bacteria into caspase-4 signaling platforms.* Nat Immunol, 2020. **21**(8): p. 880-891.
118. Pilla, D.M., et al., *Guanylate binding proteins promote caspase-11-dependent pyroptosis in response to cytoplasmic LPS.* Proc Natl Acad Sci U S A, 2014. **111**(16): p. 6046-51.
119. Li, P., et al., *Ubiquitination and degradation of GBPs by a Shigella effector to suppress host defence.* Nature, 2017. **551**(7680): p. 378-383.
120. Li, Z., et al., *Shigella evades pyroptosis by arginine ADP-riboxanation of caspase-11.* Nature, 2021. **599**(7884): p. 290-295.
121. Oh, C., et al., *OspC3 suppresses murine cytosolic LPS sensing.* iScience, 2021. **24**(8): p. 102910.
122. Sandstrom, A., et al., *Functional degradation: A mechanism of NLRP1 inflammasome activation by diverse pathogen enzymes.* Science, 2019. **364**(6435).
123. Chavarría-Smith, J., et al., *Functional and Evolutionary Analyses Identify Proteolysis as a General Mechanism for NLRP1 Inflammasome Activation.* PLoS Pathog, 2016. **12**(12): p. e1006052.
124. Tsu, B.V., et al., *Diverse viral proteases activate the NLRP1 inflammasome.* Elife, 2021. **10**.
125. Hansen, J.M., et al., *Pathogenic ubiquitination of GSDMB inhibits NK cell bactericidal functions.* Cell, 2021. **184**(12): p. 3178-3191.e18.

126. Faherty, C.S. and A.T. Maurelli, *Spa15 of Shigella flexneri is secreted through the type III secretion system and prevents staurosporine-induced apoptosis.* Infect Immun, 2009. **77**(12): p. 5281-90.
127. Clark, C.S. and A.T. Maurelli, *Shigella flexneri inhibits staurosporine-induced apoptosis in epithelial cells.* Infect Immun, 2007. **75**(5): p. 2531-9.
128. Faherty, C.S., et al., *Microarray analysis of Shigella flexneri-infected epithelial cells identifies host factors important for apoptosis inhibition.* BMC Genomics, 2010. **11**: p. 272.
129. Bergounioux, J., et al., *Calpain activation by the Shigella flexneri effector VirA regulates key steps in the formation and life of the bacterium's epithelial niche.* Cell Host Microbe, 2012. **11**(3): p. 240-52.
130. Günther, S.D., et al., *Cytosolic Gram-negative bacteria prevent apoptosis by inhibition of effector caspases through lipopolysaccharide.* Nat Microbiol, 2020. **5**(2): p. 354-367.
131. Ashida, H., et al., *A bacterial E3 ubiquitin ligase IpaH9.8 targets NEMO/IKKgamma to dampen the host NF-kappaB-mediated inflammatory response.* Nat Cell Biol, 2010. **12**(1): p. 66-73; sup pp 1-9.
132. Ashida, H., H. Nakano, and C. Sasakawa, *Shigella IpaH0722 E3 ubiquitin ligase effector targets TRAF2 to inhibit PKC-NF-κB activity in invaded epithelial cells.* PLoS Pathog, 2013. **9**(6): p. e1003409.
133. de Jong, M.F., et al., *Shigella flexneri suppresses NF-κB activation by inhibiting linear ubiquitin chain ligation.* Nat Microbiol, 2016. **1**(7): p. 16084.
134. Kim, D.W., et al., *The Shigella flexneri effector OspG interferes with innate immune responses by targeting ubiquitin-conjugating enzymes.* Proc Natl Acad Sci U S A, 2005. **102**(39): p. 14046-51.
135. Newton, H.J., et al., *The type III effectors NleE and NleB from enteropathogenic E. coli and OspZ from Shigella block nuclear translocation of NF-kappaB p65.* PLoS Pathog, 2010. **6**(5): p. e1000898.
136. Sanada, T., et al., *The Shigella flexneri effector OspI deamidates UBC13 to dampen the inflammatory response.* Nature, 2012. **483**(7391): p. 623-6.
137. Wang, F., et al., *Shigella flexneri T3SS effector IpaH4.5 modulates the host inflammatory response via interaction with NF-κB p65 protein.* Cell Microbiol, 2013. **15**(3): p. 474-85.
138. Ashida, H., C. Sasakawa, and T. Suzuki, *A unique bacterial tactic to circumvent the cell death crosstalk induced by blockade of caspase-8.* EMBO J, 2020. **39**(17): p. e104469.
139. Bernardini, M.L., et al., *Identification of icsA, a plasmid locus of Shigella flexneri that governs bacterial intra- and intercellular spread through interaction with F-actin.* Proc Natl Acad Sci U S A, 1989. **86**(10): p. 3867-71.
140. Goldberg, M.B. and J.A. Theriot, *Shigella flexneri surface protein IcsA is sufficient to direct actin-based motility.* Proc Natl Acad Sci U S A, 1995. **92**(14): p. 6572-6.
141. DuPont, H.L., et al., *The response of man to virulent Shigella flexneri 2a.* J Infect Dis, 1969. **119**(3): p. 296-9.
142. DuPont, H.L., et al., *Inoculum size in shigellosis and implications for expected mode of transmission.* J Infect Dis, 1989. **159**(6): p. 1126-8.

143. Jeong, K.I., et al., *A piglet model of acute gastroenteritis induced by Shigella dysenteriae Type 1.* J Infect Dis, 2010. **201**(6): p. 903-11.
144. West, N.P., et al., *Optimization of virulence functions through glucosylation of Shigella LPS.* Science, 2005. **307**(5713): p. 1313-7.
145. Yum, L.K. and H. Agaisse, *Mechanisms of bacillary dysentery: lessons learnt from infant rabbits.* Gut Microbes, 2019: p. 1-6.
146. Islam, D., et al., *Evaluation of an intragastric challenge model for Shigella dysenteriae 1 in rhesus monkeys (Macaca mulatta) for the pre-clinical assessment of Shigella vaccine formulations.* APMIS, 2014. **122**(6): p. 463-75.
147. Ranallo, R.T., et al., *Oral administration of live Shigella vaccine candidates in rhesus monkeys show no evidence of competition for colonization and immunogenicity between different serotypes.* Vaccine, 2014. **32**(15): p. 1754-60.
148. Martino, M.C., et al., *Mucosal lymphoid infiltrate dominates colonic pathological changes in murine experimental shigellosis.* J Infect Dis, 2005. **192**(1): p. 136-48.
149. Rathinam, V.A. and K.A. Fitzgerald, *Inflammasome Complexes: Emerging Mechanisms and Effector Functions.* Cell, 2016. **165**(4): p. 792-800.
150. Zhao, Y. and F. Shao, *The NAIP-NLRC4 inflammasome in innate immune detection of bacterial flagellin and type III secretion apparatus.* Immunol Rev, 2015. **265**(1): p. 85-102.
151. Vance, R.E., *The NAIP/NLRC4 inflammasomes.* Curr Opin Immunol, 2015. **32**: p. 84-9.
152. Kayagaki, N., et al., *Caspase-11 cleaves gasdermin D for non-canonical inflammasome signalling.* Nature, 2015. **526**(7575): p. 666-71.
153. Shi, J., et al., *Cleavage of GSDMD by inflammatory caspases determines pyroptotic cell death.* Nature, 2015. **526**(7575): p. 660-5.
154. Ashida, H., M. Kim, and C. Sasakawa, *Manipulation of the host cell death pathway by Shigella.* Cell Microbiol, 2014. **16**(12): p. 1757-66.
155. Lamkanfi, M. and V.M. Dixit, *Manipulation of host cell death pathways during microbial infections.* Cell Host Microbe, 2010. **8**(1): p. 44-54.
156. Crowley, S.M., et al., *Intestinal restriction of Salmonella Typhimurium requires caspase-1 and caspase-11 epithelial intrinsic inflammasomes.* PLoS Pathog, 2020. **16**(4): p. e1008498.
157. Ducarmon, Q.R., et al., *Gut Microbiota and Colonization Resistance against Bacterial Enteric Infection.* Microbiol Mol Biol Rev, 2019. **83**(3).
158. Rauch, I., et al., *NAIP proteins are required for cytosolic detection of specific bacterial ligands in vivo.* J Exp Med, 2016. **213**(5): p. 657-65.
159. Raqib, R., et al., *Innate immune responses in children and adults with Shigellosis.* Infect Immun, 2000. **68**(6): p. 3620-9.
160. Collins, T.A., et al., *Safety and colonization of two novel VirG(IcsA)-based live Shigella sonnei vaccine strains in rhesus macaques (Macaca mulatta).* Comp Med, 2008. **58**(1): p. 88-94.
161. Mani, S., T. Wierzba, and R.I. Walker, *Status of vaccine research and development for Shigella.* Vaccine, 2016. **34**(26): p. 2887-2894.
162. Orr, N., et al., *Community-based safety, immunogenicity, and transmissibility study of the Shigella sonnei WRSS1 vaccine in Israeli volunteers.* Infect Immun, 2005. **73**(12): p. 8027-32.

163. Coster, T.S., et al., *Vaccination against shigellosis with attenuated Shigella flexneri 2a strain SC602.* Infect Immun, 1999. **67**(7): p. 3437-43.
164. Kotloff, K.L., et al., *Safety, immunogenicity, and transmissibility in humans of CVD 1203, a live oral Shigella flexneri 2a vaccine candidate attenuated by deletions in aroA and virG.* Infect Immun, 1996. **64**(11): p. 4542-8.
165. Barthel, M., et al., *Pretreatment of mice with streptomycin provides a Salmonella enterica serovar Typhimurium colitis model that allows analysis of both pathogen and host.* Infect Immun, 2003. **71**(5): p. 2839-58.
166. Becattini, S., et al., *Commensal microbes provide first line defense against Listeria monocytogenes infection.* J Exp Med, 2017. **214**(7): p. 1973-1989.
167. Bou Ghanem, E.N., et al., *Oral transmission of Listeria monocytogenes in mice via ingestion of contaminated food.* J Vis Exp, 2013(75): p. e50381.
168. Barry, E.M., et al., *Progress and pitfalls in Shigella vaccine research.* Nat Rev Gastroenterol Hepatol, 2013. **10**(4): p. 245-55.
169. Mattock, E. and A.J. Blocker, *How Do the Virulence Factors of Shigella work together to cause disease?* Front Cell Infect Microbiol, 2017. **7**: p. 64.
170. Ashida, H., H. Mimuro, and C. Sasakawa, *Shigella manipulates host immune responses by delivering effector proteins with specific roles.* Front Immunol, 2015. **6**: p. 219.
171. Williams, G.T., *Programmed cell death: a fundamental protective response to pathogens.* Trends Microbiol, 1994. **2**(12): p. 463-4.
172. Koch, S. and A. Nusrat, *The life and death of epithelia during inflammation: lessons learned from the gut.* Annu Rev Pathol, 2012. **7**: p. 35-60.
173. Doran, A.C., A. Yurdagul, and I. Tabas, *Efferocytosis in health and disease.* Nat Rev Immunol, 2020. **20**(4): p. 254-267.
174. Yatim, N., S. Cullen, and M.L. Albert, *Dying cells actively regulate adaptive immune responses.* Nat Rev Immunol, 2017. **17**(4): p. 262-275.
175. Deets, K.A., et al., *Inflammasome activation leads to cDC1-independent cross-priming of CD8 T cells by epithelial cell-derived antigen.* Elife, 2021. **10**.
176. Sellin, M.E., et al., *Epithelium-intrinsic NAIP/NLRC4 inflammasome drives infected enterocyte expulsion to restrict Salmonella replication in the intestinal mucosa.* Cell Host Microbe, 2014. **16**(2): p. 237-248.
177. Ashida, H., T. Suzuki, and C. Sasakawa, *Shigella infection and host cell death: a double-edged sword for the host and pathogen survival.* Curr Opin Microbiol, 2021. **59**: p. 1-7.
178. Boulard, O., et al., *Identification of a genetic locus controlling bacteria-driven colitis and associated cancer through effects on innate inflammation.* J Exp Med, 2012. **209**(7): p. 1309-24.
179. Alphonse, N., et al., *A family of conserved bacterial virulence factors dampens interferon responses by blocking calcium signaling.* Cell, 2022. **185**(13): p. 2354-2369.e17.
180. Zychlinsky, A., et al., *Interleukin 1 is released by murine macrophages during apoptosis induced by Shigella flexneri.* J Clin Invest, 1994. **94**(3): p. 1328-32.
181. Zychlinsky, A., et al., *In vivo apoptosis in Shigella flexneri infections.* Infect Immun, 1996. **64**(12): p. 5357-65.

182. Sansonetti, P.J., et al., *Caspase-1 activation of IL-1beta and IL-18 are essential for Shigella flexneri-induced inflammation.* Immunity, 2000. **12**(5): p. 581-90.
183. Arondel, J., et al., *Increased interleukin-1 (IL-1) and imbalance between IL-1 and IL-1 receptor antagonist during acute inflammation in experimental Shigellosis.* Infect Immun, 1999. **67**(11): p. 6056-66.
184. Liu, H., et al., *TNF-alpha-induced apoptosis of macrophages following inhibition of NF-kappa B: a central role for disruption of mitochondria.* J Immunol, 2004. **172**(3): p. 1907-15.
185. Patankar, J.V. and C. Becker, *Cell death in the gut epithelium and implications for chronic inflammation.* Nat Rev Gastroenterol Hepatol, 2020. **17**(9): p. 543-556.
186. Persson, J. and R.E. Vance, *Genetics-squared: combining host and pathogen genetics in the analysis of innate immunity and bacterial virulence.* Immunogenetics, 2007. **59**(10): p. 761-78.
187. van Dullemen, H.M., et al., *Treatment of Crohn's disease with anti-tumor necrosis factor chimeric monoclonal antibody (cA2).* Gastroenterology, 1995. **109**(1): p. 129-35.
188. Gitlin, A.D., et al., *Integration of innate immune signalling by caspase-8 cleavage of N4BP1.* Nature, 2020. **587**(7833): p. 275-280.
189. Woznicki, J.A., et al., *TNF-α synergises with IFN-γ to induce caspase-8-JAK1/2-STAT1-dependent death of intestinal epithelial cells.* Cell Death Dis, 2021. **12**(10): p. 864.
190. Schwarzer, R., et al., *FADD and Caspase-8 Regulate Gut Homeostasis and Inflammation by Controlling MLKL- and GSDMD-Mediated Death of Intestinal Epithelial Cells.* Immunity, 2020. **52**(6): p. 978-993.e6.
191. Stolzer, I., et al., *STAT1 coordinates intestinal epithelial cell death during gastrointestinal infection upstream of Caspase-8.* Mucosal Immunol, 2022. **15**(1): p. 130-142.
192. Philip, N.H., et al., *Activity of Uncleaved Caspase-8 Controls Anti-bacterial Immune Defense and TLR-Induced Cytokine Production Independent of Cell Death.* PLoS Pathog, 2016. **12**(10): p. e1005910.
193. Lee, B.L., et al., *ASC- and caspase-8-dependent apoptotic pathway diverges from the NLRC4 inflammasome in macrophages.* Sci Rep, 2018. **8**(1): p. 3788.
194. Wen, S., et al., *Necroptosis is a key mediator of enterocytes loss in intestinal ischaemia/reperfusion injury.* J Cell Mol Med, 2017. **21**(3): p. 432-443.
195. Knoop, K.A., et al., *RANKL is necessary and sufficient to initiate development of antigen-sampling M cells in the intestinal epithelium.* J Immunol, 2009. **183**(9): p. 5738-47.
196. Louie, A., et al., *A Multiorgan Trafficking Circuit Provides Purifying Selection of Listeria monocytogenes Virulence Genes.* mBio, 2019. **10**(6).
197. Hullahalli, K., J.R. Pritchard, and M.K. Waldor, *Refined Quantification of Infection Bottlenecks and Pathogen Dissemination with STAMPR.* mSystems, 2021. **6**(4): p. e0088721.
198. Abel, S., et al., *Sequence tag-based analysis of microbial population dynamics.* Nat Methods, 2015. **12**(3): p. 223-6, 3 p following 226.

199. Gaidt, M.M., et al., *The DNA Inflammasome in Human Myeloid Cells Is Initiated by a STING-Cell Death Program Upstream of NLRP3.* Cell, 2017. **171**(5): p. 1110-1124 e18.
200. Maurelli, A.T., B. Blackmon, and R. Curtiss, 3rd, *Loss of pigmentation in Shigella flexneri 2a is correlated with loss of virulence and virulence-associated plasmid.* Infect Immun, 1984. **43**(1): p. 397-401.
201. Makino, S., et al., *A genetic determinant required for continuous reinfection of adjacent cells on large plasmid in S. flexneri 2a.* Cell, 1986. **46**(4): p. 551-5.
202. Miyoshi, H. and T.S. Stappenbeck, *In vitro expansion and genetic modification of gastrointestinal stem cells in spheroid culture.* Nat Protoc, 2013. **8**(12): p. 2471-82.
203. Wang, H., et al., *One-step generation of mice carrying mutations in multiple genes by CRISPR/Cas-mediated genome engineering.* Cell, 2013. **153**(4): p. 910-8.
204. Tenthorey, J.L., et al., *NLRC4 inflammasome activation is NLRP3- and phosphorylation-independent during infection and does not protect from melanoma.* J Exp Med, 2020. **217**(7).
205. Chen, S., et al., *Highly Efficient Mouse Genome Editing by CRISPR Ribonucleoprotein Electroporation of Zygotes.* J Biol Chem, 2016. **291**(28): p. 14457-67.